HOMOCLINIC BIFURCATION AND SADDLE CONNECTIONS FOR DUFFING TYPE OSCILLATORS

by

N. M. DAVENPORT

FOR THE DEGREE OF DOCTOR OF PHILOSOPHY 1987

ACKNOWLEDGEMENT

The author is extremely grateful for the computer facilities provided by the Department of Mathematics during his period of study at Keele. He is even more indebted to his supervisor Dr. Peter Smith for all the help, encouragement and patience he has afforded him throughout.

N. M. Davenport

AN ABSTRACT

The study primarily considers the nondimensionalised Duffing's equation

$$x'' + kx' - x + x^3 = F \cos \omega t, \quad (k, F, \omega) > 0,$$

and investigates the various phenomena associated with small damping and forcing amplitude.

Through the use of Liapunov functions global stability of solutions is established for the forced and the unforced cases.

A basic averaging process establishes a frequency/amplitude relationship for $2\pi/\omega$ periodic solutions which is subsequently tested for stability of solutions: Computer plots not only reveal stable $2\pi/\omega$ solutions but solutions that period double over a small ω-range when k and F are fixed bringing with them structural instability or bifurcation. Period doubling is known to be rife in one dimensional nonlinear mappings and a section is devoted to one such mapping where investigations reveal behaviour analogous to the Duffing's equation.

The underlying structure of Duffing's equation is revealed through the use of the Poincaré map. The complex windings of the manifolds of the saddle points result in homoclinic intersections another type of structural instability known as homoclinic bifurcation. Before homoclinic intersection comes homoclinic tangency and this is predicted through a result obtained by Mel'nikov's method. The horseshoe map explains the complicated windings of the manifold that produce the

strange attractor associated with chaotic motion.

The analysis is made easier when a piecewise linear system is investigated which behaves in the same way as Duffing's equation. Coordinates of homoclinic points are found, equations of manifolds obtained and saddle connections drawn.

Using a perturbed equation saddle connections of Duffing's equation are sought. The analysis unfurls simple saddle connections, double-loop, transverse and multiple loop connections. Odd periodic solutions are also investigated in a similar way.

Finally, the perturbed equation is solved exactly and used to find equations of saddle connections and coordinates of homoclinic points of Duffing's equation.

CONTENTS

/continued . . .

PREFACE

The aim of this thesis is to gain a better understanding of Duffing type oscillators particularly in the areas of homoclinic bifurcation and saddle connections. Although a great deal has already been written on Duffing's equation itself there are still many questions left unanswered, and many areas not dealt with to any real depth (I'm thinking here particularly of saddle connections where virtually nothing has been written at all). Through the use of standard numerical techniques and computer plots the novel phenomenon introduced by the presence of the nonlinear terms are depicted, and where possible analysed and explained.

Chapter 0 brings to the attention of the reader four physical systems whose behaviour can be modelled by Duffing's equation with negative linear restoring force, three of which are known through experimentation to exhibit extraordinary behaviour such as period doubling and chaotic motion. The fourth example is given in the form of an exercise in Jordan & Smith (1987).

Chapter 1 is a review of the global attraction property of the Duffing's equation as presented by Holmes (1979). It makes use of a number of Liapunov functions to determine the global stability of both the unforced and forced equations. The chapter also concentrates on the behaviour of solution curves that both enter and leave the saddle point of the unforced system. These invariant solutions or manifolds are first explained in

terms of eigenlines of linear systems after which a definition is introduced to include nonlinear manifolds expressed using the notation $W^{S}_{Loc}(\bar{X})$ and $W^{U}_{Loc}(\bar{X})$ for the stable and unstable manifolds respectively.

Chapter 2 is likewise a review of the general behaviour of Duffing's equation for small damping and forcing. Using the harmonic balance method frequency/amplitude curves can be drawn revealing $2\pi/\omega$ periodic solutions for fixed damping and forcing amplitude but varying forcing frequency. Stability conditions of these solutions are obtained using the Routh-Hurwitz criterion. This approach, unfortunately, has the disadvantage of obscuring the existence of $2^{n}\pi/\omega$ periodic solutions ($n = 0, 1, 2 \ldots$), known as period doubling, but these are picked up from computer plots.

When a solution changes from one stable period to another we say that it is structurally unstable and is associated with a bifurcation of the system. The term 'bifurcation' is first explained in the context of simple linear systems using the ideas of perturbation and topological equivalence.

To understand the phenomenon of period doubling use is made of a one dimensional nonlinear mapping and its composites. It turns out that the iteration scheme not only exhibits period doubling but passes through similar stages to Duffing's equation. Further results of the mapping therefore carry over to Duffing and similar systems.

Chapter 3 explains and makes use of the Poincaré map as a necessary tool in understanding the underlying structure of nonlinear systems. Mapping out the stable and unstable manifolds of the saddle point(s) reveals the complex structure of such systems. In the Duffing case a series of Poincaré diagrams are drawn showing how the structure increases in complexity as the forcing frequency is decreased. The ultimate case reveals a strange attractor corresponding to motion that is said to be chaotic: attracting motions are neither periodic nor even quasiperiodic.

Poincaré plots reveal homoclinic points where the stable and unstable manifolds intersect. This is a homoclinic bifurcation situation since the system can behave in one of two ways depending upon the choice of initial conditions. Before intersection, tangency occurs and the parameter link predicting homoclinic tangency is obtained using Mel'nikov's method.

The final section deals with the Smale horseshoe map and uses it to explain the complex structure of a strange attractor.

Systems such as Duffing's equation are usually difficult to analyse. If a simpler system could be found that behaves in the same way it may be possible to gain further insight into the original. Chapter 4 deals with a piecewise linear system that behaves precisely the same way as Duffing's equation but is easier to analyse. We are able to locate exactly the position of certain

homoclinic points, draw saddle connections and part draw from exact solutions the stable and unstable manifolds.

The very existence of a homoclinic point confirms the existence of a saddle connection. This is a solution that emanates from an unstable saddle solution only to return to it in some future time and remain there. Because of the very nature of a saddle solution, saddle connections are usually very difficult to locate and plot. Chapter 5 is devoted to the investigation of such solutions of Duffing's equation using a perturbation method. The result is a new equation which is considerably easier to analyse thus enabling a number of different saddle connections to be found. The various types investigated are simple saddle connections, double loop, transverse and multiple-loop connections. Finally, using the approach of the chapter odd periodic solutions are investigated and obtained.

It turns out that the transformed equation dealt with in chapter 5 can be solved completely. The general solution is obtained in Chapter 6 and when the necessary boundary conditions are satisfied we have the equation of a simple saddle connection. The coordinates of the homoclinic points of the original Duffing's equation are then determined and displayed for varying parameter values.

0.1 PHYSICAL SYSTEMS THAT LEAD TO DUFFING TYPE OSCILLATORS

The nonlinear differential equation of the second order

$$x'' + f(x, x')x' + g(x) = e(t)$$

with e(t) of period L, is of considerable interest in applied mathematics and various fields of engineering. It describes the oscillatory phenomena of nonlinear systems driven by a periodic external force, e(t). One such equation that fits this type is Duffing's equation

$$x'' + Bx' + Cx + Dx^3 = E \cos WT, \quad B, C, D, \Sigma \text{ and } W \text{ constant} \qquad (0.1.1)$$

being one of the simplest yet most important nonlinear differential equations. Aside from the harmonic, higher harmonic and subharmonic motions (Hayashi (1964), Levenson (1949)) which are known well to exist, it also exhibits period doubling oscillations and chaotic motions. [Ueda (1980) has produced a picture book of regular and chaotic motions exhibited by Duffing's equation and so too have Abraham & Shaw.] Many researchers have found that the nonlinear partial differential equations obtained as mathematical models of various electrical and structural experiments can be reduced further, taking a suitable approximation, often a Galerkin approximation

(See Guckenheimer & Holmes, 1983), to a Duffing type equation as above. Our interest lies with a particular form of Duffing's equation obtained on putting $x = \alpha X$, $t = \beta T$ where $\alpha^2 = -C/D$, $(D > 0)$ and $\beta^2 = -1/C$, $(C < 0)$ and writing $k = \beta B$, $F = -E/\alpha C$, $\omega = \beta W$. The resulting transformation gives the equation, in terms of the original variables,

$$x'' + kx' - x + x^3 = F \cos \omega t. \qquad (0.1.2)$$

This form will be used throughout this thesis. The behaviour of solutions is effectively controlled by three parameters - the damping coefficient k, and the amplitude F and frequency ω of the harmonic forcing term. Clearly, it is those investigations whose mathematical model reduces to this form that are of interest here. Four such examples follow.

Tseng & Dugandji (1971) considered the dynamic behaviour of a buckled beam with fixed ends, excited by the harmonic motion of its supporting base. The governing equation turned out to be a fourth order partial differential equation which upon application of Galerkin's method and assuming harmonic excitation of the base reduced to the Duffing's equation above with negative linear stiffness. This enabled the authors to investigate the snap-through problem of the system.

Perhaps the most well-known investigation was undertaken by Moon & Holmes (1979) who investigated the behaviour of the forced vibration of a cantilevered beam

which is buckled by magnetic forces. Consider a slender elastic road, clamped at one end in a rigid framework and constrained to move in a plane with one degree of freedom. [Fig[0.1].) Two magnets attached to the frame as indicated cause the beam to buckle either to the left or to the right, the central position being unstable. The whole framework is now moved sinusoidally, so that

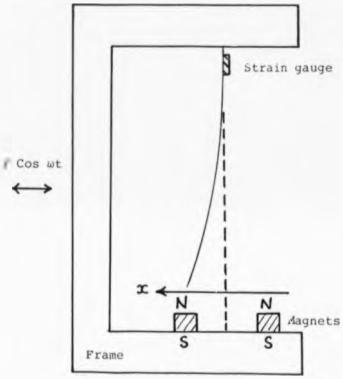

FIG[0.1] Magnetoelastic beam

the beam vibrates under 'inertial' excitation. For small excitation amplitudes, periodic motions are observed about either stable equilibrium, but as the amplitude is increased an apparently sudden transition to a 'chaotic snap-through' motion is observed. In this state, the beam oscillates irregularly about first one and then the other equilibrium. An example of such a motion, measured from a strain gauge at the beam's roots, displays irregular tip displacement. The nonlinear partial differential equation of an inextensible elastic rod in a nonuniform magnetic field can be truncated using a Galerkin approximation to yield the unforced, undamped Duffing's equation,

$$x'' - x + x^3 = 0, \qquad (0.1.3)$$

where $x = x(t)$ is the (nondimensional) displacement of the vibration and dissipation is ignored. Introduce a weak dissipation (aerodynamic damping) and periodic forcing and one obtains

$$x'' - x + x^3 = \varepsilon(f \cos \omega t - \delta\dot{x}). \qquad (0.1.4)$$

[Moon, (1980) investigated the behaviour of a buckled beam with two degrees of freedom, which also exhibited chaotic behaviour.]

In an electrical context Odyniec & Chua (1983) used a second-order circuit to model the complex dynamical behaviour of a typical Josephson-junction circuit. Josephson-junction devices are used in many applications

ranging from supersensitive detectors to superfast computers. The device is imbued with rich dynamics and displays a wide variety of nonlinear phenomena.

A Josephson-junction circuit model is shown in Fig[0.2] where the basic Josephson element is a nonlinear inductor described by

$$i = I_c \sin\left(\frac{4\pi e}{h}\right)\phi$$

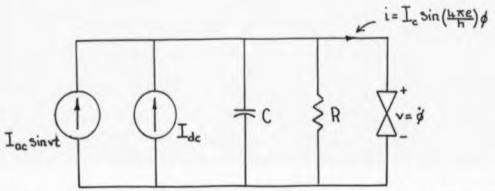

FIG[0.2] A second-order Josephson-junction circuit model driven by a dc and ac current source.

where ϕ denotes the flux linkage, e denotes the electron charge, and h denotes Planck's constant and I_c a suitable amplitude. The equation governing the second-order circuit in Fig[0.2] is given by

$$C\frac{d^2\phi}{dt^2} + \frac{1}{R}\frac{d\phi}{dt} + I_c \operatorname{Sin}\left(\frac{4\pi e}{h}\right)\phi = I_{dc} + I_{ac} \operatorname{Sin} \nu t. \quad (0.1.5)$$

Equation (0.1.5) can be transformed into the dimensionless form

$$\beta x'' + x' + \operatorname{Sin} x = \alpha + \varepsilon \operatorname{Sin} \omega\tau \quad (0.1.6)$$

where differentiation is now with respect to τ.

A further problem that can be modelled by Duffing's equation of this type is given in the form of an exercise in Jordan & Smith (1987) where the dynamic behaviour of a very simple system is considered. Two rings can slide on two fixed horizontal wires which lie in the same vertical plane with separation a. The two rings are connected by a spring of unstretched length ℓ and stiffness μ. The upper ring is forced to move with displacement $\phi(t)$ from a fixed point 0 as shown in Fig[0.3]. The resistance on the lower ring which has mass m is assumed to be mk × (speed). Let x be the relative displacement between the rings where x = x(t), T the tension (or compression) in the spring and R the total resistence due to velocity. Applying Newton's 2nd Law (that of force = mass × acceleration), the equation governing the behaviour of the lower ring is given by

$$m(x'' + \phi'') = -R - T \operatorname{Cos} \theta, \quad (0.1.7)$$

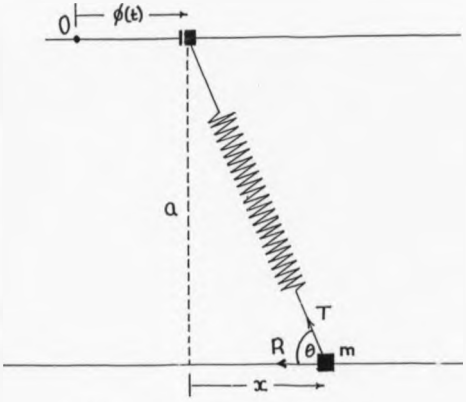

FIG[0.3]

where θ is the angle the spring makes with the lower wire, and

$T = \mu(\sqrt{a^2 + x^2} - \ell)$

$R = mk(\ddot{x} + \frac{1}{\phi})$

$\cos\theta = x/\sqrt{a^2 + x^2}$, hence

$$x'' + kx' + \frac{\mu}{m}x - \frac{\mu \ell x}{m\sqrt{a^2 + x^2}} = -\phi'' - k\phi'. \qquad (0.1.8)$$

Assuming that the displacement, x is small compared to a, the nonlinear term of (0.1.8) can be approximated to x^3 to give the new equation

$$x'' + kx' + \frac{\mu}{ma}(a - \ell)x + \frac{\ell\mu x^3}{2ma^3} = -\phi'' - k\phi'. \qquad (0.1.9)$$

If we ensure beforehand that the unstretched length ℓ of the spring is greater than the perpendicular distance, a, between the wires and reproduce the cosine forcing simply by putting $-\phi'' - k\phi' = F \cos \omega t$ then after a simple redimensionalising we obtain Duffing's equation in the form given by (0.1.2). Hence, for the appropriate choice of parameter values the behaviour of the lower ring should be in accordance with the known behaviour of this form of Duffing's equation; unfortunately, there are no results of any practical experiments carried out in this particular case. The question naturally arises, what type of behaviour might we expect from such systems? It is hoped that in the remainder of this thesis this, and similar questions, will be answered.

CHAPTER 1

GLOBAL ATTRACTIONS OF SOLUTIONS TO DUFFING'S EQUATION

1.1 GLOBAL ATTRACTION - THE UNFORCED CASE

Consider the differential equation

$$x'' + kx' - x + x^3 = F \cos \omega t, \quad x(0) = x_0, \quad x'(0) = y_0 \tag{1.1.1}$$

which is Duffing's equation with negative linear stiffness and cubic restoring force. Holmes (1979) used this equation as the simplest model of a buckled beam undergoing lateral vibrations. From numerical evidence Eqn(1.1.1) has stable closed-loop solutions in the (x, x') plane disposed about $x = \pm 1$ and $x = 0$. Fig[1.1] displays the form of the restoring function $R(x) = x - x^3$, the arrows indicating the direction of the restoring force about $x = \pm 1$ and 0. When $|x| > 1$ a strong restoring force attempts to pull the response back towards $|x| = 1$. In the regions $0 < x < 1$ and $-1 < x < 0$, the restoring force acts in the opposite direction forcing the response back towards $|x| = 1$. In fact, in both of these two regions two separate forces are at work, one pulling back to $|x| = 1$, the other pushing away from $x = 0$. Fig[1.2]

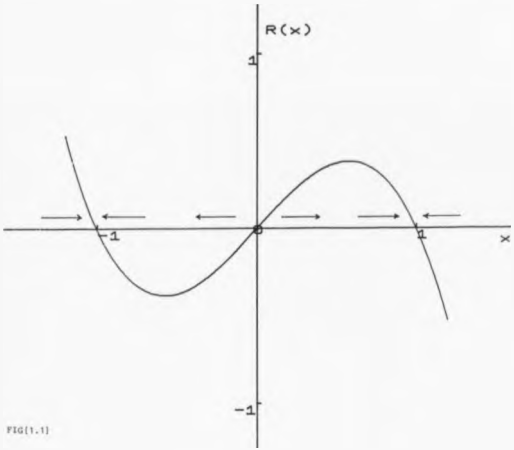

FIG(1.1)

shows typical results in the (x, x') phase plane of the unforced, Duffing equation in which F = 0. In this case, the net result of the restoring force just described, along with the presence of damping (kx') in the system creates the spiralling into either of the two equilibrium states at x = 1 or x = -1. When, however, the forcing term is present, for suitable parameter values, one can expect two distinct stable solutions positioned about

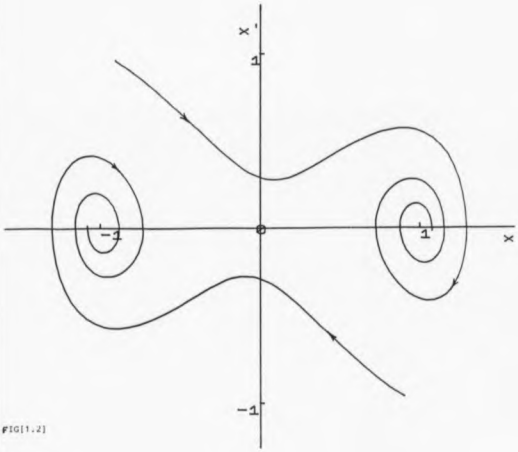

FIG[1.2]

$x = \pm 1$ with obvious rotation symmetry of 180° about (0, 0).

If F is set to zero in Eqn(1.1.1), that is, without external forcing, we have the autonomous differential equation

$$x'' + kx' - x + x^3 = 0, \quad x(0) = x_0, \quad x'(0) = y_0. \tag{1.1.2}$$

Expressing (1.1.2) as the first-order nonlinear system

$$x' = y = X(x, y)$$

$$y' = x - ky - x^3 = Y(x, y) \qquad (1.1.3)$$

we can obtain the co-ordinates of the equilibrium points in the (x, x') plane by setting x' = y' = 0. From (1.1.3) we have the three fixed points at (0, 0) and (±1, 0). Through the process of linearization about each of the equilibrium points we find the latter two points are sinks with eigenvalues $\frac{1}{2}(-k \pm \sqrt{k^2 - 8})$, and the origin is a saddle with eigenvalues $\frac{1}{2}(-k \pm \sqrt{k^2 + 4})$. Examples of both a sink and a saddle are shown in Fig[1.2] and Fig[1.3] respectively. All three equilibrium points have eigenvalues with non-zero real parts and are called hyperbolic or non-degenerate equilibrium points. (See Abraham and Shaw, Part Two.) However, although linearization or calculation of eigenvalues provide local stability conditions it cannot detect global phenomena such as limit cycles.

For global stability we follow the account given by Holmes (1979) based on the Liapunov Stability Theorem. First the theorem is explained as outlined in Hayashi (1964).

Consider an autonomous system of differential equations

$$\frac{dx}{dt} = \underline{X}(\underline{x}) \quad \text{or}$$

$$\frac{dx_i}{dt} = X_i(x_1, x_2, \ldots, x_n) \quad i = 1, 2, 3, \ldots, n \qquad (1.1.4)$$

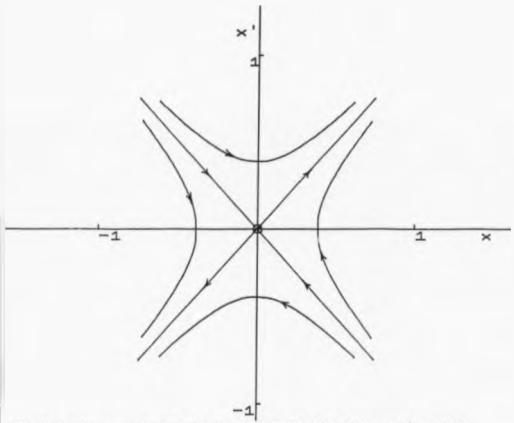

FIG[1.3] A saddle point (x' = y, y' = x). The asymptotes show eigenvector directions.

and assume that the origin is a singular equilibrium point of this system. Introduce a positive definite function V(x) with the following properties:

1. V is continuous together with its first partial derivatives in a certain domain D containing the origin.

2. Outside the origin V is positive; it vanishes only at the origin. The time derivative of V along a trajectory of the system (1.1.4) is given by

$$\frac{dV}{dt} = \sum_{i=1}^{n} \text{grad } V.\frac{dx}{dt} = \sum_{i=1}^{n} \text{grad } V.\underline{X} = W(\underline{x}). \qquad (1.1.5)$$

Let the function $dV/dt = W(\underline{x}) \leq 0$ in the domain of D. such a function is called a Liapunov function.

With the aid of these definitions Liapunov's Stability Theorem may be stated as follows:

If there exists in a certain domain D about the origin a Liapunov function $V(\underline{x})$ then the origin is stable. Furthermore, if $dV/dt = W(\underline{x}) < 0$ is negative definite in the domain D, then the stability is asymptotic.

Applying the method to Duffing's equation we first translate Eqn(1.1.2) from the two stable sinks by putting

$$z_1 = x \pm 1$$
$$z_2 = y, \qquad (1.1.6)$$

that is, translate the system so that the fixed points are at the origin. (The x_1 translation in Holmes' paper (1979) result (2.2) is incorrect.) This results in the new system

$$z_1' = z_2$$
$$z_2' = -2z_1 - kz_2 \pm 3z_1^2 - z_1^3. \qquad (1.1.7)$$

Holmes (1979) then takes as the Liapunov function

$$V(z_1, z_2) = \tfrac{1}{2}z_2^2 + z_1^2 + \tfrac{1}{4}z_1^4 + \alpha(kz_1^2/2 + z_1z_2) \tag{1.1.8}$$

$$= \tfrac{1}{2}z_2^2(1 - \alpha/k) + z_1^2 + \tfrac{1}{4}z_1^4 + \tfrac{\alpha}{2}k(z_1 + z_2/k)^2. \tag{1.1.9}$$

(There is an error in the corresponding Liapunov function used by Holmes (1979) where $\frac{1}{4}\alpha$ should read $\frac{1}{4}\alpha y_1^4$.) Then $V(z_1, z_2) > 0$ outside the origin provided that $0 < \alpha < k$. Hence, $V(z_1, z_2)$ is globally positive definite. Differentiating $V(z_1, z_2)$, with respect to time, along solution curves of Eqn(1.1.2) we have

$$\frac{dV}{dt} = (\alpha - k)z_2^2 - 2\alpha z_1^2 \pm 3\alpha z_1^3 \pm 3z_1^2z_2 - \alpha z_1^4. \tag{1.1.10}$$

We demand that

$$\frac{dV}{dt} \leq 0. \tag{1.1.11}$$

(i) If z_1 is fixed then, for z_2 large, $(\alpha - k)z_2^2$ dominates $\Rightarrow V' \leq 0$.

(ii) If z_2 is fixed then, for z_1 large, $-\alpha z_1^4$ dominates $\Rightarrow V' \leq 0$.

(iii) If $z_1 = mz_2$ then, for z_1 large, $-\alpha m^4 z_2^4$ dominates $\Rightarrow V' \leq 0$.

Thus if z_1 and z_2 are sufficiently large, we have $dV/dt \leq 0$. Therefore, all solutions of (1.1.7) and hence (1.1.2) remain bounded for all time and approach and enter a bounded set $A \subset R^2$.

In differentiating $V(z_1, z_2)$ along solution curves we attempt to verify that all solutions cross the level curve V "inwards". If this proves to be the case then, as previously stated, all solutions enter a bounded region and remain there for all time.

By way of a simple example which illustrates Liapunov's Stability Theorem, consider the linear differential equation

$$x'' + kx' + x = 0. \tag{1.1.12}$$

Expressed as a first-order system (1.1.12) becomes

$$x' = y$$

$$y' = -ky - x$$

with the single equilibrium point (a sink) at (0, 0). Consider the level curve

$$V(x, y) = x^2(1 + \beta k/2) + y^2 + \beta xy \tag{1.1.14}$$

which is positive definite for all $0 < \beta < 2k$.

At a point of intersection, P, of a solution curve and the level curve (1.1.14), see Fig[4.1], we can test the behaviour of the trajectory by using the gradient vector ∇V and the tangent vector X. If the projection of the gradient vector onto the tangent vector is negative (that is, along $-\vec{PT}$) then the trajectory crosses the level curve "inwards". Since it is only the sign of the projection that is important we can apply the dot-product

procedure as used for finding the directional derivative.

We require the sign of the projection

$$\nabla V.X < 0 \qquad (1.1.15)$$

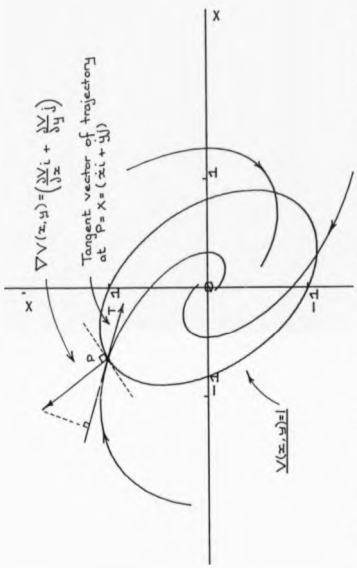

FIG(1.4) All trajectories of the equation $x'' + x' + x = 0$ cross the Liapunov function $V(x, y) = \frac{3}{4}x^2 - xy + y^2$ "inwards". $(x = \beta = 1)$

that is,

$$\left(\frac{\partial V}{\partial x}\mathbf{i} + \frac{\partial V}{\partial y}\mathbf{j}\right).(\dot{x}_1 + \dot{y}_2) < 0 \qquad (1.1.16)$$

or

$$\frac{\partial V}{\partial x}\dot{x} + \frac{\partial V}{\partial y}\dot{y} < 0 \qquad (1.1.17)$$

giving

$$\frac{dV}{dt} < 0 \qquad (1.1.18)$$

where V(x, y) is differentiated along solution curves of (1.1.13). Hence, V'(x, y) must be negative definite.

In the example

$$V' = (\beta - 2k)y^2 - \beta x^2 < 0 \qquad (1.1.19)$$

when (x, y) ≠ (0, 0), hence the trajectory in Fig[1.4] crosses the level curve "inwards". The level curve in Fig[1.4] is in the form V(x, y) = c, c > 0. Simply reducing the value of c produces a set of (decreasing) concentric ellipses with solution curves that continue to cross inwards. All solutions of Eqn(1.1.13) therefore, must tend towards the origin, hence the origin is an asymptotic stable equilibrium point.

Holmes continues to show that almost all solutions of Eqn(1.1.2) approach one or other of the sinks at (±1, 0) by using a second Liapunov function (actually a pair of functions, one for (1, 0), one for (-1, 0)):

$$V_1 = \frac{1}{2}z_2^2 + z_1^2 \mp z_1^3 + \frac{1}{4}z_1^4 + \alpha\left[\frac{k}{2}z_1^2 + z_1z_2\right] \tag{1.1.20}$$

$$= \frac{1}{4}z_1^2(z_1 \pm 2)^2 + \alpha\frac{k}{2}\left(z_1 + \frac{z_2}{k}\right)^2 + \frac{z_2^2}{2}\left(1 - \frac{\alpha}{k}\right) > 0,$$

$$(z_1, z_2) \neq (0, 0), \tag{1.1.21}$$

that is, V_1 is positive definite except at the origin. (An error exists in the corresponding Liapunov function used by Holmes (1979) where $\pm 3(\alpha\beta)^{\frac{1}{3}}y_1^3$ should read $\pm(\alpha\beta)^{\frac{1}{3}}y_1^3$).

The functions, (1.1.20), are defined within the two areas enclosed by the loop, in Fig[1.5], whose equation is given by

$$H(x, y) = \frac{1}{2}y^2 - \frac{1}{2}x^2 + \frac{1}{4}x^4 = 0 \tag{1.1.22}$$

and which after the translation given by (1.1.6) becomes

$$H(z_1, z_2) = \frac{1}{2}z_2^2 + z_1^2 \mp z_1^3 + \frac{1}{4}z_1^4 = \frac{1}{4}. \tag{1.1.23}$$

Differentiating $V_1(z_1, z_2)$, with respect to time, along solution curves of Eqn(1.1.2), we have

$$\frac{dV_1}{dt} = (\alpha - k)z_2^2 - 2\alpha z_1^2 \pm 3\alpha z_1^3 - \alpha z_1^4 \tag{1.1.24}$$

$$= (\alpha - k)z_2^2 - \alpha z_1^2\left[\left(z_1 \mp \frac{3}{2}\right)^2 - \frac{1}{4}\right] \tag{1.1.25}$$

where $\left(z_1 \mp \frac{3}{2}\right)^2 - \frac{1}{4} \geq 0$ inside the 'new' loops given by

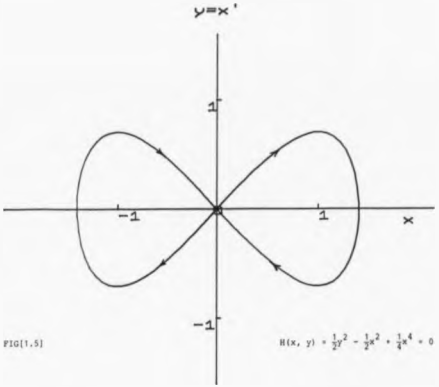

FIG(1.5) $H(x, y) = \frac{1}{2}y^2 - \frac{1}{2}x^2 + \frac{1}{4}x^4 = 0$

(1.1.23). Therefore, all solutions starting within the loop, H(x, y), approach one or other of the sinks as $t \to \infty$. It finally remains to check that there are no attractors outside H(x, y). As there are no other equilibrium points and the system is planar, the only possibility is a limit cycle. Taking the Hamiltonian energy, H(x, y), of Eqn(1.1.22) and differentiating along solution curves of (1.1.3), we obtain $dH/dt = -ky^2$. The

energy is therefore decreasing on any closed curve and thus no limit cycles exist.

Returning to the unstable equilibrium (saddle) point of Eqn(1.1.2) at the origin we concentrate on the behaviour of the curves that both enter and leave this point for forward time. To understand this better consider the first-order linear system

$$\begin{aligned} x' &= y \\ y' &= x - ky. \end{aligned} \tag{1.1.26}$$

Expressed in matrix form Eqns(1.1.26) become

$$\begin{pmatrix} x' \\ y' \end{pmatrix} = \begin{pmatrix} 0 & 1 \\ 1 & -k \end{pmatrix} \begin{pmatrix} x \\ y \end{pmatrix} = M \begin{pmatrix} x \\ y \end{pmatrix}. \tag{1.1.27}$$

In this set certain solutions play a special role; those which lie in the linear subspaces spanned by the eigenvectors. The subspaces are invariant under the solution matrix, M, in particular if V_i is a (real) eigenvector of M then a solution based at a point $aV_i \in R^2$ remains on span$\{V_i\}$ for all time.

Eigenvectors of the matrix M in Eqn(1.1.27) are

$$e_1 = \begin{pmatrix} 1 \\ \lambda_1 \end{pmatrix} \quad \text{and} \quad e_2 = \begin{pmatrix} 1 \\ \lambda_2 \end{pmatrix} \tag{1.1.28}$$

where $\lambda_{1,2} = \frac{1}{2}[-k \pm (k^2 + 4)^{\frac{1}{2}}]$, and the general solution of Eqn(1.1.27) is given by

$$x(t) = c_1\begin{bmatrix}1\\ \lambda_1\end{bmatrix}e^{\lambda_1 t} + c_2\begin{bmatrix}1\\ \lambda_2\end{bmatrix}e^{\lambda_2 t}. \qquad (1.1.29)$$

Hence, taking initial conditions $\begin{bmatrix}x_0\\ x_0'\end{bmatrix} = p\begin{bmatrix}1\\ \lambda_1\end{bmatrix}$ or $q\begin{bmatrix}1\\ \lambda_2\end{bmatrix}$

$p, q \in \mathbb{R}$, the response will remain on the linear subspace spanned by the respective eigenvectors. This means all solutions starting with initial conditions on the span of the eigenvector e_1 tend to infinity along the line $x' - \lambda_1 x = 0$. This is referred to as the unstable eigenspace, E^u. Those with initial conditions on the span of the eigenvector e_2 tend to the origin along the line $x' - \lambda_2 x = 0$, referred to as the stable eigenspace, E^s. In recent terminology (See Guckenheimer and Holmes, 1983) these special eigenspaces are referred to as the stable and unstable manifolds respectively. A generalised definition of an n-dimensional manifold $M \subset \mathbb{R}^n$ is a set for which each $x \in M$ has a neighbourhood U for which there is a smooth invertible mapping (diffeomorphism) $\phi : \mathbb{R}^n \to U$ $(n \leq N)$.

We can now define (in a general sense to include nonlinear systems) the local stable and unstable manifolds of a hyperbolic equilibrium point, $\bar{x}$, $W^s_{LOC}(\bar{x})$, $W^u_{LOC}(\bar{x})$ as follows,

$$W^s_{LOC}(\bar{x}) = \{x \in U | \phi_t(t) \to \bar{x} \text{ as } t \to \infty, \text{ and } \phi_t(x) \in U \text{ for all } t \geq 0\} \qquad (1.1.30)$$

$$W^u_{LOC}(\bar{x}) = \{x \in U | \phi_t(x) \to \bar{x} \text{ as } t \to \infty, \text{ and } \phi_t(x) \in U \text{ for all } t \leq 0\} \quad (1.1.31)$$

where $U \subseteq \mathbb{R}^n$ is a neighbourhood of the equilibrium point $\bar{x}$, and $\phi_t(x) = \phi(x, t)$ is a smooth function defined for all x in U and t in some interval $I \subseteq \mathbb{R}$. The invariant manifolds W^s_{LOC} and W^u_{LOC} provide nonlinear analogues of the stable and unstable eigenspaces E^s and E^u of the linear problem. The Stable Manifold Theorem (see G. and H. 1983) for a fixed point tells us that W^s_{LOC} and W^u_{LOC} are in fact tangent to E^s and E^u at $\bar{x}$, see Fig[1.6]. The Hartman-Grobman Theorem also states that if $\bar{x}$ is a hyperbolic equilibrium point then there is a homeomorphism* h defined on some neighbourhood U of $\bar{x}$ in $\mathbb{R}^n$ locally taking orbits of the nonlinear flows ϕ_t of the nonlinear differential equation $\dot{x} = f(x)$; $x \in \mathbb{R}^n$, $x(0) = x_0$ to those of the linear flow under local linearization. (See Guckenheimer and Holmes, 1983.) See Fig[1.7].

The local invariant manifolds W^s_{LOC}, W^u_{LOC} have global analogues W^s, W^u, obtained by letting points in W^s_{LOC} flow backwards in time and those in W^u_{LOC} flow forwards in time:

---

* A homeomorphism or topological transformation is a one-to-one correspondence between the points of two geometric figures A and B which is continuous in both directions.

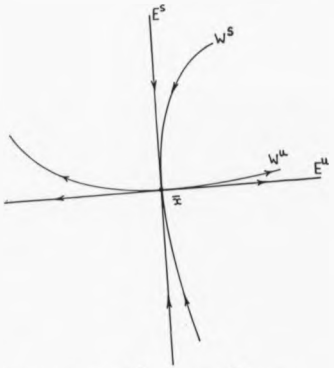

FIG[1.6] Local stable (W^s) and unstable (W^u) manifolds.

$$W^s(\bar{x}) = \bigcup_{t\leq 0} \phi_t(W^s_{LOC}(\bar{x})) \qquad (1.1.32)$$

and

$$W^u(\bar{x}) = \bigcup_{t\geq 0} \phi_t(W^u_{LOC}(\bar{x})) \qquad (1.1.33)$$

Existence and uniqueness of solutions of such equations ensure that two stable (or unstable) manifolds

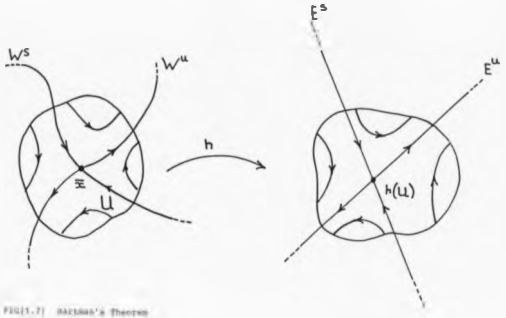

FIG(1.7) Hartman's Theorem

of distinct equilibrium points $\bar{x}_1$, $\bar{x}_2$ cannot intersect, nor can $W^s(\bar{x})$ (or $W^u(\bar{x})$) intersect itself. However, intersections of stable and unstable manifolds of distinct fixed points or the same fixed point can occur and, in fact, are a source of much of the complex behaviour found in dynamical systems.

In Eqn(1.1.3) all solutions starting at a point on an unstable manifold (in the (x, x') plane) move away

from the saddle point at the origin. Previous results have shown that globally there is a 'Liapunov' bound and since no limit-cycles exist the unstable manifolds get themselves trapped inside the local 'Liapunov' bounds and spiral in towards the stable equilibrium points at (±1, 0) as $t \to \infty$. All solutions starting on the stable manifolds, however, spiral globally into the origin as $t \to \infty$, avoiding the unstable manifolds. The existence and uniqueness of solutions of Eqn(1.1.3) ensure that intersections of stable and unstable manifolds do not occur. (See Fig[1.8].) The stable manifolds divide the (x, x') plane into two separate regions called DOMAINS OF ATTRACTION.* All initial conditions within one domain of attraction lead solutions ultimately to one of the two equilibrium points corresponding to constant solutions. Fig[1.8] shows (dotted) the typical behaviour of a response with initial conditions (x_0, x_0') wending its way to the equilibrium point (1, 0). When x is plotted against time the result is $x(t) \to 1$ as $t \to \infty$. The motion up to (±1, 0) is referred to as the TRANSIENT. The

---

* A closed invariant set $A \subset \mathbb{R}^n$ is called an attracting set if there is some neighbourhood U of A such that $\phi_t(x) \in U$ for $t \geq 0$ and $\phi_t(x) \to A$ as $t \to \infty$, for all $x \in U$. The set $\bigcup_{t \leq 0} \phi_t(U)$ is the domain of attraction of A - it is, of course, the stable manifold of A. An attracting set ultimately captures all orbits starting in its domain of attraction.

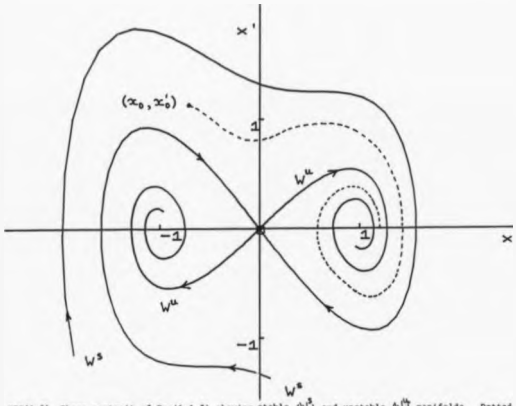

FIG(1.8) Phase portrait of Eqn(1.1.3) showing stable (W^s) and unstable (W^u) manifolds. Dotted line - - - - shows typical trajectory.

transient disappears in time leaving the stable solution either $x(t) = 1$ or $x(t) = -1$. The stable manifold is often referred to as the SEPERATRIX, in the unforced case.

1.2 GLOBAL ATTRACTION - THE FORCED CASE

We start by considering the stability of the non-autonomous system (1.1.1), that is, with $F \neq 0$. Written as a first order autonomous ordinary differential

equation on $R^2 \times S^1$, where R^2 is the (x, y) plane and $\theta \in S^1$ denotes points on the unit circle:

$$\begin{aligned} x' &= y \\ y' &= F \cos\theta - ky + x - x^3 \\ \theta' &= \omega \end{aligned} \tag{1.2.1}$$

$S^1 = R/(\text{Mod } 2\pi)$ and this copes with the 2π periodicity of the vector field.

Since $\omega \neq 0$, $\theta' = \omega$ shows that (1.2.1) has no equilibrium points. When $F = 0$ the behaviour in the (x, y) plane is the same for all $\theta \in [0, 2\pi]$ and the equilibrium points (0, 0) and (±1, 0) generate hyperbolic circular closed orbits in $R^2 \times S^1$, (hyperbolic because of the nature of the eigenvalues associated with the linearization at the equilibrium points). The invariant manifold* theorem (see Holmes, 1979) tells us that for (small) $F \neq 0$ orbits still exist, no longer circular but the qualitative features are retained. Therefore, we expect two stable attracting orbits 'close' to (±1, 0) and a single saddle type orbit close to (0, 0). Also since (1.1.3) is a (globally) structurally stable system for small F we expect the global structures of the

---

* An invariant manifold (or set) for a flow ϕ_t on R^n is a subset $S \subset R^n$ such that

$\phi_t(x) \in S$ for $x \in S$ for all $t \in R$.

manifolds of the autonomous case (1.1.3) to be preserved, that is, we expect 'complex' manifolds to exist which ultimately account for the two responses about $x = \pm 1$.

To confirm the stability of the response we again use the Liapunov function V_1 of (1.1.20) and differentiate along solution curves of the forced system,

$$\begin{aligned} x' &= y \\ y' &= F \operatorname{Cos} \omega t - ky + x - x^3. \end{aligned} \tag{1.2.2}$$

This gives,

$$\frac{dV_1}{dt} = (\alpha - k)z_2^2 - 2\alpha z_1^2 \pm 3\alpha z_1^3 - \alpha z_1^4 + (z_2 + \alpha z_1) \times F \operatorname{Cos} \omega t \tag{1.2.3}$$

$$\leq (\alpha - k)z_2^2 - 2\alpha z_1^2 \pm 3\alpha z_1^3 - \alpha z_1^4 + |z_2 F| + |\alpha z_1 F| \tag{1.2.4}$$

where z_1 and z_2 are given by (1.1.6).
Now (1.2.4) can be written

$$\frac{dV_1}{dt} \leq (\alpha - k)z_2^2 - 2\alpha z_1^2 - \alpha z_1^2\left[\left(z_1 \mp \frac{3}{2}\right)^2 - \frac{9}{4}\right] + |z_2 F| + |\alpha z_1 F|. \tag{1.2.5}$$

Splitting the inequality up (as a means of establishing the negative definite condition) we first require that

$$(\alpha - k)z_2^2 + |z_2 F| < 0 \tag{1.2.6}$$

or $$|z_2 F| < (k - \alpha)z_2^2.$$

Squaring and dividing throughout by z_2^2, $(z_2 \neq 0)$,

$$F^2 < (k - \alpha)^2 z_2^2. \tag{1.2.7}$$

Hence,

$$(k - \alpha)^2 \frac{z_2^2}{F^2} > 1. \tag{1.2.8}$$

Setting

$$F^2 = 0(\varepsilon^2) = \varepsilon^2 m + \ldots \tag{1.2.9}$$

and

$$z_2 = 0(\varepsilon^{1-\gamma}) = \varepsilon^{1-\gamma}\sqrt{n} + \ldots \tag{1.2.10}$$

and substituting into (1.2.8) we must have that

$$(K - \alpha)^2 \frac{n}{m}\varepsilon^{-2\gamma} > 1 \tag{1.2.11}$$

and this is achieved by choosing a suitable γ sufficiently small.

Secondly, we require that

$$-2\alpha z_1^2 - \alpha z_1^2\left[\left(z_1 \mp \frac{3}{2}\right)^2 - \frac{9}{4}\right] + |\alpha F z_1| < 0 \tag{1.2.12}$$

that is,

$$-\alpha z_1^2\left[\left(z_1 \mp \frac{3}{2}\right)^2 - \frac{1}{4}\right] + |\alpha F z_1| < 0. \tag{1.2.13}$$

From section (1.1) it is known that the function inside the square brackets in (1.2.13) is positive definite inside the loops given by (1.1.23). We write

$$M = \left(z_1 \mp \frac{3}{2}\right)^2 - \frac{1}{4} \tag{1.2.14}$$

and consider from (1.2.13)

$$-\alpha z_1^2 M + |\alpha z_1 F| < 0. \tag{1.2.15}$$

By the same argument as applied to condition (1.2.6), condition (1.2.15) is also satisfied. Hence, if z_1 and z_2 are (slightly) greater than $0(\varepsilon)$ then we have $dV_1/dt < 0$. Thus solutions remain bounded and in some neighbourhood of $(z_1, z_2) = (0, 0)$ for small F. This means that in terms of the response in the (x, y) plane, for small F solutions tend to remain in either of the two regions R_1 and R_2 as shown in Fig[1.10].

General stability of (1.2.2), for large F, is confirmed by again using the first Liapunov function (1.1.8), that is,

$$V = \frac{1}{2}z_2^2 + z_1^2 + \frac{1}{4}z_1^4 + \alpha\left(\frac{k}{2}z_1^2 + z_1 z_2\right)$$

and as before differentiate along solution curves of the forced system.

We have,

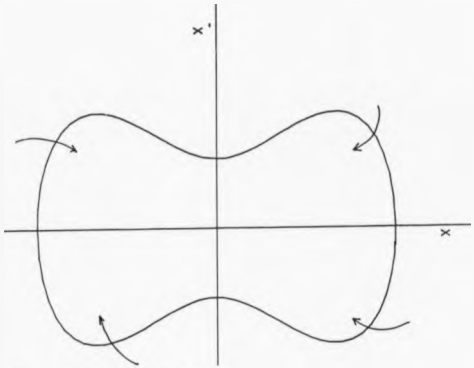

FIG[1.9] Global stability for F large.

$$\frac{dV}{dt} = (\alpha - k)z_2^2 - 2\alpha z_1^2 \pm 3z_1^2(z_2 - \alpha z_1) - \alpha z_1^4 + (z_2 + z_1)F \cos \omega t \qquad (1.2.16)$$

$$\leq (\alpha - k)z_2^2 - 2\alpha z_1^2 + 3|z_1^2 z_2| + 3\alpha|z_1^3| + |z_2 F| + |\alpha z_1 F| \qquad (1.2.17)$$

and again we want dV/dt < 0. This is shown to be true by an argument similar to that used in section (1.1).

(i) If z_1 is fixed then for large z_2, $(\alpha - k)z_2^2$ (< 0) dominates.

(ii) If z_2 is fixed then for large z_1, $-\alpha z_1^4$ (< 0) dominates.

(iii) Writing $z_1 = mz_2$, then for large z_2, $-\alpha m^4 z_2^4$ (< 0) dominates.

Hence, for large F solutions remain within the large region L as shown in Fig[1.9].

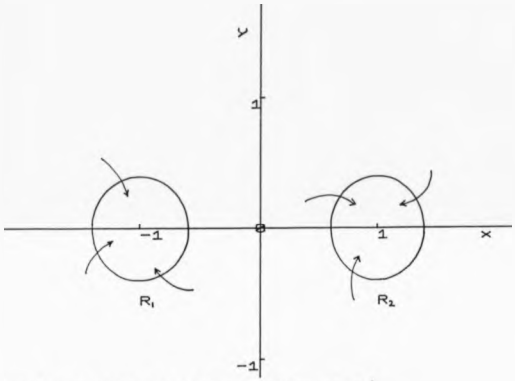

FIG[1.10] Global stability for $F \neq 0$; $k, \alpha > 0$. Small force. $F = O(\epsilon^2)$

The results of this section and section (1.1) have shown clearly that all solutions are bounded regardless of parameter values used and initial values taken. However, they do not draw attention to the fact that within these bounded regions the response can be extremely complicated. In Chapter 2 we look at the way in which the behaviour changes quite dramatically over a small range of parameter values.

CHAPTER 2

PERIOD DOUBLING BIFURCATIONS AND NON-LINEAR MAPPINGS

2.1 BEHAVIOUR IN THE (x, x') PLANE

In this section we intend to shed some light on the general behaviour of Duffing's equation given by (1.1.1) with fixed damping, k, and fixed forcing amplitude F, while the forcing frequency, ω, is varied. We shall first investigate some stable periodic solutions which appear as closed loops in the (x, x') plane. These are obtained using standard numerical techniques. We take $k^2 = 0.1$ and $F = 0.25$ throughout.

When the forcing frequency ω is large ($\omega \geq 2$ in this case) the closed-loop solutions (obtained after the transient behaviour has died away) are disposed very tightly about $x = 1$ and $x = -1$, with each response dependent upon its own region of initial conditions or domain of attraction. As ω is increased beyond $\omega = 2$ it appears that the solution of (1.1.1) can be approximated by the linear equation

$$x'' + kx' + 2x = \pm 2 + F \cos \omega t \qquad 2.1.1$$

where the original restoring function, $x - x^3$, has been

replaced by the tangent approximation $-2x \pm 2$ at $x = \pm 1$ respectively. The assumption that large forcing frequencies produce small amplitude response follows from averaging and is evident in the frequency-amplitude curve in Fig[2.2]. Equally as important is the fact that the period of the original response is $2\pi/\omega$ and is unchanged by this approximation.

As ω decreases so the solution loses its elliptic form and the amplitude increases ($F = 0.25$, $k =$ [illegible])

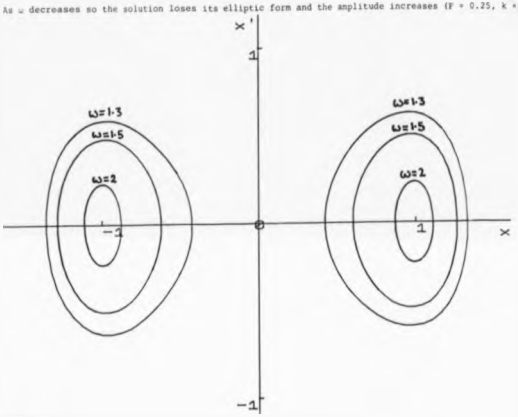

Ignoring the transient part (2.1.1) has particular solution

$$x_p(t) = \pm 1 + f_1 \operatorname{Cos} \omega t + f_2 \operatorname{Sin} \omega t \qquad (2.1.2)$$

where

$$f_1 = \frac{F(2 - \omega^2)}{(2 - \omega^2)^2 + k^2\omega^2}, \qquad f_2 = \frac{Fk\omega}{(2 - \omega^2)^2 + k^2\omega^2} \qquad (2.1.3)$$

with response in the (x, x') plane being the ellipses

$$(x \pm 1)^2 + (x'/\omega)^2 = R^2 = f_1^2 + f_2^2. \qquad (2.1.4)$$

As ω decreases over a short range of values (below $\omega = 2$) two noticeable changes occur to the elliptic closed loop. Firstly, the size increases rapidly with a corresponding increase in the amplitude response and secondly, the elliptic nature starts to disappear as the effect of the restoring force in the region $|x| < 1/\sqrt{3}$, which is fairly relaxed in comparison with its behaviour, elsewhere, comes into play. See Fig[2.1]. Furthermore, for a short while, each pair of stable solutions retains the same period $2\pi/\omega$ as that of the forcing term. We can account for the presence of the two solutions as follows.

If $x(t)$ is a steady state solution of Eqn(1.1.1) then

$$\bar{x}(t) = -x(t + \pi/\omega) \qquad (2.1.5)$$

is also a steady state solution. This can be shown by

multiplying (1.1.1) by -1, by replacing t by $t + \pi/\omega$ and by using (2.1.5).

Qualitatively, the behaviour of these closed-loop solutions are similar to the forced, damped linear ordinary differential equation given by

$$x'' + kx' + x = F \cos \omega t, \quad 0 < k^2 < 4 \qquad (2.1.6)$$

since for large ω, small oscillations occur and there is a region where the amplitude increases, as ω-decreases, attaining a maximum amplitude at $\omega^2 = 1$. As ω is reduced further so the amplitude decreases; this describes the standard frequency-amplitude curve for a forced linear ordinary differential equation. With Duffing's equation, however, this run to 'maximum-amplitude' is far from straight forward, the oscillations passing through a phase of what is termed period doubling where the period of the stable solutions increases as a power of 2 over a small range of ω-values. This leads eventually to large (possibly infinite) periodic or chaotic oscillations. This phenomenon of period doubling will be described further in section 2.2.

For the moment we turn our attention to modelling these $2\pi/\omega$-oscillations by following the method given by Jordan & Smith (1987) and write

$$x(t) = c(t) + a(t) \cos \omega t + b(t) \sin \omega t \qquad (2.1.7)$$

where the amplitudes a(t), b(t) and c(t) are slowly varying compared with Cos ωt and Sin ωt so that their

second derivatives in subsequent working may be neglected. This is the usual averaging approach used widely to find resonant solutions.

Substituting (2.1.7) into (1.1.1) and equating the coefficients of the terms containing Cos ωt and Sin ωt (known as the method of harmonic balance) and the nonoscillatory term c to zero, yields

$$ka' + 2\omega b' + Aa + k\omega b = F \qquad (2.1.8a)$$

$$-2\omega a' + kb' - k\omega a + Ab = 0 \qquad (2.1.8b)$$

$$kc' + Bc + c^3 = 0 \qquad (2.1.8c)$$

where $A = -1 - \omega^2 + \frac{3}{4}r^2 + 3c^2$

and $B = -1 + \frac{3}{2}r^2, \quad r^2 = a^2 + b^2.$

The equilibrium points of the system in the van de Pol space (a, b, c), which correspond to the steady state oscillations are obtained by equating to zero, a', b' and c' to give

$$Aa + k\omega b = F \qquad (2.1.9a)$$

$$-k\omega a + Ab = 0 \qquad (2.1.9b)$$

$$Bc + c^3 = 0. \qquad (2.1.9c)$$

From (2.1.9c) either $c = 0$, or

$$c = \pm(1 - 3r^2/2)^{\frac{1}{2}}. \qquad (2.1.10)$$

Our interest lies with the pair of solutions given by (2.1.10) where we see that the constant term is dependent upon the amplitude, r. Also a real solution in this case can only occur if

$$r^2 \leq 2/3. \tag{2.1.11}$$

Squaring and adding Eqns(2.1.9a) and (2.1.9b) we have

$$r^2\left[k^2\omega^2 + \left(-1 - \omega^2 + \frac{3}{4}r^2 + 3c^2\right)^2\right] = F^2 \tag{2.1.12}$$

which is the frequency-amplitude equation for Duffing's equation (1.1.1) for this approximation. Eliminating c in Eqns(2.1.10) and (2.1.12) we obtain the frequency-amplitude equation independent of c given by

$$r^2\left[k^2\omega^2 + \left(\omega^2 - 2 + \frac{15}{4}r^2\right)^2\right] = F^2 \tag{2.1.13}$$

Fig[2.2] shows the frequency-amplitude curve when $k^2 = 0.1$ and $F = 0.25$. The horizontal line at the top is the amplitude-constraint imposed by (2.1.11). Corresponding to certain small ω-values as many as three responses are possible; however, this is not the case in practice. The periodic states of equilibrium determined by Eqns(2.1.9) are not always realized, but are actually able to exist in practice only so long as they are stable. We now investigate the stability of the equilibrium states and find the periodic solutions which are sustained in the stable state.

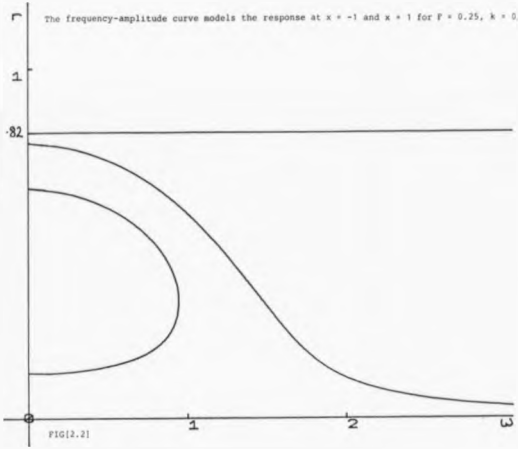

FIG[2.2]

In order to investigate the stability of a system near a chosen equilibrium point, we apply a sufficiently small disturbance to the system by changing the a's, b's and c's in Eqn(2.1.8) from their equilibrium values. If, as the time t increases indefinitely all the a's, b's and c's return to their original equilibrium values, the system is said to be asymptotically stable at this equilibrium point. On the other hand, if all or some of

the a's, b's or c's depart further from their original equilibrium values with increasing t, the system is unstable. This is the Routh-Hurwitz criterion. [See Hayashi 1964.]

Denoting the equilibrium values of Eqn(2.1.8) by a_0, b_0, c_0 we consider small variations defined by

$$\begin{aligned} a &= a_0 + \varepsilon(t) \\ b &= b_0 + \eta(t) \\ c &= c_0 + \psi(t). \end{aligned} \tag{2.1.14}$$

Substituting Eqn(2.1.14) into Eqn(2.1.8) and discarding terms of order higher than the first in ε, η and ψ, gives

$$\begin{aligned} \frac{d\varepsilon}{dt} &= a_{11}\varepsilon + a_{12}\eta + a_{13}\psi \\ \frac{d\eta}{dt} &= a_{21}\varepsilon + a_{22}\eta + a_{23}\psi \\ \frac{d\psi}{dt} &= a_{31}\varepsilon + a_{32}\eta + a_{33}\psi \end{aligned} \tag{2.1.15}$$

where

$$\begin{aligned} a_{i1} &= \partial X_1/\partial a \\ a_{i2} &= \partial X_2/\partial b \\ a_{i3} &= \partial X_3/\partial c \end{aligned} \tag{2.1.16}$$

and $X_1(a, b, c) = da/dt = 0$

$$X_2(a, b, c) = db/dt = 0 \qquad (2.1.17)$$

$X_3(a, b, c) = dc/dt = 0$

from Eqn(2.1.8).

Writing Eqn (2.1.14) in matrix form

$$E' = ME \qquad (2.1.18)$$

where $E = \begin{pmatrix} \varepsilon \\ \eta \\ \psi \end{pmatrix}$, and M the 3 × 3 coefficient matrix, we assume a solution of the form $E = se^{\lambda t}$, which, when substituted into Eqn(2.1.17) gives

$$(I\lambda - M)s = 0,$$

where I is the 3 × 3 identity matrix, and this has non-trivial solutions provided that

$$|I - M| = 0. \qquad (2.1.19)$$

Eqn(2.1.19) is called the characteristic equation and it is to the roots of this equation that we look to determine the state of the equilibrium points. When Eqn(2.1.19) is expanded, this 3rd-order determinant leads to the characteristic equation

$$A_0\lambda^3 + A_1\lambda^2 + A_2\lambda + A_3 = 0. \qquad (2.1.20)$$

If the real parts of the roots of the characteristic equation of the system are negative, the corresponding

equilibrium state is stable; if, however, at least one root has a positive real part, the equilibrium point is unstable. The Routh-Hurwitz criterion states that the real parts of the roots λ_i are negative provided that all the coefficients A_0, A_1, A_2, A_3 (of Eqn(2.1.20)) are positive and that the determinant

$$\Delta = \begin{vmatrix} A_1 & A_0 \\ A_3 & A_2 \end{vmatrix} \tag{2.1.21}$$

is positive also, that is

$$A_1A_2 - A_0A_3 > 0. \tag{2.1.22}$$

We will refer to this as Condition I.

Applying the above procedure to Eqn(2.1.8) we arrive at the cubic characteristic equation (2.1.20) where

$$A_0 = k^3 + 4\omega^2 k, \tag{2.1.23a}$$

$$A_1 = k^2([1] + [4] + [5] + 4\omega^2) + 4\omega^2[5], \tag{2.1.23b}$$

$$A_2 = k([4][5] + [1][4] + [1][5] - [3][2]) + 4k^2\omega^2[5] - 18kr_0^2c_0^2, \tag{2.1.23c}$$

$$A_3 = [1][4][5] - [2][3][5] + 18c_0^2r_0^2\left(1 + \omega^2 - \frac{3}{4}r_0^2 - 3c_0^2\right) \tag{2.1.23d}$$

and

$$[1] = -1 - \omega^2 + \frac{3}{4}r_0^2 + \frac{3}{2}a_0^2 + 3c_0^2 \qquad (2.1.24a)$$

$$[2] = k\omega + \frac{3}{2}a_0 b_0 \qquad (2.1.24b)$$

$$[3] = -k\omega + \frac{3}{2}a_0 b_0 \qquad (2.1.24c)$$

$$[4] = -1 - \omega^2 + \frac{3}{4}r_0^2 + \frac{3}{2}b_0^2 + 3c_0^2 \qquad (2.1.24d)$$

$$[5] = 3c_0^2 - 1 + \frac{3}{2}r_0^2 \qquad (2.1.24e)$$

where $r_0^2 = a_0^2 + b_0^2$.

The first requirement is for each of the coefficients A_j (j = 0, 1, 2, 3) to be positive. A_0 is positive since ω and k are both positive

(i) Setting $A_1 > 0$ gives

$$r_0^2 < \frac{(8 + 2k^2)\omega^2 + 6k^2}{12\omega^2 + 9k^2} = L. \qquad (2.1.25)$$

However, $L \geq 2/3$ and so we stay with the amplitude condition imposed by (2.1.11).

(ii) Setting $A_2 > 0$ gives

$$\frac{855}{16}r_0^4 - 54r_0^2 + (\omega^4 + k^2\omega^2 + 12) > 0 \qquad (2.1.26)$$

which is always greater than zero for all r_0, ω and k.

(iii) Setting $A_3 > 0$ gives

$$\left(\frac{3}{2}r_0^2 - 1\right)\left[k^2\omega^2 + \left(\omega^2 - 2 + \frac{15}{4}r_0^2\right)\left(\omega^2 - 2 + \frac{45}{4}r_0^2\right)\right] < 0, \qquad (2.1.27)$$

which will be referred to as Condition II and is a slight extension of the conventional condition given by $d(F^2)/dr^2 > 0$ (See Hayashi, 1964)*. The boundary curve between the stable and the unstable regions given by Condition II, shows the vertical tangency of the frequency-response curve at the stability limit.

Fig[2.3] shows computer plots of Conditions I and II drawn on the frequency-amplitude curve of Fig[2.2]. Only oscillations that are outside the shaded unstable regions occur in practice. Immediately, large amplitude solutions predicted for small forcing frequencies are removed, leaving a single solution for each frequency ω. Removing the regions of instability we are left with the discontinuous curve of Fig[2.4], which models the averaged amplitude response for each ω. Period $2\pi/\omega$ response persist for ω down to about $\omega_1 \approx 1.130$ after which period doubling occurs. At $\omega = \omega_1$, the closed-loop (stable) solutions in the (x, x') plane start to split producing multiple closed-loop (stable) $4\pi/\omega$ periodic oscillations still disposed about $x = \pm 1$. Such a response is shown in Fig[2.5]. At $\omega = \omega_1$, a bifurcation has occurred. This

---

* Since $r_0^2 < \frac{2}{3}$, we can actually write inequality (2.1.27) as

$$k^2\omega^2 + \left(\omega^2 - 2 + \frac{15}{4}r_0^2\right)\left(\omega^2 - 2 + \frac{45}{4}r_0^2\right) > 0$$

which now agrees with Hayashi's result.

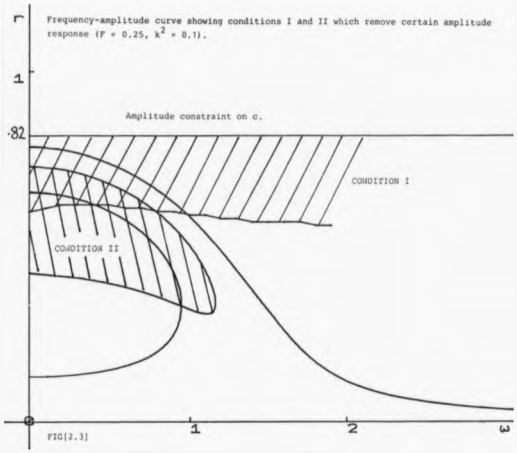

FIG[2.3]

solution type persists until a second critical frequency is reached at which point the loops split again giving off $8\pi/\omega$ periodic stable solutions - a second bifurcation has occurred. An example of such a response is shown in Fig[2.6]. This extraordinary behaviour continues over a small range of ω-values giving stable oscillations of period $16\pi/\omega$, $32\pi/\omega$ .... This phenomenon is known as period doubling. A response of period T (in this case

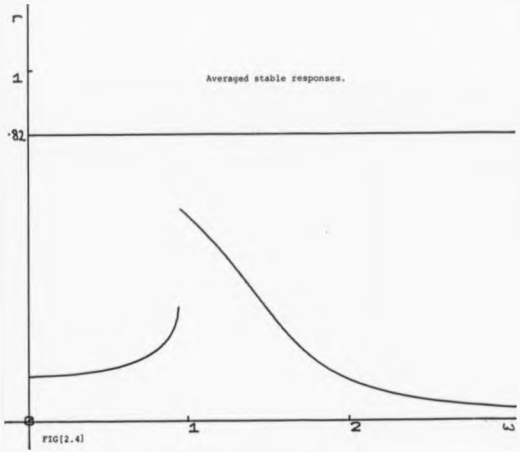

FIG[2.4]

$2\pi/\omega$) is said to have period 1. Period doubling, therefore, creates the sequence of periods 1, 2, 4, 8, 16, ..., 2^n, ... ($n \in \mathbb{Z}_0^+$). As period doubling occurs over such a small range of ω-values it soon becomes difficult numerically to find when further splitting takes place and to show high period oscillations with any degree of precision since the additional loops thrown off are very close to the previous ones. As ω is decreased

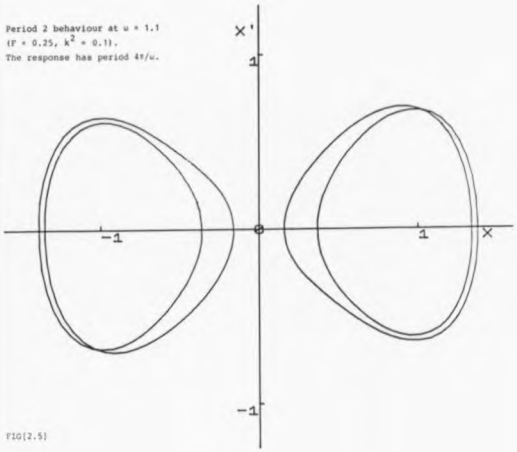

FIG(2.5)

further the sequence of period doubling bifurcations continues indefinitely ending in chaotic responses. It is believed that the bifurcation points of ω corresponding to a change of period doubling follow a Feigenbaum (1983) sequence; see section (2.3). The chaotic responses manifest themselves as a complicated mass of windings and tangles when projected onto the (x, x') plane. We know from Chapter 1 that such a solution is

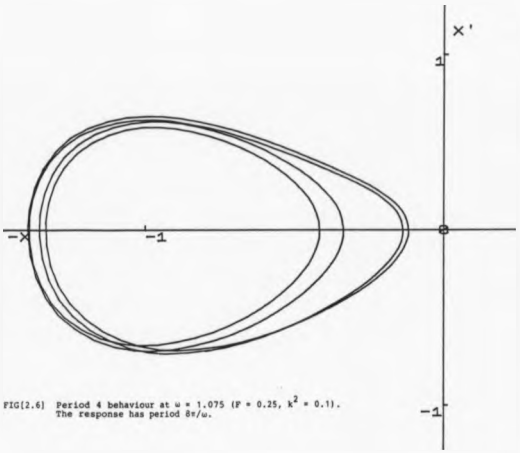

FIG[2.6] Period 4 behaviour at $\omega = 1.075$ ($F = 0.25$, $k^2 = 0.1$). The response has period $8\pi/\omega$.

bounded and what was previously two separate solutions has come together to produce a response that orbits erratically from one half plane to the other. Chapter 3 shows us that below this unpredictable behaviour lies a fascinating yet definite structure which accounts largely for the behaviour of such a system.

We can summarise the behaviour of the system as ω is varied with the help of Fig[2.7]. The number line

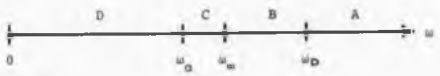

Fig[2.7]

$[0, \infty)$ for ω can be split up into four regions A, B. C and D with boundary points given by ω_D, where period doubling commences, ω_∞, where period doubling ends, and ω_a, the end of the chaotic region. In region A all solutions have period $2\pi/\omega$. In region B the progression of period doubling solutions occur which ends at ω_∞, after which in region C, most solutions are chaotic. The latter persist until at ω_a solutions of period $2\pi/\omega$ emerge and continue through to 0. Holmes (1979) uses an analogue computer to solve Duffing's equation and records the peak amplitude for F varying with the other parameters fixed. The results shown in Figure 5 of his paper display similar behaviour to that just described for varying ω. In both cases the general behaviour agrees with that of certain non-linear iteration schemes - see section (2.3).

2.2 BIFURCATIONS

What do we mean by a bifurcation? According to Holmes & Guckenheimer (1983) the term bifurcation was

originally used by Poincaré to describe the 'splitting' of equilibrium solutions in a family of differential equations. If

$$\dot{x} = F_\mu(x); \quad x \in \mathbb{R}^n, \quad \mu \in \mathbb{R} \tag{2.2.1}$$

is a system of differentiable equations depending on the single parameter μ, then the equilibrium solutions of (2.2.1) are given by the solution of the equation $F_\mu(x) = 0$. The graph of each of the solutions in the (x, μ) space is then a branch of the equilibria. The stability of an equilibrium point is determined by first linearizing locally (2.2.1) at the equilibrium point and then solving the n^{th} order polynomial characteristic equation to determine the corresponding eigenvalues. [See section (2.1).] If a solution of the characteristic equation has zero real part then we have what is termed a bifurcation point where a sudden change in behaviour occurs as the parameter, μ, passes through the critical value. In fact, the stability of the equilibrium point changes either from stable or unstable or vice-versa at a bifurcation point.

Consider the simple system

$$\dot{x} = y, \qquad \dot{y} = \mu x \tag{2.2.2}$$

containing the parameter $\mu \in (-\infty, \infty)$. It has a single equilibrium point at $x = 0$, $y = 0$ in the phase plane. We want to know how the phase paths change as the parameter μ varies. The corresponding characteristic equation

$$\lambda^2 - \mu = 0 \qquad (2.2.3)$$

has a zero real-part solution (actually $\lambda = 0$) when $\mu = 0$. The phase diagram has a centre at (0, 0) for $\mu < 0$ and a saddle at (0, 0) for $\mu > 0$. The system has a bifurcation point at $\mu = 0$, since the system is structurally unstable for this value.

It is important to add that a change in the nature of an equilibrium point and consequently the phase paths does not correspond necessarily to a bifurcation point. A transition from a stable spiral to a stable node, for example, does not signify a bifurcation point as both points are asymptotically stable. This is illustrated in the following example.

The behaviour of the system

$$\begin{aligned} \dot{x} &= x - y \\ \dot{y} &= x + \mu y \end{aligned} \qquad (2.2.4)$$

depends on the roots of the characteristic equation

$$\lambda^2 - (1 + \mu)\lambda + 1 = 0 \qquad (2.2.5)$$

which has roots

$$\lambda_{1,2} = \tfrac{1}{2}[(1 + \mu) \pm \sqrt{(\mu + 3)(\mu - 1)}].$$

For $\mu < -3$, the eigenvalues λ_1 and λ_2 both take negative real values so the equilibrium point at (0, 0) is a stable node.

For $-3 < \mu < -1$, the eigenvalues are complex with negative real parts so the equilibrium point is a stable spiral. For $-1 < \mu < 1$, the eigenvalues are complex with positive real part so the equilibrium point is an unstable spiral. For $\mu > 1$, the eigenvalues are both positive reals and the equilibrium point is an unstable node.

The only bifurcation point in this example occurs at $\mu = -1$ because at this value the change has been accompanied by a change of stability. The system is structurally unstable.

The criteria for structural stability rely upon two notions: perturbation and topological equivalence. [See Palis & de Malo (1982), Abraham & Shaw 3(1984)]. A perturbation of a vector field $V(x)$, $x \in R^n$, means the addition to it of a relatively small vector field $v(x)$. Topological equivalence of two phase portraits means there is a homeomorphism [See section (1.1)] of the phase plane or continuous 'rubber sheet' deformation, which maps one of the portraits to the other, preserving the arrows of time on each trajectory.

The two point attractors of Fig[2.8a,b] are topologically equivalent. A homeomorphism can deform one stable spiral into the other preserving the integral curves. Likewise, a homeomorphism can deform a stable spiral into a stable node. However, the point attractor of Fig[2.8c] is not topologically equivalent to the centre. A homeomorphism cannot map a spiral onto a centre.

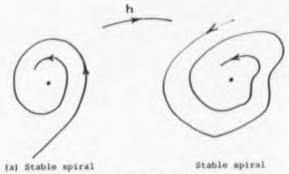

(a) Stable spiral Stable spiral

A HOMEOMORPHISM EXISTS

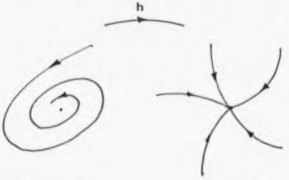

(b) Stable spiral Stable node

A HOMEOMORPHISM EXISTS

(c) Stable spiral Centre

NO HOMEOMORPHISM EXISTS

FIG[2.8]

As for the perturbation we want to know whether a phase diagram will remain qualitatively unchanged when the right-hand side of the system is slightly changed. If the output characteristics are liable to change radically, for example by the appearance of a new equilibrium point, then the system is said to be structurally unstable. The special case where a change in a parameter has such an effect, as at a bifurcation

point, involves similar considerations.

Consider the system

$$\dot{x} = -y, \qquad \dot{y} = x \tag{2.2.7}$$

whose equilibrium point (0, 0) is a centre. If we perturb the system slightly by writing

$$\dot{x} = -y + \varepsilon x, \qquad \dot{y} = x \qquad |\varepsilon| \leq 1 \tag{2.2.8}$$

then the equilibrium point, still at (0, 0) becomes an unstable spiral if $\varepsilon > 0$, and a stable spiral if $\varepsilon < 0$. The slight perturbation has shown that the system (2.2.7) is structurally unstable.

This brief section has allowed us to look into the reasons for bifurcations in the context of C^2 differentiable equations. [For an account of multiple bifurcation problems the reader is referred to the paper by Guckenheimer, 1984.] However, for a better understanding of period-doubling bifurcations (or flip-bifurcations*) we have to turn away from nonlinear flows to nonlinear maps and in particular the part the Poincaré map plays in bringing some sort of order to an otherwise chaotic response.

2.3 ONE DIMENSIONAL NONLINEAR MAPPING

Consider a real interval I and a nonlinear function f which transforms any point $x \in I$ into some point $x' \in I$.

---

* See Guckenheimer and Holmes (1983)

This is called a map of the interval

$$f : I \to I. \tag{2.3.1}$$

In general, the function f may depend on a parameter μ and we can write the one dimensional mapping in the form

$$x_{n+1} = f(\mu, x_n), \quad n = 0, 1, 2, \ldots \tag{2.3.2}$$

where f is considered sufficiently smooth. We can choose an arbitrary initial point (or 'seed') $x_0 \in I$ and generate a sequence of values by iteration. Some mappings are simple enough to be accessible to certain analytical tools and are not very time consuming in numerical study. At the same time they are rich enough to show many of the universal properties of chaotic transitions observed in higher dimensional systems particularly Duffing's equation.

In general, the property of the sequence $\{x_n, n = 0, 1, 2, \ldots\}$ depends on the function f and on the choice of x_0 and μ. Here we consider only those functions f which have only one maximum on the interval I and are referred to as unimodal mappings.

A basic equation in the analysis is to describe the behaviour of the sequence $\{x_n, n = 0, 1, 2, \ldots\}$ generated by iteration from the given initial value x_0. The sequences most commonly encountered are periodic and asymptotically periodic: x is periodic if $f^n(x) = x$ for all n, where $f^n(x)$ denotes the n^{th}-iterate of f, that is, the system reproduces itself every period or single

iteration; it is asymptotically periodic if its iterates converge to the iterates of a periodic point. Such points are called fixed points.

In addition to these fixed points characterized by

$$x = f(x) \tag{2.3.3}$$

we can also observe periodic orbits of period k, defined by k points such that

$$\begin{aligned} x_{i+1} &= f(x_i) \\ x_{i+2} &= f(f(x_i)) \equiv f^2(x_i) \\ &\cdot \\ &\cdot \\ &\cdot \\ x_{i+k} &= f^k(x_i) = x_i. \end{aligned} \tag{2.3.4}$$

The fixed point(s) of the iterations behave in the same way as equilibrium points of autonomous differential equations - some turn out to be stable and some do not. Suppose that $x = \bar{x}$ is a fixed point of the map $x_{n+1} = f(x_n)$, so that

$$\bar{x} = f(\bar{x}). \tag{2.3.5}$$

Perturb the fixed point $\bar{x}$ slightly by setting

$$x = \bar{x} + \varepsilon \tag{2.3.6}$$

so that

$$x_{n+1} = \bar{x} + \varepsilon_{n+1} = f(x_n) = f(\bar{x} + \varepsilon_n). \tag{2.3.7}$$

Assuming that f has a power series expansion around $x = \bar{x}$ we can write

$$\bar{x} + \varepsilon_{n+1} = f(\bar{x}) + f_x\varepsilon_n + \frac{1}{2}f_{xx}\varepsilon_n^2 + \frac{1}{6}f_{xxx}\varepsilon_n^3 + \ldots \tag{2.3.8}$$

where $f_x \equiv f_x(\bar{x})$, etc.

Writing the coefficients of the series as C, D, E, ... and using the equilibrium condition $\bar{x} = f(\bar{x})$, the mapping becomes

$$\varepsilon_{n+1} = C\varepsilon_n + D\varepsilon_n^2 + E\varepsilon_n^3 + \ldots. \tag{2.3.9}$$

When ε_{n+1} is small we need retain only the linear term of this expansion so that

$$\varepsilon_{n+1} = C\varepsilon_n. \tag{2.3.10}$$

Constant reapplication of this linear map gives us ε_i in terms of the initial point ε_0 as

$$\varepsilon_n = C^n\varepsilon_0. \tag{2.3.11}$$

The fixed point is, therefore, linearly stable if $-1 < C < 1$, where

$$C = f_x \equiv \frac{df}{dx}(\bar{x}) \tag{2.3.12}$$

for one dimensional mappings. Notice that C here behaves in the same way as an eigenvalue in determining the

stability of an equilibrium point in a continuous dynamical system.

An example that fits nicely into this category of mappings is given by

$$x_{n+1} = \mu \, \mathrm{Sin}(x_n), \qquad (x_n, \mu) \in [0, \pi] \tag{2.3.13}$$

where x_n is in radians. The function $f \equiv \mu \, \mathrm{Sin}(x_n)$ is unimodal, is zero at the interval end points and smooth everywhere.

It can easily be shown using a simple computer program that (2.3.13) is able to reproduce itself every single iteration and describe the behaviour of the single fixed point as having period 1, and write

$$x_{n+1} = \bar{x} = \mu \, \mathrm{Sin}(\bar{x}) \tag{2.3.14}$$

where $\bar{x}$ is the fixed point.

As μ is varied $\bar{x} = 0$ is always a fixed point but beyond a minimum value of μ a second solution is possible and we will refer to this other fixed point as $\bar{x}_1$.

For $0 < \mu < 1$, only $\bar{x} = 0$ is possible whereas for $1 < \mu < \pi$ both fixed points can occur. If we set $\mu = \pi/2$ and start at $x_0 = \pi/2$, then $x_1 = x_2 = \ldots = \pi/2$; and similarly if $x_0 = 0$, $x_1 = x_2 = \ldots = 0$. This shows that if we start at a fixed point then computing the n^{th} iterate is a trivial matter but if we start with an x_0 not a fixed point what happens then?

The easiest way to see what happens is to perform a graphical analysis. We graph $y = f(\mu, x_n)$ together with

$y = x_n$. Where the lines intersect we have

$$x_n = y = f(x_n) = \mu \, \mathrm{Sin}(x_n) \tag{2.3.15}$$

so that the intersections are the fixed points. To iterate an initial x_0 successively,

1. move vertically to the graph of $f(x_n)$
2. move horizontally to the graph of $y = x_n$, and
3. repeat steps 1 and 2 etc.

Fig[2.9] depicts this process for $\mu = 1.5$ along with the two fixed points $\bar{x} = 0$ and $\bar{x}_1 = 1.496$. Starting from any $x_0 \in (0, \pi)$ upon continued iteration x_n will converge to $\bar{x}_1 = 1.496$ no matter how close x_0 is to the fixed point $\bar{x} = 0$. All iterates diverge from the latter fixed point. The fixed point $\bar{x} = 0$ is unstable while the second fixed point $\bar{x}_1 = 1.496$ is stable or is referred to as an attractor of period 1. In this case, after the transients (terms of the sequence leading to the fixed value) have died away the existence of the attractor determines the solution independently of the initial condition x_0 provided that x_0 is within what we call the basin of attraction.

We can check on the stability of $x = 0$ and $x_1 = 1.496$ by finding C as given by (2.3.12). It turns out that

$$C(x) = \mu \, \mathrm{Cos}(x_n), \quad \mu = 1.5 \tag{2.3.16}$$

so

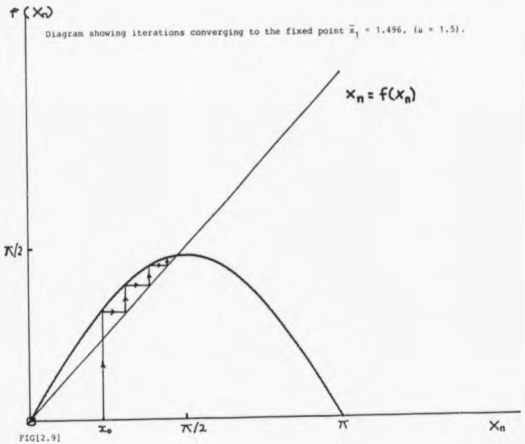

FIG[2.9]

C(0) = 1.5

and

C(1.496) = 0.1118

hence, the latter point only is stable. Fig[2.10] displays the behaviour of iterations around two fixed points. The figure shows all subsequent iterations tending towards the stable fixed point in (a), whereas in

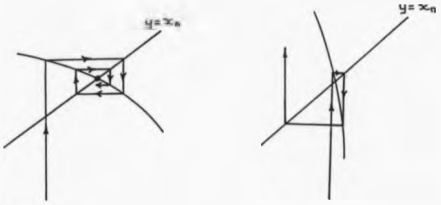

FIG[2.10]

(a) Stable fixed points
|gradient| < 1

(b) Unstable fixed point
|gradient| > 1

(b) all iterations move away from the fixed point which is unstable.

Increasing μ we find that this behaviour persists until $\mu \approx 2.2618 = \Lambda_1$ when the system undergoes period doubling. That is, instead of having a stable cycle of period 1 corresponding to one fixed point, the system has a stable cycle of period 2. It turns out that these two fixed points are fixed points of the function f^2 (f o f)

and the stability is again determined by C in (2.3.12) the slope of the f^2 function at its fixed points. Suppose that the period 2 solutions of $f \equiv \mu \text{ Sin } x$ are given by p and q. Then

$$\mu \text{ Sin } p = q$$

and

$$\mu \text{ Sin } q = p$$

hence

$$\mu \text{ Sin}(\mu \text{ Sin } p) = p$$

that is,

$$f \circ f(p) = p \quad \text{and} \quad f \circ f(q) = q$$

so that the two fixed points p and q are separately fixed points of f^2.

The graph of

$$f \circ f = f^2 = \mu \text{ Sin}(\mu \text{ Sin}(x_n)) \tag{2.3.17}$$

is shown in Fig[2.11]. Since f is symmetric about $x = \pi/2$, f^2 is also symmetric about $x = \pi/2$. It also has three turning points because f has values greater than $\pi/2$. The fixed point of f, $\bar{x}_1$, is stable up to the point where the local minimum of f^2 touches the line $y = x_n$ as μ varies. The gradient of f at this point is -1. For subsequent values of μ, the lines $y = x_n$ intersects f^2 at 3 points (excluding $\bar{x} = 0$), the middle point u being

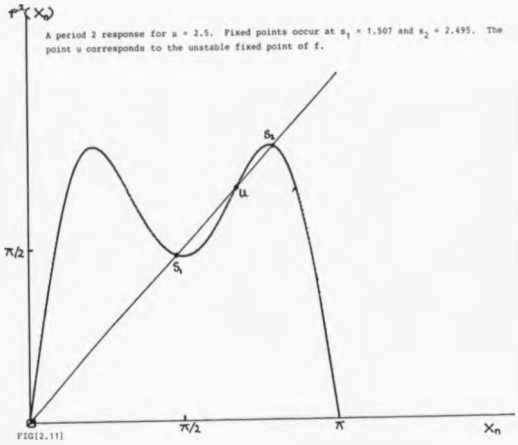

A period 2 response for $a = 2.5$. Fixed points occur at $s_1 = 1.507$ and $s_2 = 2.495$. The point u corresponds to the unstable fixed point of f.

FIG[2.11]

unstable and corresponding to the unstable fixed point of f, the other two, s_1 and s_2 are stable. Since s_1 and s_2 are not the fixed points of f, f sends one into the other:

$$s_1 = f(s_2)$$
$$s_2 = f(s_1). \qquad (2.3.18)$$

Such a pair of points is called a stable 2-cycle or

an attractor of period 2 and is the first example of period doubling as μ is increased.

It is worth mentioning that f^2 has the same slope at s_1 and s_2. Applying the function of a function rule we have

$$f^{2\prime} = f'(x_n).f'[f(x_n)]. \tag{2.3.19}$$

Therefore,

$$f^{2\prime}(s_1) = f'(s_1).f'[f(s_1)] \tag{2.3.20}$$

$$= f'(s_1).f'(s_2), \quad \text{from (2.3.18).} \tag{2.3.21}$$

Likewise

$$f^{2\prime}(s_2) = f^2(s_2).f'(s_1). \tag{2.3.22}$$

Therefore

$$f^{2\prime}(s_1) = f^{2\prime}(s_2). \tag{2.3.23}$$

Generally, if $s_1, s_2, s_3, \ldots, s_n$ is an n-cycle so that

$$s_{r+1} = f(s_r), \quad r = 1, 2, \ldots, n-1 \tag{2.3.24}$$

and

$$s_1 = f(s_n), \tag{2.3.25}$$

then each is a fixed point of f^n with identical slopes:

$$s_r = f^n(s_r), \quad r = 1, 2, \ldots, n, \tag{2.3.26}$$

and

$$f^{n\prime}(s_r) = f'(s_1)\ f'(s_2)\ \ldots\ f'(s_n). \tag{2.3.27}$$

As we increase μ further, the minimum of f^2 drops still lower so that both s_1 and s_2 have negative slopes. At $\mu = \Lambda_2 = 2.616501$ the slope at s_1 and s_2 becomes equal to -1. The same thing occurs at this stage that occurred for f at Λ_1. Each fixed point of f^2 at Λ_2 splits creating a 4-cycle or period 4 response. This is the second period doubling phase.

To resolve the period 4 behaviour into fixed points we consider the f^4 iteration which is computed from f^2 using

$$f^4 = f^2 \circ f^2. \tag{2.3.28}$$

The graph of f^4 appears in Fig[2.12] along with the four fixed points for $\mu = 2.69$. As μ increases the local maximum of f^4 at $x_n = \pi/2$ moves up developing a fixed point with negative slope. Finally at $\mu = \Lambda_3 = 2.696373$ when the slope of the fixed points is again -1, each fixed point will split into a pair giving rise to an 8-cycle or period 8 response - see Fig[2.13]. Again, using $f^8 = f^4 \circ f^4$ we follow the behaviour of the gradients of the fixed points of f^8. Then at $\mu = \Lambda_4 =$ the slope is again -1 and another period

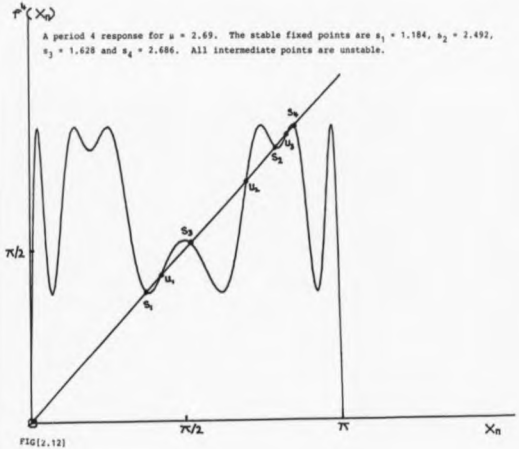

A period 4 response for $\mu = 2.69$. The stable fixed points are $s_1 = 1.184$, $s_2 = 2.492$, $s_3 = 1.628$ and $s_4 = 2.686$. All intermediate points are unstable.

FIG[2.12]

doubling occurs. Through the use of

$$f^{2^{n+1}} = f^{2n} \circ f^{2n}$$

the period doubling behaviour occurs ad infinitum over the interval $[0, \pi]$. As μ increases beyond Λ_4 the system exhibits an ordered 16, 32, 64, ... cycle at Λ_n; $n = 3, 4, 5, \ldots$.

The first few values Λ_n where a 2^n-period is born

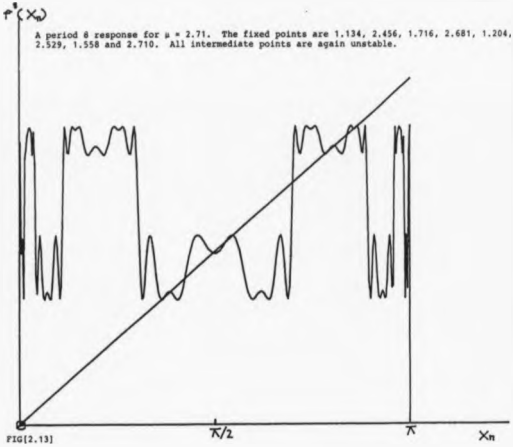

are brought together in the following table:

$\Lambda_1 = 2.261829$ $\Lambda_2 = 2.616501$

$\Lambda_3 = 2.696373$ $\Lambda_4 = 2.71416.$

According to Lauwerier (1986) it can be shown that the sequence of Λ_n's approximates to the geometric progression whose n^{th} term is given by

$$A_n \simeq A_\infty - c(F)^{-n}$$

where F, the Feigenbaum constant, is the rate of onset of complex behaviour. If we define

$$F_n = \frac{A_{n+1} - A_n}{A_{n+2} - A_{n+1}}, \quad (n = 1, 2, 3, \ldots)$$

F_n quickly approaches the constant value F. The three values of F_n, (n = 1, 2, 3) are

$F_1 = 4.4409$

$F_2 = 4.4905$

$F_3 = 4.5375$

with the limit value

$F = 4.6692016 \ldots$

c turns out to be approximately 2.417.

Feigenbaum (1983) says that this number, F, must appear as a natural rate in oscillatory-type systems and all systems exhibiting a period-doubling route to chaos. It also makes a prediction possible of A_∞ as soon as the first few period-doubling values are known. This holds for any map with a single parameter. We have using

$$A_\infty \simeq \frac{FA_{n+1} - A_n}{F - 1}$$

$= 2.71919 \quad (n = 5).$

Fig[2.14] shows a bifurcation diagram of fixed points $\bar{x}_n$ against the parameter μ, where $2 \leq \mu \leq \pi$ and μ is taken in intervals of 0.025. The start of each period doubling regime, marked Λ_1, Λ_2, ... can be clearly seen to be converging to Λ_∞.

Beyond Λ_∞ the behaviour for each μ is mostly chaotic. Once the period of transition has ended the iteration produces values that jump about in a random fashion within a bounded set. Such a set of fixed points is said to be countable infinite. This chaotic behaviour continues ad infinitum with no noticeable repetitions. When each random set of fixed points is plotted against its μ-value it appears as a straight line as in Fig[2.14].

The interval (Λ_∞, π) appears to contain largely infinite sets of unstable cycles or chaotic behaviour. These appear as straight line segments terminating in the line segment at $\mu = \pi$ which runs from $]0, \pi[$. However, μ-values do exist in this range for which stable m-cycles occur. Two such 'windows' run from $\mu = 2.7493$ to 2.7505 and from $\mu = 2.946$ to 2.974 with the latter window particularly evident in Fig[2.14]. 'Blown-up' versions of both windows appear in Fig[2.15] and Fig[2.16] respectively, the former showing a stable 10-cycle response emerging from an otherwise chaotic response and period-doubling back to chaos; the latter starts as a stable 3-cycle and behaves in a similar manner. Although not detected many such windows may exist. For similar diagrams see May (1976), (1982); Lauwerier (1986).

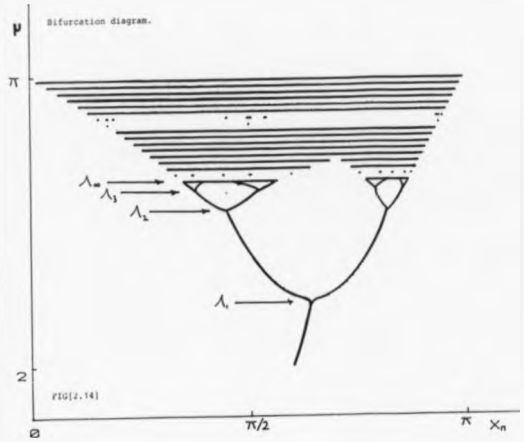

FIG[2.14]

A theorem due to Li & Yorke (1975) states quite simply that if there is a periodic point with period 3, then for each integer n = 1, 2, 3, ..., there is a periodic point with period n (the converse is not necessarily true). Furthermore, there is an uncountable subset of points $x \in I$ which are not even "asymptotically periodic". Hence, the title of their paper - 'Period three implies chaos'.

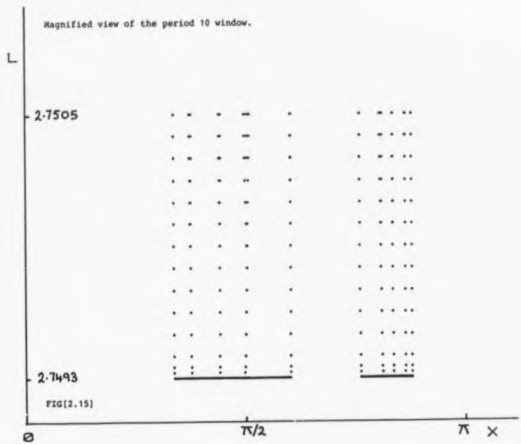

FIG[2.15]

We have seen in section (2.1) that despite the good approximation given by the frequency-amplitude equation used in determining the amplitude response of a Duffing oscillator it does not contain evidence of any period-doubling oscillations - unless it is in the form of an average amplitude result. Such a change in the behaviour of a system signifies a bifurcation and section (2.2) informed us that a bifurcation accompanies a structural

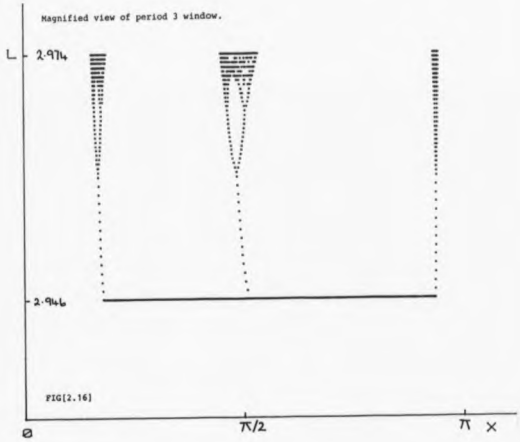

change in stability through the concepts of perturbation and topological equivalence. Such bifurcation points and 'fixed point splitting' can be a very time consuming activity and even difficult to locate with any degree of accuracy when numerical methods are employed even with the help of a computer but Feigenbaum (1983) and Henon (1976) have shown that analogies of bifurcation behaviour occur in one and two dimensional mappings respectively and that

the bifurcation to chaos has universal implications not restricted to mappings alone. Such a result aids the understanding of bifurcation to chaos in oscillatory systems.

CHAPTER 3

MANIPOLDS, HOMOCLINIC POINTS AND HORSESHOES

3.1 THE POINCARÉ MAP

For nonautonomous systems of ordinary differential equations of order 2 the diagram of solution curves when projected on to the (x, x') plane often appear as a tangle of intersecting and self-intersecting curves, since, in general, each initial state or point in the plane generates an infinite number of curves corresponding to the various initial times t_0. At first sight such a diagram appears extremely complicated with important features totally obscured. However with the aid of the so-called Poincaré map we can detect and graph underlying structure by deleting the phase paths but retaining what are commonly referred to as 'first-return' points only. To understand this transformation we follow the explanation given by Holmes & Guckenheimer, (1983) who consider the behaviour of a flow in n-space. But first, however, it is necessary to define a system of differential equations and the flow it generates.

Regard a differential equation as a system

$$\frac{dx}{dt} = \dot{x} = f(x) \qquad (3.1.1)$$

where $x = x(t) \in \mathbb{R}^n$ is a vector valued function of time t and $f : U \to \mathbb{R}^n$ is a smooth function defined on some subset $U \subseteq \mathbb{R}^n$, see for example (1.2.1). We say that the vector field f generates a flow $\phi_t : U \to \mathbb{R}^n$, where $\phi_t(x) = \phi(x, t)$ is a smooth function defined for all x in U and t in some interval $I = (a, b) \subseteq \mathbb{R}$, and ϕ satisfies (3.1.1)in the sense that

$$\frac{d}{dt}[\phi(x, t)]_{t=\tau} = f[\phi(x, \tau)] \qquad (3.1.2)$$

for all $x \in U$ and $\tau \in I$. [For flow read general solution.]

Let ψ be a periodic orbit of some flow ϕ_t in $\mathbb{R}^n$ arising from a nonlinear vector field f(x). Let Σ be a curve or cross-section such that $\Sigma \subset \mathbb{R}^n$ of dimension (n - 1), with the property that Σ cuts each phase space path transversely; that is, it is nowhere tangential to them. Denote the point where ψ intersects Σ by p, and let U be some neighbourhood of p. Then the first return or Poincaré map $P : U \to \Sigma$ for a point $q \in U$ is

$$P(q) = \phi_\tau(q), \qquad (3.1.3)$$

where $\tau = \tau(q)$ is the time taken for the orbit (particular solution) based at q to first return to Σ. Generally, τ depends upon q and need not be equal to $T = T(p)$ the period of ψ. However as q tends to p so τ tends to T.

The procedure is particularly easy to understand

for the second order autonomous system of the form

$$\dot{x} = X(x, y), \qquad \dot{y} = Y(x, y) \tag{3.1.4}$$

and its phase diagram in the (x, y) plane. Consider a point $p_0 : (x_0, y_0)$ in the cross-section Σ shown in Fig[3.1] if we follow the phase path through p_0 in its direction of flow then it next cuts Σ at $p_1 : (x_1, y_1)$.

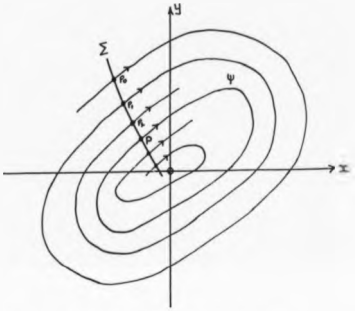

FIG[3.1] The Poincaré map for forced oscillations.

P_1 is the first return or Poincaré map of P_0. If we continue on the phase path, then the first return of P_1 is $P_2 : (x_2, y_2)$. In general terms we can say that the operator P is such that for the particular $\sum$ chosen and for every (x, y) on $\sum$,

$$P(x, y) = (x', y') \in \sum \tag{3.1.5}$$

where (x', y') is a point of first return of the path from (x, y). For successive returns starting from (x_0, y_0) we can use the notation

$$(x_2, y_2) = P(P(x_0, y_0)) = P^2(x_0, y_0); \tag{3.1.6}$$

or in general

$$(x_n, y_n) = P^n(x_0, y_0) \tag{3.1.7}$$

where n stands for the number of first-returns or Poincaré maps.

Since the system is autonomous the starting time for a sequence of first-returns is immaterial; we can for example always translate solutions to initial time $t_0 = 0$.

Fig[3.1] also shows a limit cycle and in this case successive first-returns approach the limit cycle both from outside or from the inside; a sequence of first-returns will not cross over a limit cycle. From point p : (x_0, y_0) on the limit cycle the first-returns map onto themselves, that is,

$$p = (x_0, y_0) = P(x_0, y_0) \text{ or} \tag{3.1.8}$$

$$p = (x_0, y_0) = P^n(x_0, y_0), \quad n = 1, 2, 3, \ldots. \tag{3.1.9}$$

In other words, the point p is a fixed point of P and the sequence $P_0, P_1, P_2, \ldots$ approaches the fixed point p. The same is true for a sequence of first-returns on the inside of the limit cycle. In addition, the sequence of time-lapses between returns tends towards the natural period of the limit cycle response. We would also expect the behaviour of these first returns to imply stability for the limit cycle.

As an example consider the first-returns of the autonomous system

$$\begin{aligned} \dot{x} &= y + x(1 - x^2 - y^2) \\ \dot{y} &= -x + y(1 - x^2 - y^2) \end{aligned} \tag{3.1.10}$$

for the section $\sum$ given by $x > 0$, $y = 0$ starting at $(r_0, 0)$.

Using polar co-ordinates

$$r^2 = x^2 + y^2, \qquad \text{Tan } \theta = \frac{y}{x} \tag{3.1.11}$$

and differentiating with respect to time

$$\dot{r} = \frac{x\dot{x} + y\dot{y}}{r}, \qquad \dot{\theta} = \frac{x\dot{y} - y\dot{x}}{r^2} \tag{3.1.12}$$

we find that the system reduces to

$$\dot{r} = r(1 - r^2), \qquad \dot{\theta} = -1 \tag{3.1.13}$$

with solutions

$$r(t) = (1 + r_0 e^{-2t})^{-\frac{1}{2}}, \qquad \theta(t) = -t \tag{3.1.14}$$

from which

$$x = \frac{\text{Cos } t}{(1 + r_0 e^{-2t})^{-\frac{1}{2}}}, \qquad y = \frac{-\text{Sin } t}{(1 + r_0 e^{-2t})^{-\frac{1}{2}}}. \tag{3.1.15}$$

As $t \to \infty$ so $x(t) \to \text{Cos } t$ and $y(t) \to -\text{Sin } t$, hence, the circle $x^2 + y^2 = 1$ is a limit cycle. If $r_0 > 0$, then the solution is a spiral in the phase plane, starting inside the circle and tending to the circle has a limit as t varies from $-\infty$ to ∞. If $r_0 < 0$, the spiral approaches the circle from the outside. (See Fig[3.2].)

Eliminating t between the paths, r(t) and $\theta(t)$, the paths are given by

$$r(\theta) = (1 + r_0 e^{2\theta})^{-\frac{1}{2}} \tag{3.1.16}$$

and the required successive returns on $\sum$ occur for $\theta = 0, -2\pi, -4\pi, \ldots$ with corresponding radius vector

$$\left.\begin{aligned} r_n &= (1 + r_0 e^{4\pi n})^{-\frac{1}{2}} \\ \text{and } \theta_n &= 0 \end{aligned}\right\} \quad (n = -1, -2, -3, \ldots). \tag{3.1.17}$$

As $n \to -\infty$, the sequence of points approach the fixed point p = (1, 0).

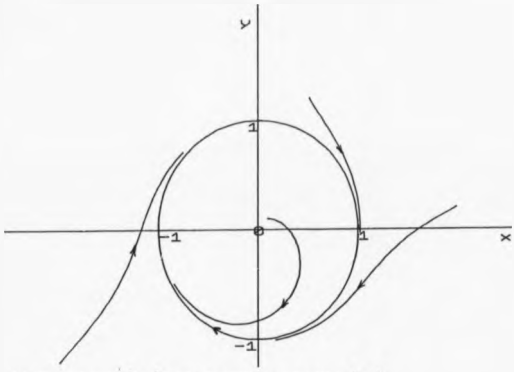

FIG[3.2] Limit cycle $x^2 + y^2 = 1$ of the equation $\dot{x} = y + x(1 - x^2 - y^2)$
$\dot{y} = -x + y(1 - x^2 - y^2)$

Unfortunately, many differential equations do not lend themselves to accessible solutions in terms of elementary functions, but require the use of numerical methods to allow investigations to take place. Although certain features of a given differential equation suggest certain types of solutions one cannot be certain that they will occur in practice particularly when nonlinear terms are present. The modern computer is an invaluable

tool, playing a significant part nowadays to aid such investigations. A search for hidden periodicities, such as subharmonics periods, is best carried out by starting with a period (usually a resonant period) in mind and then looking for solutions with this period. The method of analysis is based on the transformation theory of differential equations. This method, when combined with the use of computers, provides an effective means of finding various types of solutions, and is the method employed throughout this thesis. We apply this theory of transformation to Duffing's equation as stated in the paper by Hayashi (1969).

3.2 MANIFOLDS FOR DUFFING'S EQUATION

Equation (1.1.1) can be transformed into the system of first-order equations

$$\frac{dx}{dt} = y \quad \equiv X(x, y, t) \tag{3.2.1a}$$

$$\frac{dy}{dt} = -ky + x - x^3 + F \cos \omega t \quad \equiv Y(x, y, t) \tag{3.2.1b}$$

where the forcing term, F Cos ωt, has period $L = 2\pi/\omega$.

Let $[x(x_0, y_0, t), y(x_0, y_0, t)]$ be a solution of (3.1.2) which when $t = 0$ is at the point $P_0(x_0, y_0)$ of the (x, y) plane. We focus our attention on the location of the point P_n whose co-ordinates are

$x_n = x(x_0, y_0, nL)$, $y_n = y(x_0, y_0, nL)$, $n = 0, \pm1, \pm2, \ldots$.

Call the transformation $P_0 \rightarrow P_1$ the mapping T and write

$P_1 = TP_0$. Similarly, for successive mappings we write $P_2 = TP_1 = T^2P_0$, $P_3 = TP_2 = T^3P_0$ etc. For the inverse mapping we write $P_0 = T^{-1}P_1 = T^{-2}P_2 = \ldots$. The mapping thus defined is known as a one-to-one continuous transformation of the plane into itself.

A point in the (x, y) plane which is invariant under the mapping T is called a fixed point. If P_0 is a fixed point, then $TP_0 = P_1 = P_0$. Let m be the smallest positive integer for which $T^mP_0 = P_m = P_0$. Then P_0 will iterate periodically through a set of m distinct points and is therefore called an m-periodic point. The set of these m-periodic points is called a periodic group. A solution of Eqs(3.2.1) which lies on a fixed point at t = 0 is periodic with period L. Similarly, a solution with an m-periodic point is a subharmonic solution of period mL.

At first sight it might appear that this transformation is simply a repeat of the Poincaré map. The Poincaré map, however, does not entail any mention of time intervals but picks out intersections of a particular phase path with another curve (the so-called 'section').

The two procedures can, however, be brought together. Rewrite (3.2.1) as a system of autonomous first order equations (of one dimension higher) by putting $\theta = t$, where $\theta(0) = 0$. The new system is

$$\begin{aligned} \dot{x} &= y \\ \dot{y} &= -ky + x - x^3 + F \cos \omega\theta \qquad (3.2.2) \\ \dot{\theta} &= 1. \end{aligned}$$

The system now has the property that if θ is replaced by $\theta + 2n\pi/\omega$, n being any integer, then the system is unchanged. We can now relate a plot of calculated values of x and y at each time step $2\pi/\omega$ to a Poincaré map associated with (3.2.2) not in the (x, y, θ) space but on a torus. The space is constructed by picking out the space block

$$-\infty < x < \infty, \quad -\infty < y < \infty, \quad 0 \leq \theta \leq 2\pi/\omega$$

from the (x, y, θ) space and bending the plane $\theta = 2\pi/\omega$ round to coincide with the $\theta = 0$ plane. The torus thus formed is in 4-space. On this space, and for all time, the equations hold good and the solutions are represented by curves which wrap round the torus and, in the case of periodic solutions, wrap round it, perhaps more than once, and join up smoothly. Other solutions wrap round the torus tending towards the periodic limit cycle.

By marking the isolated values of x(t) and y(t) at times $t = 0, 2\pi/\omega, 4\pi/\omega, \ldots$ these are the intersections of the solution curves in the new 4-space with the plane (the 'section') $\theta = 0$, and this then constitutes a Poincaré map.

Application then of the Poincaré map to a periodically forced system is relatively straight forward both to compute and display graphically. A step-by-step numerical solution of the system (autonomous or not) is organised to print out a result at the end of every period with the points normally displayed on continuous

linking curves with the direction of movement indicated. The procedure can be thought of in terms of a stroboscope which illuminates the representative point once in every cycle. [See Abraham & Shaw Book 1.] Clearly a fixed point for the Poincaré map has the same stability as its corresponding oscillation and we look to the Poincaré map to behave as a phase (map) diagram as opposed to a phase (flow) diagram.

Consider the Poincaré map $P : \sum \to \sum$ as defined in the previous section, where P depends on the parameters F, k and ω of the Duffing equation (1.1.1). Here we shall fix F and k and vary ω. We concentrate our attentions on $W^s(s)$ and $W^u(s)$, the stable and unstable manifolds which enter and leave the hyperbolic saddle point S, see section (1.1). When F = 0, the manifolds become the separatices of the unforced system with unstable equilibrium point at (0, 0), (see Chapter 1, Fig[1.8]).

Generally, one would not use a Poincaré mapping to plot a Duffing separatrix but it helps here to explain the general procedure. On applying the Poincaré map to the unforced equation it is first necessary to linearise locally about the equilibrium point (0, 0). This gives the linear differential equation

$$x'' + kx' - x = 0. \qquad (3.2.3)$$

It was shown in Chapter 1, section (1.1), that this equation has two eigenvectors $x' - \lambda_1 x = 0$, $x' - \lambda_2 x = 0$

which are the unstable and stable manifolds respectively and that locally these can be used to approximate $W^u(s)$ and $W^s(s)$. Armed with this knowledge one can choose initial values on either of the unstable or stable manifolds, close to the equilibrium point and plot their first returns (in the case of the unforced equation any time period is acceptable). All forward time first-returns started on $x' - \lambda_1 x = 0$ will map out the unstable manifold $W^u(s)$, while reversed time first-returns on $x' - \lambda_2 x = 0$ will map out the stable manifold $W^s(s)$. Other solutions not starting on either manifold have first-returns that tend ultimately (as $W^u(s)$) to one of the two stable equilibrium points at (-1, 0) or (1, 0). Locally, the manifolds are at right-angles to each other at (0, 0).

When the forcing term is present ($F \neq 0$) the manifolds are computed in exactly the same way by first linearising locally about the equilibrium point of the unstable response, marked S in Fig[3.3]. This time we consider the equation

$$x'' + kx' - x = F \cos \omega t \qquad (3.2.4)$$

whose solution allows us to determine the local manifolds at the equilibrium point given by $S = (f_1, \omega f_2)$ where

$$f_1 = \frac{-F(1 + \omega^2)}{(1 + \omega^2)^2 + k^2\omega^2} \qquad (3.2.5a)$$

and

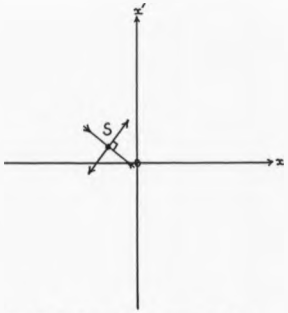

FIG[3.3] Local eigenline approximation of the manifolds close to the saddle point S.

$$f_2 = \frac{Fk\omega}{(1 + \omega^2)^2 + k^2\omega^2}. \qquad (3.2.5b)$$

The unstable manifold is approximated by

$$x' = m_1 x + \omega f_2 - m_1 f_1, \qquad (3.2.6)$$

and the stable manifold by

$$x' = m_2 x + \omega f_2 - m_2 f_1, \qquad (3.2.7)$$

and correspond to the eigenvectors of (3.2.4). Fig[3.3] shows how the manifolds behave at the unstable equilibrium point S.

Returning to the full Duffing's equation Poincaré points on each manifold are then obtained as before by plotting $2\pi/\omega$ first-returns from initial points on these straight-line segments close to the equilibrium point S.

The manifolds have been computed for the cases $\omega = 1.3$, 1.2, 1.0967 (the significance of this value will be stated later) and $\omega = 1$ (with $F = 0.25$ and $k^2 = 0.1$ throughout), and their graphs displayed in Fig[3.4]. In Fig[3.4a], the unstable manifolds SA and SB approach fixed points on the stable periodic solution; the fixed points u and v correspond to the oscillations in Fig[2.1].

Unlike the manifolds of the unforced case both sets of manifolds are drawn in sharply alongside manifolds from the saddle point as ω is reduced, see Fig[3.4a,b]. Eventually, the 'spikes' of the manifolds touch tangentially the manifolds of S; simultaneously, the main branches of the stable and unstable manifolds also touch tangentially away from S at points marked H_1 and H_2 in Fig[3.4c,d]. It is explained in the next section why the occurrence of such tangential point or homoclinic points marks the set of an infinite number of such points and in consequence the unstable manifolds no longer approach any other fixed point, and a bifurcation must therefore take place for some value of ω. It occurs when homoclinic tangency first appears between the manifold at about

$\omega = 1.0967$. This phenomena is known as homoclinic bifurcation. Even though the unstable manifolds break away from the fixed point at the onset of tangency the fixed points remain. As ω is decreased further so the stable manifold intersect the unstable manifolds and the 'spiked' parts continue to push forward following the general curvature of the unstable manifolds. In Fig[3.4e] we see how the 'lower' stable manifold turns back on itself and pushes through the tangle of unstable curves before turning round and back again. The manifold behaviour at this point is becoming complex. (See Jordan & Smith (1987), Holmes (1979), Guckenheimer & Holmes (1983), Greenspan & Holmes (1982) for further manifold diagrams.)

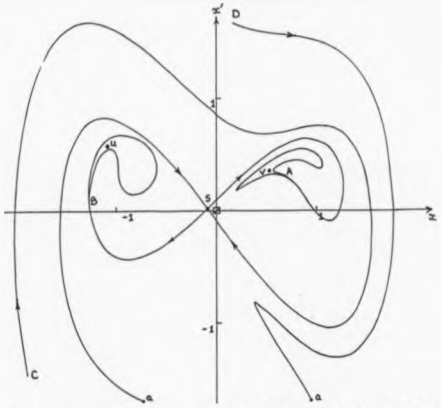

FIG[3.4a] Poincaré map showing invariant manifolds of the saddle point s for $F = 0.25$, $\omega = 1.3$, $k^2 = 0.1$. u and v are the fixed points of the stable $2\pi/\omega$-periodic solutions.

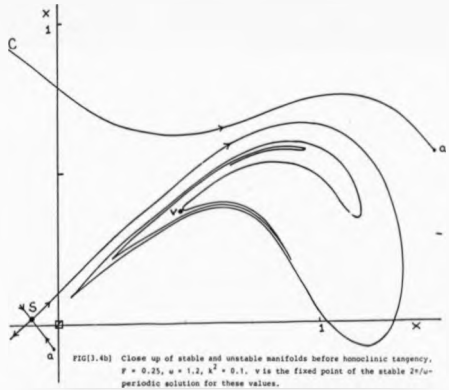

FIG[3.4b] Close up of stable and unstable manifolds before homoclinic tangency. $F = 0.25$, $\omega = 1.2$, $k^2 = 0.1$. v is the fixed point of the stable $2\pi/\omega$-periodic solution for these values.

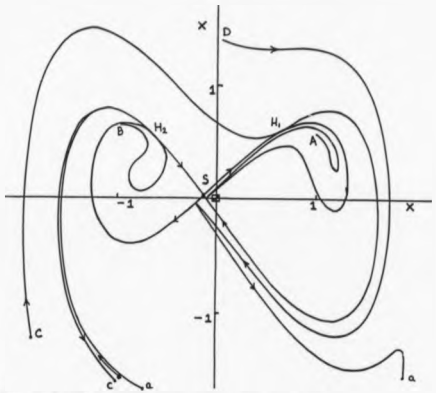

FIG[3.4c] Poincaré map revealing homoclinic points of tangency H_1 and H_2 and the complicated nature of the invariant manifolds. $F = 0.25$, $\omega = 1.0947$, $k^2 = 0.1$.

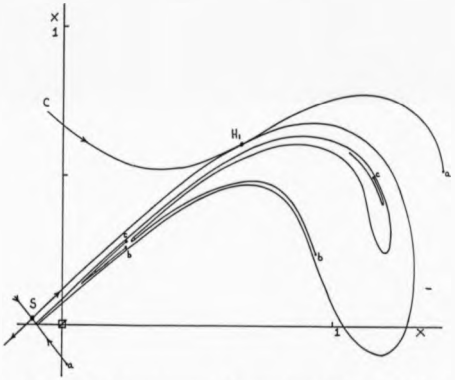

FIG[3.4d] Close up of the manifold behaviour when homoclinic tangency occurs, $F = 0.25$, $\omega = 1.0967$, $k^2 = 0.1$.

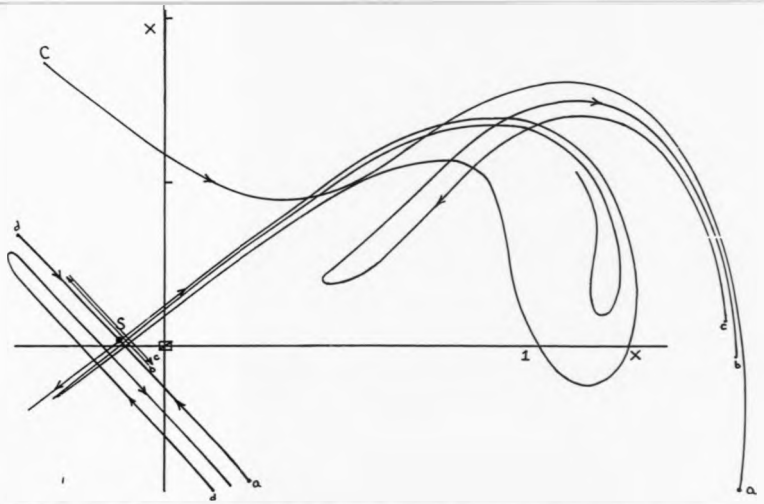

FIG[3.4a] Complex behaviour of the manifolds as the right hand stable manifold turns and runs back inside (b, c) cutting the unstable manifold before running out again.

3.3 MEL'NIKOV'S METHOD

In Fig[3.4] we saw that the unstable and stable manifolds intersect tangentially at a (infinite) number of homoclinic points. Mel'nikov (1963) produced a perturbation method for establishing a relationship between the parameter values of the differential equation to show when homoclinic tangency occurs.

To apply the method of Mel'nikov we first write Duffing's equation as a perturbation of a Hamiltonian system which possesses a 'saddle connection' in this case the four seperatrices leaving and entering the saddle point, which form the two loops of the unforced case, F = 0. See Fig[1.5]. We then have

$$\dot{x} = y \tag{3.3.1a}$$

$$\dot{y} = x - x^3 + \varepsilon(f \cos \omega t - k_0 y) \tag{3.3.1b}$$

where $\varepsilon k_0 = k$, $\varepsilon f = F$ and $\varepsilon \ll 1$.

The structure of the Poincaré map, P, (Holmes (1979)), is easily found for the trivial case $\varepsilon = 0$. P possesses three fixed points at (0, 0) and (±1, 0) and the saddle seperatrix become the stable and unstable manifolds W^S and W^U. The structure of these manifolds play an important part in determining the nature of solutions. In the trivial case, the manifolds are

structurally unstable and split in one of three ways as the parameter values change. The three possibilities are: (a) each loop splits so that the unstable manifold W^u passes 'outside' the stable manifold W^s; (b) W^u passes 'inside' W^s or (c) W^u and W^s meet transversely (at homoclinic points). The last case can only occur in the case of nonautonomous systems, see Fig[3.5]. Since W^s

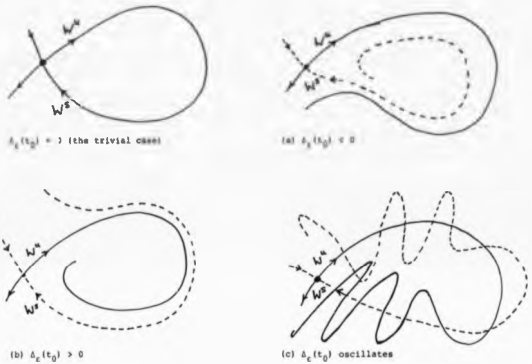

$\Delta_c(t_0) = 0$ (the trivial case)

(a) $\Delta_c(t_0) < 0$

(b) $\Delta_c(t_0) > 0$

(c) $\Delta_c(t_0)$ oscillates

FIG[3.5]

and W^u are invariant under the Poincaré map the existence of one intersection implies the existence of infinitely many.

Fig[3.6] shows that if q is an homoclinic point then by definition it is on both manifolds. Let the first return of q on W^u be $P^u(q)$. Let the first return of q on W^s be $P^s(q)$. By the uniqueness of solution of

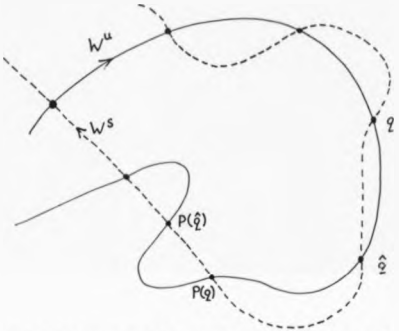

FIG[3.6] The existence of one homoclinic point implies the existence of infinitely many.

the differential equation it implies that $P^U(q) = P^S(q) = P(q)$, since if this were not the case there would exist two distinct solutions from q at time $t = 0$. Hence, the first return of an homoclinic point is another homoclinic point, and this behaviour occurs indefinitely. In the figure the homoclinic points start as a dense, yet countable set leaving the saddle point S along W^U terminating with yet another dense, countable set entering S along W^S. Such sets are accompanied by violent windings of the unstable manifolds: Holmes (1979) tells us that as the Poincaré map is orientation preserving so we can expect an homoclinic point $\bar{q}$ to occur between the intersections q and P(q) and so on.

The presence of homoclinic points does not signify a structure change alone but also signifies the existence of saddle connections. A saddle connection is a solution curve in the (x, x') plane that leaves the saddle point at $t = -\infty$ and returns to the saddle point as $t \to \infty$. In practice such solutions are not easily found due to the unstable nature of the saddle point. However, Chapter 5 is devoted to finding such curves using a new equation obtained from a co-ordinate transformation of Duffing's equation.

Returning to Mel'nikov's method he showed how a function $\Delta_\varepsilon(t_0)$ could be derived for systems of the form

$$\begin{aligned} \dot{x} &= p_0(x, y) + \varepsilon p_1(x, y, \omega t, \varepsilon) \\ \dot{y} &= q_0(x, y) + \varepsilon q_1(x, y, \omega t, \varepsilon) \end{aligned} \qquad (3.3.2)$$

so that the value of $\Delta_\varepsilon(t_0)$ determines the structure of W^u and W^s, see Fig[3.5]. In particular, if $\Delta_\varepsilon(t_0) < 0$ we have case (a); if $\Delta_\varepsilon(t_0) > 0$, we have case (b). If $\Delta_\varepsilon(t_0)$ oscillates and takes both positive and negative values then case (c) occurs. (If $\Delta_\varepsilon(t_0) = 0$, we have the trivial case associated with $F = 0$.)

According to Mel'nikov we can write

$$\Delta_\varepsilon(t_0) = -q_0(x_0, y_0)\{x_\varepsilon^+(t_0, \omega, t_0) - x_\varepsilon^-(t_0, \omega, t_0)\} + p_0(x_0, y_0)\{y_\varepsilon^+(t_0, \omega, t_0) - y_\varepsilon^-(t_0, \omega, t_0)\}. \tag{3.3.3}$$

The point (x_0, y_0) is chosen to lie on the separatrix of the unforced system with $(x_0, y_0) \neq (0, 0)$ and $x_\varepsilon^\pm(t, \omega, t_0)$, $y_\varepsilon^\pm(t, \omega, t_0)$ denote the solution curves of the perturbed ($\varepsilon \neq 0$) system at the points $(x_\varepsilon^\pm(t_0, \omega, t_0), y_\varepsilon^\pm(t_0, \omega, t_0))$ at time t_0 and tending to $(0, 0)$ as $t \to \pm\infty$ respectively. $(x_\varepsilon^\pm(t_0, \omega, t_0), y_\varepsilon^\pm(t_0, \omega, t_0))$ lie on the normal of the unforced seperatrix passing through $(0, 0)$.

Mel'nikov defines $\Delta_\varepsilon(t_0) = r \times P_+P_-$ where P_+P_- is the distance between the two branches of the seperatrix of the unperturbed system. P_+ and P_- lie on the normal to the seperatrix at $P = (x_0, y_0)$. r is the tangent vector at P. Fig[3.7] shows the coordinates of points P_+ and P_-.

Start by finding P_+P_-. From ΔRP^+P^-

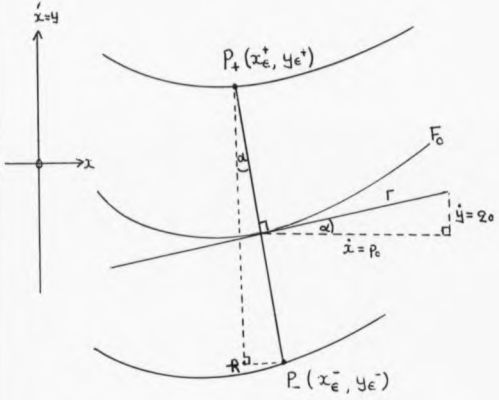

FIG[3.7]

$$\text{Sin } \alpha = \frac{x_\epsilon^- - x_\epsilon^+}{P^+P^-}$$

$$\text{so } P^+P^- = \frac{x_\epsilon^- - x_\epsilon^+}{\text{Sin } \alpha}$$

$$= \frac{r(x_\epsilon^- - x_\epsilon^+)}{q_0}$$

therefore, $\Delta_\varepsilon(t_0) = r \times P^+P^- = r^2\dfrac{(x_\varepsilon^- - x_\varepsilon^+)}{q_0}$

$$= \frac{(q_0^2 + p_0^2)(x_\varepsilon^- - x_\varepsilon^+)}{q_0}. \qquad (3.3.4)$$

From the two similar triangles RP^+P^- and PAB

$$\text{Tan } \alpha = \frac{q_0}{p_0} = \frac{x_\varepsilon^- - x_\varepsilon^+}{y_\varepsilon^+ - y_\varepsilon^-}$$

$$p_0 = \frac{q_0(y_\varepsilon^+ - y_\varepsilon^-)}{(x_\varepsilon^- - x_\varepsilon^+)}$$

and (3.3.4) becomes

$$\Delta_\varepsilon(t_0) = -q_0(x_\varepsilon^+ - x_\varepsilon^-) + p_0(y_\varepsilon^+ - y_\varepsilon^-).$$

Mel'nikov shows using the previous result how $\Delta_\varepsilon(t_0)$ can be constructed as a power series in ε,

$$\Delta_\varepsilon(t_0) = \sum_{n=1} \Delta^n(t_0)\varepsilon^n.$$

For small ε only the first term is necessary and is given by

$$\Delta^1(t_0) = \int_{-\infty}^{\infty} p_1(x_0(t - t_0),\ y_0(t - t_0)).$$

$$q_0(x_0(t - t_0),\ y_0(t - t_0))$$

$$- q_1(x_0(t - t_0),\ y_0(t - t_0)).$$

$$p_0(x_0(t - t_0),\ y_0(t - t_0))$$

$$\times \exp\left| -\int_0^{t-t_0} \left\{ \frac{\partial p_0}{\partial x}(x_0(s),\ y_0(s)) \right.\right.$$

$$\left.\left. + \frac{\partial q_0}{\partial y}(x_0(s) + y_0(s)) \right\} ds \right| dt, \qquad (3.3.6)$$

where $(x_0(t - t_0),\ y_0(t - t_0))$ denotes the solution of the unperturbed system starting at $(x_0(0),\ y_0(0))$.

From (3.3.1) $p_0 = y$, $p_1 = 0$, $q_0 = x - x^3$, $q_1 = f \cos \omega t - k_0 y$ and on substitution into (3.3.6) it turns out that [See Appendix A]

$$\Delta^1(t_0) = \frac{4}{3}k_0 - f\pi\omega\sqrt{2}\ \mathrm{Sech}(\pi\omega/2)\ \sin(\omega t_0). \qquad (3.3.7)$$

From (3.3.7) we infer that a homoclinic point occurs when $\Delta^1(t_0) = 0$, or

$$\sin(\omega t_0) = 4k_0 \cosh(\pi\omega/2)/3\sqrt{2}f\pi\omega < 1. \qquad (3.3.8)$$

Single solutions occur when $t_0 = (4n - 3)\pi/2\omega$ $(n = 0, \pm 1, \pm 2, \ldots)$ hence

$$F = \frac{2\sqrt{2}k}{3\pi\omega} \cosh(\pi\omega/2) \qquad (3.3.9)$$

in terms of the original parameters.

Fig[3.8] displays the result of plotting F against

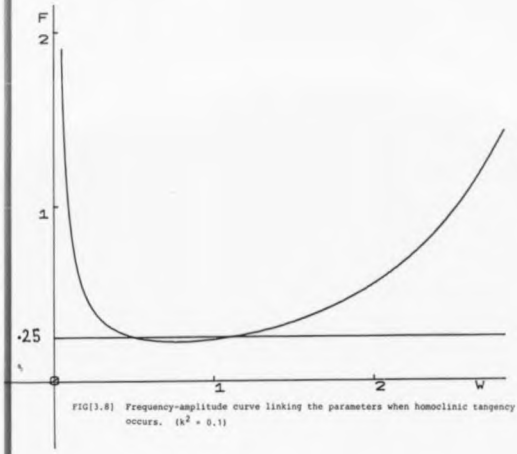

FIG[3.8] Frequency-amplitude curve linking the parameters when homoclinic tangency occurs. ($k^2 = 0.1$)

ω and although it is considerably easier to determine F given ω we concentrate on finding ω when $F = 0.25$ and $k^2 = 0.1$. ω turns out to be 0.5059 or 1.0967, but our interest lies only with the latter value, which was used to produce Fig[3.4c,d]. Holmes (1979) shows that the predicted value of F, using (3.3.9) turns out to be very close to that obtained using Poincaré plots.

3.4 THE HORSESHOE MAP

In practice it is impossible to show the multitude of complex windings that result from homoclinic points of intersection. The windings become so compressed against each other to be practically indistinguishable. In Fig[3.6] there is no suggestion in this simplified view that it is possible for the unstable manifold to

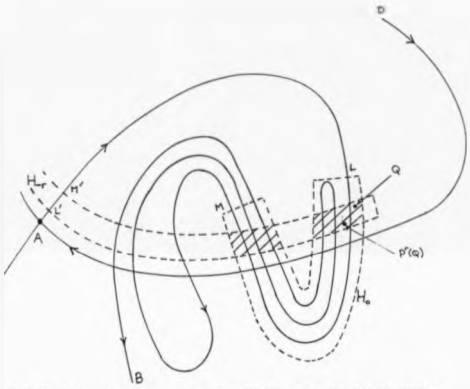

FIG[3.9] The horseshop map reveals further windings of the manifolds and possible periodic solutions if $P^r(Q) = Q$.

backtrack on itself and intersect the stable manifold between the two previous intersections; nor that this can happen an infinite number of times, see also results by Jordan & Smith (1987), Holmes & Gruckenheimer (1983), Greenspan & Holmes (1983), Ueda (1980).

To understand this behaviour choose a segment of the first loop of the unstable manifold between two points L and M on AB as shown in Fig[3.9]. L and M must be chosen to be on the same side of AD. Let H_0 consist of a set of initial points lying close to the segment LM in the form of a horseshoe crossed twice by the stable manifold AD.

Now consider mappings of the horseshoe generated by P. Let H_0 be mapped by P, P^2, P^3, ..., P^r into H_1, H_2, H_3, ..., H_r; or backwards by P^{-1}, P^{-2}, ..., P^{-r} into H_{-1}, H_{-2}, ..., H_{-r}. The latter sets would appear as rectangles that are compressed and stretched as they map back towards the saddle point at A in Fig[3.9]. Eventually, for some r, the set $P^{-r}(H_0)$, or H_{-r}, will fall into a narrow strip which overlaps the horseshoe as shown in Fig[3.9] where LM maps into L'M'. The intersections are shown shaded. Choose a point $q \in H_0$ such that $P^{-r}(q) = Q \in H_{-r} \cap H_0$, then $P^r(Q) = P^r(P^{-r}(q)) = q \in H^r$. But $q \in H_0$, hence H_0 and H_r have the point q in common and so H_0 and H_r also intersect implying that the loop of the unstable manifold which is contained in H_r is carried along with it into the neighbourhood of LM. The picture that emerges is

illustrated in Fig[3.9] for the case r = 1. If we next choose a point $q \in H_0 \cap H_{-r}$ such that $P^{-r}(q) = Q \in H_0 \cap H_{-r}$ then as before $P^r(Q) = q \in H_r \cap H_0 \cap H_{-r}$ and $P^{2r}(Q) = P^r(q)$. Now $q = P^{-r}(\bar{q})$ where $\bar{q} \in H_0$, hence $P^{2r}(Q) = \bar{\bar{q}} \in H_0$ with the result that another loop has to interlace between the existing paths. There also exists the possibility of $P^r(Q) = Q$ giving rise to period r solutions. (See Abraham & Shaw 3, 1984.)

As ω decreases the fixed points of the period doubling solutions are limit points for initial values which are not on either the stable or unstable manifolds. The increasing complexity of both branches of the unstable manifolds means that the first-returns of solutions of the differential equation rapidly become trapped inside the unstable manifolds and thereafter approach a limit set which lies on the unstable manifold. The limit set in the chaotic region, see Fig[3.10] is called a strange attractor where it would appear that under Poincaré first returns points wander aimlessly within a bounded region. For examples of strange attractors see Seydel (1985), Jordan & Smith (1987), Holmes (1979), Guckenheimer & Holmes (1983). For further work on strange attractors see Ruelle (1980), Shaw (1980).

The mechanism which creates the attracting set of the strange attractor can be explained in a general way by analysing the repeated effect of the horseshoe map described earlier by following the method outlined in

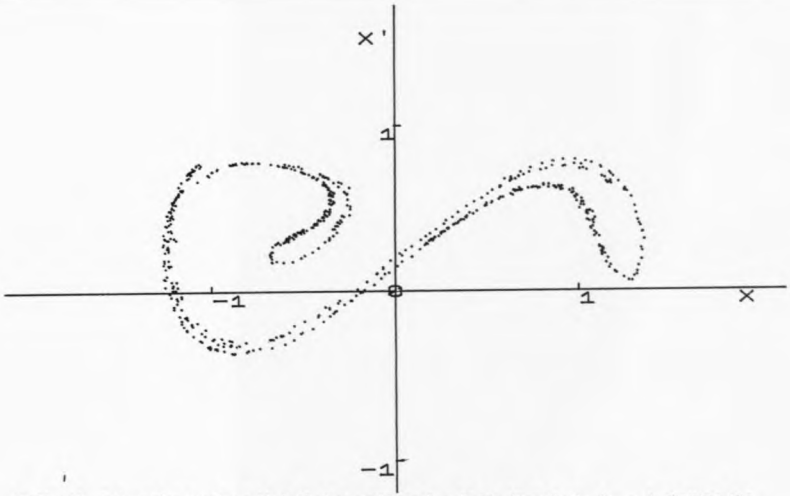

Fig[3.10] Poincaré map of eqn(1.1.1) for sections $t = 2n\pi/\omega$ ($n = 0, 1, 2, \ldots$) showing the strange attractor for a single orbit when $F = 0.4$, $\omega = 1$.

Jordan & Smith (1987). The procedure models the general behaviour of iterated points that fall into the region of overlap shown shaded in Fig[3.9].

Assume that the 'rectangular strip' through L'M' (in Fig[3.9]) is replaced by a square ABCD and that a homoclinic bifurcation causes the square to be mapped into a horseshoe A'B'C'D' by the operator P of first-returns. The mapping behaves this way: the square is stretched in the direction AD and compressed in the direction AB, bent over in the form of a horseshoe, and placed back over the original square and the process is repeated; see Fig[3.11]. We are interested, at each stage, in the parts of the codomain which are shared by the regions from which they are mapped. Fig[3.12] shows the results after two mappings. The two vertical strips u' and v' are those points of the original square that remain within the square after the first mapping being mapped originally from the horizontal strips labelled u and v. The four smaller squares contain those points belonging to u and v which are shared with u' and v'. The second iteration results in the two vertical strips u' and v' being mapped onto the pair of thinner horseshoes with the shared region this time being the intersection of the two thinner horseshoes and two pairs of horizontal strips contained in u and v. Hence, a second mapping produces 16 squares, a third mapping 64 squares and so on. The limit set, as the number of mappings tends to infinity, is very much like a Cantor set since a Cantor

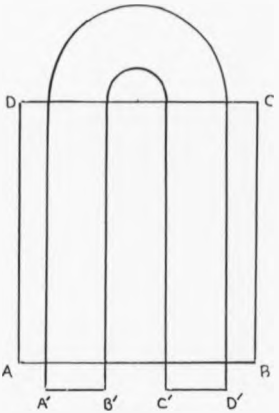

FIG[3.11] Horseshoe map.

set can be formed in a similar way. The Cantor process goes as follows: First take a line segment, at 1; see Fig[3.13]. Then remove a smaller segment from within, making a gap, as in 2. Repeat the surgery on each of the two remaining segments, obtaining 3, and continue forever. If at each step you take away the middle third of a segment, this is the middle third process. The limit set of this process is a Cantor set, and the set is

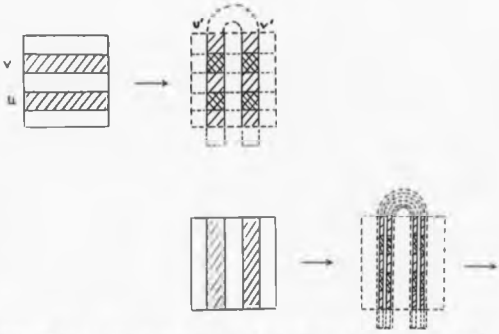

FIG[3.12] Successive horseshoe maps generating Cantor type set. Sections similarly shaded correspond under the mapping.

uncountable. The limit set of the horseshoe map has a similar structure but of course it is a two dimensional structure. There exists, therefore, an uncountable number of points in the initial square, which, when treated as initial states at t = 0 for iterated first returns, lead ultimately to endless repeated plots of a certain set of points - the limit set - which constitutes the strange attractor. The associated oscillations will

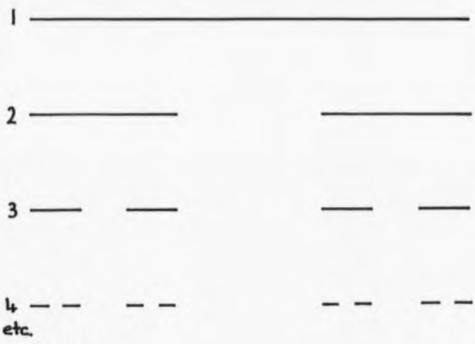

Fig[3.13]

include both periodic and non-periodic motions. The elements of this set are distributed on the unstable manifold since horseshoes can be constructed for each loop across the stable manifold. For further information on homoclinic bifurcation and horseshoes see Holmes & Guckenheimer (1983), and Holmes & Whitley (1983).

CHAPTER 4

A PIECEWISE LINEAR SYSTEM

4.1 THE MODEL PROBLEM

Mel'nikov's method for perturbed Hamiltonian systems provides us with a perturbation method for determining parameter values for which homoclinic tangency and consequently homoclinic bifurcation occur. The method also allows us to estimate to zero order the co-ordinates in the phase plane of the points of homoclinic tangency. If these co-ordinates were known then it would be a simple matter to obtain (numerically) the so-called saddle-connections; those solutions which leave the unstable saddle point only to enter it again at some later time and remain there for all time. In practice it would amount to starting the solutions with initial values given by the homoclinic point at time $t = 0$ (or any integer multiple of the period of the forcing term) and plotting the solutions both forward and backward in time. Such solutions of Duffing's equation are taken up in further detail in Chapter 5.

The construction of a model problem that exhibits such behaviour without the need to resort to perturbation methods or heavy analysis clearly provides us with the

means of understanding better those systems, such as Duffing's equation, where analytical processes are practically impossible. This has been achieved by taking as our model a simple first order piece-wise linear differential equation whose homoclinic points and manifolds are accessible to analysis.

Consider the system

$$\left.\begin{aligned} x' &= -cx + (1 + c)(y - 1) \\ y' &= -bx - b + F \cos \omega t \end{aligned}\right\} \quad x < y - 1 \qquad \text{(Region RI)}$$

$$x' = x, \qquad y' = -by + F \cos \omega t \qquad y-1 \leq x \leq y+1 \qquad \text{(Region RII)}$$

$$\left.\begin{aligned} x' &= -cx + (1 + c)(y + 1) \\ y' &= -bx + b + F \cos \omega t \end{aligned}\right\} \quad x > y + 1 \qquad \text{(Region RIII)} \qquad (4.1.1)$$

$c > 0$, $\omega \neq 0$.

Since x' and y' are uncoupled in RII it makes it considerably easier to find x and y and to deal with them subsequently. The solution in RII is given by

$$x = A_0 e^{t} \qquad (4.1.2a)$$

$$y = B_0 e^{-bt} + F^* b \cos \omega t + F^* \omega \sin \omega t \qquad (4.1.2b)$$

where $F^* = F/(\omega^2 + b^2)$ and A_0, B_0 are constants of integration.

Let $x(0) = x_0$ and $y(0) = y_0$, where $(x_0, y_0) \in$ RII . Then

$$x = x_0 e^{t} \tag{4.1.3a}$$

$$y = (y_0 - F^*b)e^{-bt} + F^*b \cos \omega t + F^*\omega \sin \omega t. \tag{4.1.3b}$$

The system has a periodic solution given by $x = 0$, $y = F^*b \cos \omega t + F^*\omega \sin \omega t$ if $x_0 = 0$, $y_0 = F^*b$ provided $|F^*\sqrt{\omega^2 + b^2}| < 1$. It's fixed point is $S = (0, F^*b)$ which is a saddle point. The stable manifold is given by $x_0 = 0$ and the unstable manifold by $y_0 = bF^*$, provided that $|x - y| \leq 1$ at all points on a solution starting at $(0, y_0)$ for $t \geq 0$, and at all points on a solution starting at (x_0, bF^*) for $t \geq 0$. These conditions require that

$$|(y_0 - F^*b)e^{-bt} + F^*b \cos \omega t + F^*\omega \sin \omega t| \leq 1 \tag{4.1.4}$$

for all $t \geq 0$, and

$$|x_0 e^{t} - F^*b \cos \omega t - F^*\omega \sin \omega t| \leq 1 \tag{4.1.5}$$

for all $t \leq 0$.

The behaviour of the stable and unstable manifolds in RII are displayed in Fig[4.1] where the point A has co-ordinates $(1 + F^*b, F^*b)$.

In RIII, where $x < y + 1$, the equations can be written

$$\begin{aligned} x' &= -cx + (1 + c)y + (1 + c) \\ y' &= -bx + b + F \cos \omega t \end{aligned} \tag{4.1.6}$$

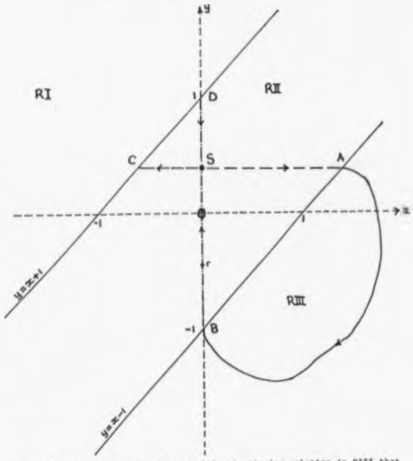

FIG[4.1] Behaviour of manifolds in RII. Particular solution in RIII that runs between boundary points A and B.

from which

$$y = (x' + cx - 1 - c)/(1 + c). \qquad (4.1.7)$$

Elimination of y gives

$$x'' + cx' + b(1 + c)x = b(1 + c) + F(1 + c)\cos \omega t. \qquad (4.1.8)$$

Consider next the point A on the unstable manifold in RII (see Fig[4.1]). All solutions through A at time

$t = 2n\pi/\omega$, $n = 0, \pm1, \pm2, \ldots$, must form the outset* of the saddle point S since in reverse time such solutions tend towards the periodic saddle response at 0. We can make A into a homoclinic point by finding a solution that starts at A at say time $t = 0$ and enters RII again at $B = (0,-1)$ on the stable manifold at time $t = t_1$, see Fig[4.1]. A first return from A will then be on the stable manifold BS at r and vice-versa provided that a response starting from r at $t = 2n\pi/\omega$, $n = 0, \pm1, \pm2, \ldots$, arrives at B at time $t = m(2\pi/\omega - t_1)$, $m = 0, \pm1, \pm2, \ldots$. thus satisfying the definition of a homoclinic point, see section (3.3), as A would then be on both the stable and unstable manifolds. To this end, it turns out that we can take a particular solution of (4.1.8) which conveniently does away with the problems of working with the transient part of the general solution.

Consider the particular solution of (4.1.8)

$$x = 1 + C \cos \omega t + D \sin \omega t \qquad (4.1.9)$$

where

---

* Fig[1.3] shows the phase portrait near a saddle fixed point in the (x, x') plane. Two are asymptotic as $t \to -\infty$ and we call these asymptotic curves the inset of the saddle. The other two are asymptotic to the saddle as $t \to +\infty$ and form the outset of the saddle. (See Thompson & Stewart, 1986.)

$$C = \frac{\{b(1 + c) - \omega^2\}(1 + c)F}{[\{b(1 + c) - \omega^2\}^2 + \omega^2 c^2]} \qquad (4.1.10)$$

$$D = \frac{c\omega(1 + c)F}{[\{b(1 + c) - \omega^2\}^2 + \omega^2 c^2]}. \qquad (4.1.11)$$

It follows that

$$y = \frac{1}{1 + c}[-1 + (D\omega + Cc)\text{Cos } \omega t + (-C\omega + Dc)\text{Sin } \omega t]. \qquad (4.1.12)$$

Let the particular solution (4.1.9) start at A at time $t = 0$, then

$$1 + F^*b = 1 + C \qquad (4.1.13)$$

$$F^*b = \frac{1}{1 + c}.(-1 + D\omega + Cc). \qquad (4.1.14)$$

Arriving at B at time $t = t_1$, where $0 \leq t_1 \leq 2\pi/\omega$, then from (4.1.9) and (4.1.12)

$$1 + C \text{ Cos } \omega t_1 + D \text{ Sin } \omega t_1 = 0$$

$$-1 + (D\omega + Cc)\text{Cos } \omega t_1 + (-C\omega + Dc)\text{Sin } \omega t_1 = -(1 + c) \qquad (4.1.15)$$

which reduce to

$$C \text{ Cos } \omega t_1 + D \text{ Sin } \omega t_1 = -1$$

$$D \text{ Cos } \omega t_1 + C \text{ Sin } \omega t_1 = 0. \qquad (4.1.16)$$

Hence,

$$\text{Cos } \omega t_1 = \frac{-C}{C^2 + D^2}, \qquad \text{Sin } \omega t_1 = \frac{-D}{C^2 + D^2} \qquad (4.1.17)$$

$$\Rightarrow C^2 + D^2 = 1. \tag{4.1.18}$$

Now from the values of C and D and (4.1.13), (4.1.14)

$$F^*b = \frac{\{b(1 + c) - \omega^2\}(1 + c)F}{[\{b(1 + c) - \omega^2\}^2 + \omega^2c^2]} \tag{4.1.19}$$

$$1 + F^*b = \frac{c\omega^2(1 + c)F}{[\{b(1 + c) - \omega^2\}^2 + \omega^2c^2]}. \tag{4.1.20}$$

From (4.1.19) we find that

$$\omega^2 = \frac{b(b + bc + 1 + 2c)}{(b + c + 1)}, \tag{4.1.21}$$

and from (4.1.20)

$$F(1 + c)^2(\omega^2 - b) = \{b(1 + c) - \omega^2\}^2 + \omega^2c^2. \tag{4.1.22}$$

Now from (4.1.18), (4.1.19) and (4.1.20)

$$F^2(1 + c)^2 = \{b(1 + c) - \omega^2\}^2 + \omega^2c^2 \tag{4.1.23}$$

and from (4.1.22) and (4.1.23)

$$F = \omega^2 - b. \tag{4.1.24}$$

From (4.1.23) and (4.1.24)

$$\omega^2 = \frac{2b + 2bc + c}{c + 2}, \tag{4.1.25}$$

hence, from (4.1.21) and (4.1.25)

$$b^2 = 1 \tag{4.1.26}$$

$$\text{i.e. } b = \pm 1. \tag{4.1.27}$$

Taking b = 1, the forcing frequency, ω, satisfies

$$\omega^2 = \frac{2 + 3c}{2 + c} \qquad (4.1.28)$$

and the forcing amplitude, F, satisfies

$$F = \frac{2c}{2 + c}. \qquad (4.1.29)$$

Hence, the point A is a homoclinic point when, on choosing c, the forcing frequency ω and amplitude F of the given system are given by (4.1.28) and (4.1.29) respectively.

4.2 SADDLE CONNECTIONS

On achieving one of our aims, that of locating the co-ordinates of a homoclinic point, we are now in a position to draw saddle connections. Saddle connections displayed in Fig[4.2] were drawn by starting at the homoclinic point A = (1 + F*, F*), at time t = 0, and in forward time solving the corresponding equations in RII and RIII using a standard numerical technique. To complete the connection plotting was again started at A at time t = 0 but with reverse time. Alternatively, the saddle connections could have been drawn using the exact equations of the three sections, namely,

$$x = (1 + F^*)e^t$$
$$y = F^* \text{ Cos } \omega t + F^* \omega \text{ Sin } \omega t \qquad t \in]-\infty, 0] \qquad (4.2.1a)$$

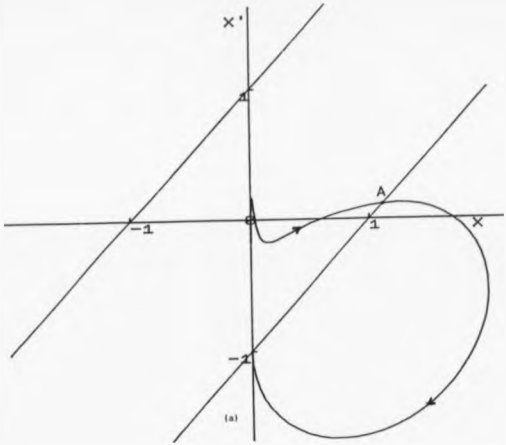

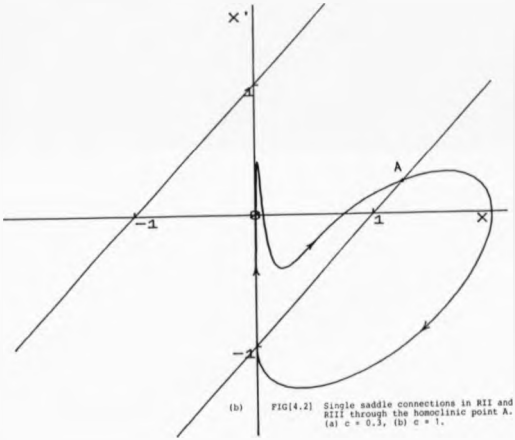

FIG[4.2] Single saddle connections in RII and RIII through the homoclinic point A. (a) c = 0.3, (b) c = 1.

$$x = 1 + \bar{C}\,\mathrm{Cos}\,\omega t + \bar{D}\,\mathrm{Sin}\,\omega t$$

$$y = \frac{1}{1+c}[-1 + (\bar{D}\omega + \bar{C}c)\mathrm{Cos}\,\omega t + (-\bar{C}\omega + \bar{D}c)\mathrm{Sin}\,\omega t]$$

$$t \in [0, t_1] \qquad (4.2.1b)$$

$$x = 0$$

$$t \in [t_1, \infty(\qquad (4.2.1c)$$

$$y = (1 - F^*)e^{-t} + F^*\,\mathrm{Cos}\,\omega t + F^*\omega\,\mathrm{Sin}\,\omega t$$

where

$$F^* = \frac{c}{2(1+c)}$$

$$\bar{C} = \frac{c}{2(1+c)} \qquad \bar{D} = \frac{\omega(2+c)}{2(1+c)}$$

and ω^2 is given by (4.1.28).

The arrival time at B is t_1 such that $n\frac{\pi}{\omega} < t_1 < \frac{3n\pi}{2}$, $n = 0, \pm1, \pm2, \ldots$, and t_1 satisfies

$$\mathrm{Tan}\,\omega t_1 = \omega(2+c)/c. \qquad (4.2.2)$$

Plotting the displacement x against the time t for the previous saddle connections we obtain the curves shown in Fig[4.3] with each response tailing off to $x = 0$ as $t \to -\infty$ but hitting the time axis at time $t = t_1$ given by (4.2.2). Notice that both responses attain the same maximum displacement, that of $x = 2$, but at different times. The maximum displacement is in fact fixed at 2 regardless of the value of c for the following reason.

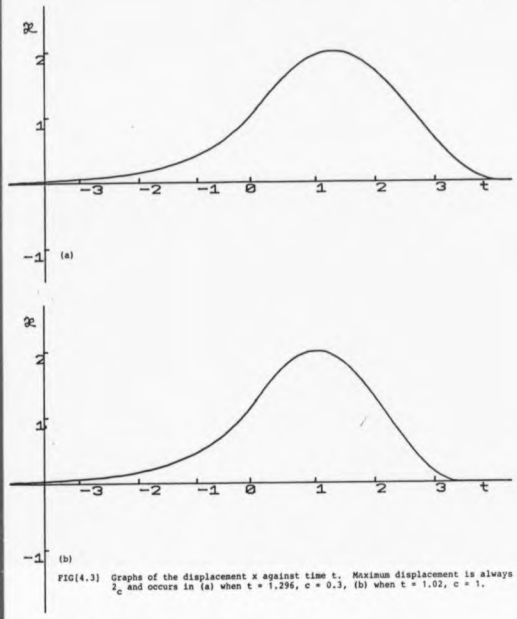

FIG[4.3] Graphs of the displacement x against time t. Maximum displacement is always 2_c and occurs in (a) when t = 1.296, c = 0.3, (b) when t = 1.02, c = 1.

The response in RIII is given by

$$x = 1 + \overline{C} \operatorname{Cos} \omega t + \overline{D} \operatorname{Sin} \omega t.$$

The maximum displacement of x occurs at time $t = t^*$, where

$$2n\frac{\pi}{\omega} < t^* < (4n + 1)\frac{\pi}{2\omega}, \quad n = 0, \pm 1, \pm 2, \ldots, \text{and}$$

$$\operatorname{Tan} \omega t^* = \overline{D}/\overline{C} = \omega(2 + c)/c$$

and as $\bar{C}^2 + \bar{D}^2 = 1$, (4.1.18), the maximum displacement of x is 2. Incidentally, there is a constant time difference of π/ω between t^* and t' the time when the saddle response arrives at B.

Plotting the displacement y against time t gives the results shown in Fig[4.4]. Here the oscillation has period $2\pi/\omega$ as it leaves the periodic saddle response at

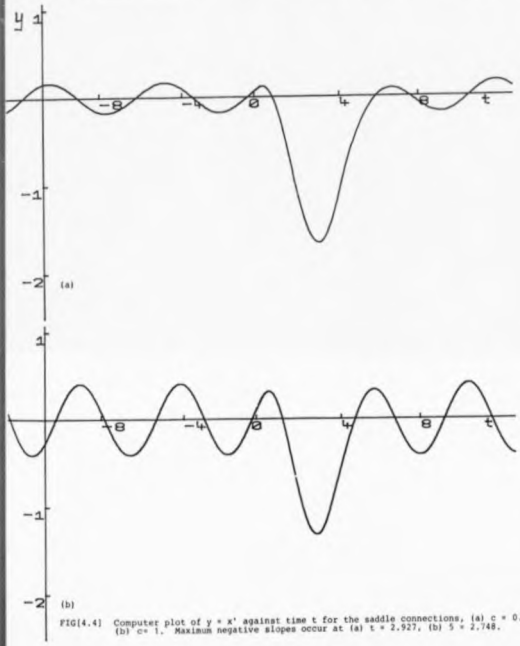

FIG[4.4] Computer plot of $y = x'$ against time t for the saddle connections, (a) $c = 0.3$, (b) $c = 1$. Maximum negative slopes occur at (a) $t = 2.927$, (b) $5 = 2.748$.

$t = -\infty$ and again when it returns as $t \to \infty$. As the response runs through RIII y attains an overall minimum value of $(-1 - \sqrt{\omega^2 + c^2})/(1 + c)$ at time $t = \hat{t}$ where $n\pi/\omega < \hat{t} < 3n\pi/2\omega$, $n = 0, \pm1, \pm2, \ldots$ and $\hat{t}$ satisfies the equation

$$\text{Tan } \omega\hat{t} = \omega c/(2 + c). \tag{4.2.3}$$

Starting at the homoclinic point A the progression of first-returns on the stable manifold BS, each one a homoclinic point, have co-ordinates given by (0, H) where

$$H = \frac{1}{2(1 + c)}\left|C - \frac{(2 + 3c)}{(1 + c)}e^{-\left(\frac{2n\pi}{\omega} - t_1\right)}\right|, \qquad n = 0, \pm1, \pm2, \ldots \tag{4.2.4}$$

and t_1 is given by (4.2.2). It is evident from (4.2.4) that as $n \to \infty$ so the sequence of homoclinic points tends towards the saddle point S.

A Poincaré map of the unstable and stable manifolds of (4.1.1) is shown in Fig[4.5] where $c = 0.3$. Qualitatively, the result compares well with the Poincare map of Duffing's equation shown in Fig[3.4c]. It should be pointed out that the point A is not however an homoclinic tangency point but an homoclinic point of intersection - see Appendix C.

4.3 THE POINT OF HOMOCLINIC TANGENCY IN RI

All solutions starting on SC in RII at time $t = \frac{2n\pi}{\omega}$, $n = 0, \pm1, \pm2, \ldots$, see Fig[4.6], will at some

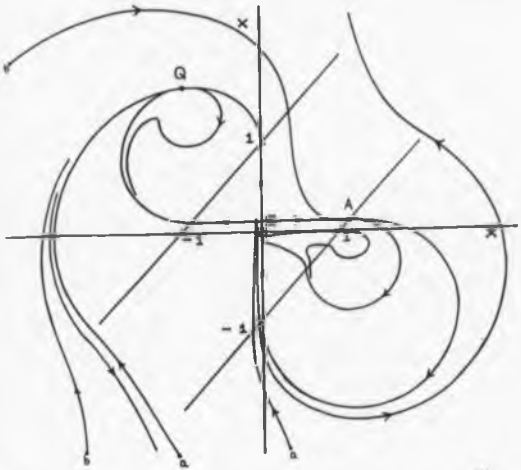

FIG(4.5) Poincaré map of the manifolds of the piecewise linear system, c = 0.3, F = 0.[illegible], ω = 1.123.

later time meet the boundary line y = x + 1 matching with a new solution set in RI. In amongst this latter set is a unique solution which eventually meets the point D. This unique solution turns out to be the particular solution of (4.1.1) in RI. Such a solution must connect an outgoing point of the unstable manifold $\mathcal{SC}$ to the point D on the incoming set, DS, of S. Hence, the fixed point of the particular solution must be common to both

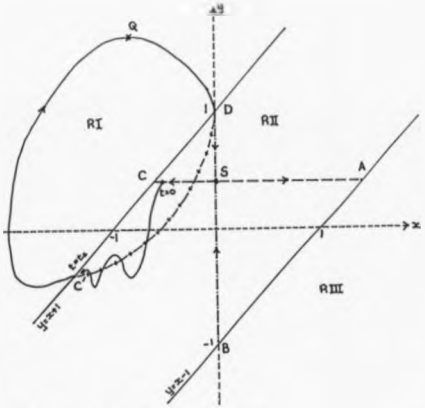

FIG[4.6] Locating the homoclinic point Q in RIII.

the outset and inset of S and is, therefore, a homoclinic point with the particular solution constituting a homoclinic connection. It is, therefore, a straightforward matter to determine the co-ordinates of this homoclinic point.

For $x < y - 1$ in RI

$$x' = -cx + (1 + c)(y - 1) \qquad (4.3.1a)$$

$$y' = -bx - b + F \cos \omega t \qquad (4.3.1b)$$

where ω and F are given by (4.1.28) and (4.1.29) respectively. From (4.3.1a)

$$y = \frac{x' + cx + (1 - c)}{1 + c}. \qquad (4.3.2)$$

Elimination of y between (4.3.1b) and (4.3.2) gives

$$x'' + cx' + (1 + c)bx + (1 + c)b = (1 + c)F \cos \omega t. \qquad (4.3.3)$$

Put b = 1 from (4.1.27) then

$$x'' + cx' + (1 + c)x + (1 + c) = (1 + c)F \cos \omega t. \qquad (4.3.4)$$

The particular solution of (4.3.4) is

$$x(t) = -1 + C \cos \omega t + D \sin \omega t \qquad (4.3.5a)$$

with

$$y(t) = \frac{1}{(1 + c)}[\omega(-C \sin \omega t + D \cos \omega t) + c(C \cos \omega t + D \sin \omega t) + 1] \qquad (4.3.5b)$$

where C and D are given by (4.1.10) and (4.1.11) respectively with b = 1.
Inserting (4.3.5a) into (4.3.5b)

$$y(t) = \frac{1}{1 + c}[\omega(-C \sin \omega t + D \cos \omega t) + c(x + 1) + 1] \qquad (4.3.6)$$

which can be re-written

$$\frac{1}{\omega}[(1 + c)(y - 1) - cx] = -C \sin \omega t + D \cos \omega t. \qquad (4.3.7)$$

Squaring and adding (4.3.5a) and (4.3.7)

$$(x + 1)^2 + \frac{1}{\omega^2}[(1 + c)(y - 1) - cx]^2 = C^2 + D^2, \quad (4.3.8)$$

As (4.3.8) passes through D at (0, 1), so

$$C^2 + D^2 = 1 \quad (4.3.9)$$

hence

$$(x + 1)^2 + \frac{1}{\omega^2}[(1 + c)(y - 1) - cx]^2 = 1 \quad (4.3.10)$$

is the equation in RII of the particular solution.

The particular solution (4.3.10) also meets the boundary line $y = x + 1$ at

$$x = -1 - F^*, \qquad y = -F^* \quad (4.3.11)$$
$$= C' \qquad \text{(see Fig[4.6])}.$$

(This response never meets C unless $c = 0$.)
The fixed point of the particular solution (4.3.10) is found by putting $t = 0$ (say) into (4.3.5) giving the co-ordinates of the homoclinic point Q,

$$[-1 + C, (\omega D + cC + 1)/(1 + c)]. \quad (4.3.12)$$

We also have at our disposal the means of finding the time $t = t_2$ at which the particular solution (4.3.5) in RI starts from the boundary line $y = x + 1$. We must look for a solution which takes us from an initial point ($t = 0$) on SC (in RII) to the point C' at time $t = t_2$

where t_2 is the same time it would take to travel from the homoclinic point Q through to C' on the completed curve given by (4.3.10); see Fig[4.6]. Hence, the time $t = t_2$ must satisfy

$$-1 - F^* = -1 + C \cos \omega t_2 + D \sin \omega t_2 \tag{4.3.13a}$$

$$-F^* = \frac{1}{(1 + c)} \cdot [\omega(-C \sin \omega t_2 + D \cos \omega t_2) + c(C \cos \omega t_2 + D \sin \omega t_2)] \tag{4.3.13b}$$

from which

$$\sin \omega t_2 = -F^*D + (F^* + 1)C/\omega = 0 \tag{4.3.14a}$$

$$\cos \omega t_2 = -F^*C - (F^* + 1)D/\omega = -1 \tag{4.3.14b}$$

and so $t_2 = (2n + 1)\frac{\pi}{2\omega}$, $n = 0, \pm 1, \pm 2, \ldots$. (4.3.15)

Now any solution starting on the unstable manifold SC, in Fig[4.6], is given by (4.1.3). If this solution is to reach C' at time $t = t_2$, then

$$x_0 = -(1 + F^*)e^{-t_2}, \tag{4.3.16}$$

hence, starting at the point

$$[-(1 + F^*)e^{-t_2}, \quad F^*] \tag{4.3.17}$$

at time $t = \frac{2n\pi}{\omega}$, $n = 0, \pm 1, \pm 2, \ldots$, the $2\pi/\omega$ first-return will be at Q. It finally remains to show that for the

same time $t - t_2$, the y-response is also at C'. This can easily be seen to be true if one considers the equation for y given by (4.1.3b) along with the results of (4.3.14).

Applying a negative time Poincare' map from a particular point on the stable manifold DS we also expect to arrive at Q. The initial point on DS is found as follows. First, find the time, t', it takes to travel along the particular solution from Q to D in Fig[4.6]. From (4.3.5), t' satisfies

$$1 = -1 + C \cos \omega t' + D \sin \omega t' \tag{4.3.18a}$$

$$0 = \omega(-C \sin \omega t' + D \cos \omega t') + c(C \cos \omega t' + D \sin \omega t') + 1 \tag{4.3.18b}$$

giving

$$\sin \omega t' = 2D + (2c + 1)C/\omega \tag{4.3.19a}$$

$$\cos \omega t' = 2C - (2c + 1)D/\omega \tag{4.3.19b}$$

hence

$$\tan \omega t' = \frac{2\omega D + (2c + 1)C}{2\omega C - (2c + 1)D}. \tag{4.3.20}$$

The solution on the stable manifold starting at $D = (0, 1)$ at time $t = t'$ is given by

$$\begin{aligned} x(t) &= 0 \\ y(t) &= (1 - F^* \cos \omega t' - F^* \omega \sin \omega t')e^{-(t-t')} \\ &\quad + F^* \cos \omega t + F^* \omega \sin \omega t \end{aligned} \tag{4.3.21}$$

and when $t = 2\pi/\omega$, the co-ordinates of the first-return from the homoclinic point Q are

$$x(2\pi/\omega) = 0$$

$$y(2\pi/\omega) = (1 - F^* \text{ Cos } \omega t' - F^* \text{ Sin } \omega t')e^{-(2\pi/\omega - t')} + F^*. \tag{4.3.22}$$

The co-ordinates of subsequent first-returns can be found using (4.3.21) where the time t is replaced by $\frac{2n\pi}{\omega}$, $n = 0, \pm1, \pm2, \ldots$.

4.4 EQUATIONS OF THE STABLE MANIFOLDS IN RIII AND RI

Let the point P_S at (x_0, y_0) in Fig[4.7] be a point on the stable manifold in RIII, which runs through to B. Let the curve PB be part of the response curve which starts at P at time $t = 0$. All points P_S on the stable manifold must have solution curves that start at P_S at time $t = 0$ and meet the point B at time $t = t_1^*$ modulo $2\pi/\omega$; otherwise, the response in RII is deflected away from the manifolds.

The complete solution in RIII is given by

$$x(t) = e^{-ct/2}[\bar{A} \text{ Cos } qt + \bar{B} \text{ Sin } qt] + C \text{ Cos } \omega t + D \text{ Sin } \omega t + 1 \tag{4.4.1a}$$

$$y(t) = \frac{ce^{-ct/2}}{2(c+1)}[\bar{A} \text{ Cos } qt + \bar{B} \text{ Sin } qt] + \frac{e^{-ct/2}}{(c+1)}[-q\bar{A} \text{ Sin } qt + \bar{B}q \text{ Cos } qt] + [-1 + (D\omega + Cc)\text{Cos } \omega t + (-C\omega + Dc)\text{Sin } \omega t]/(c+1) \tag{4.4.1b}$$

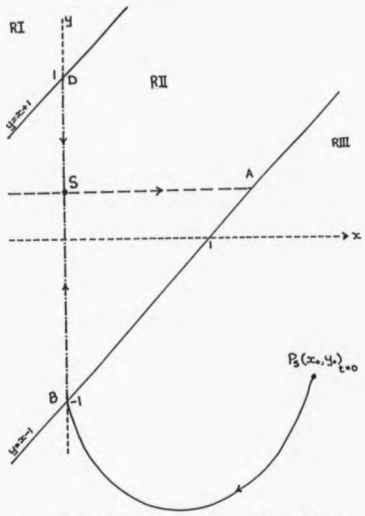

FIG[4.7] If P_* is a point on the stable manifold in RIII then a solution starting from P_* at time t = 0 must pass through the boundary point B.

where C and D are given by (4.1.10) and (4.1.11) with b = 1, and $q = \frac{1}{2}\sqrt{4 + 4c - c^2}$.

Starting at $P = (x_0, y_0)$ at time t = 0, we have

$$\bar{A} = x_0 - C - 1 \tag{4.4.2a}$$

$$\bar{B} = \left\{(1 + c)y_0 - \frac{c\bar{A}}{2} + 1 - (Dw + Cc)\right\}/q. \tag{4.4.2b}$$

Let the solution reach B on the stable manifold at

time $t = t_1^*$ where B = (0, -1). Therefore, from (4.4.1)

$$\bar{A} \text{ Cos } qt_1^* + \bar{B} \text{ Sin } qt_1^* = [-1 - C \text{ Cos } \omega t_1^* - D \text{ Sin } \omega t_1^*]e^{ct_1^*/2} = U \tag{4.4.3a}$$

$$\bar{A}\left[\frac{c}{2} \text{ Cos } qt_1^* - q \text{ Sin } qt_1^*\right] + \bar{B}\left[\frac{c}{2} \text{ Sin } qt_1^* + q \text{ Cos } qt_1^*\right] = [-c - (D\omega + Cc)\text{Cos } \omega t_1^* - (-C\omega + Dc)\text{Sin } \omega t_1^*]e^{ct_1^*/2} = V. \tag{4.4.3b}$$

In matrix form this can be written

$$\begin{bmatrix} \text{Cos } qt_1^* & \text{Sin } qt_1^* \\ \frac{c}{2} \text{ Cos } qt_1^* - q \text{ Sin } qt_1^* & \frac{c}{2} \text{ Sin } qt_1^* + q \text{ Cos } qt_1^* \end{bmatrix} \begin{bmatrix} \bar{A} \\ \bar{B} \end{bmatrix} = \begin{bmatrix} U \\ V \end{bmatrix} \tag{4.4.4}$$

from which

$$\begin{bmatrix} \bar{A} \\ \bar{B} \end{bmatrix} = \frac{1}{q} \begin{bmatrix} \frac{c}{2} \text{ Sin } qt_1^* + q \text{ Cos } qt_1^* & -\text{Sin } qt_1^* \\ q \text{ Sin } qt_1^* - q \text{ Cos } qt_1^* & \text{Cos } qt_1^* \end{bmatrix} \begin{bmatrix} U \\ V \end{bmatrix}. \tag{4.4.5}$$

The initial points (x_0, y_0) can now be expressed in terms of the time t_1^*. From (4.4.2) and (4.4.5)

$$x_0 = 1 + C + \left[\left(\frac{c}{2} \text{ Sin } qt_1^* + q \text{ Cos } qt_1^*\right)U - V \text{ Sin } qt_1^*\right]/q \tag{4.4.6a}$$

$$y_0 = \left[\frac{c}{2}(x_0 - C - 1) + (-1 + D\omega + Cc) + \left(q \text{ Sin } qt_1^* - \frac{c}{2} \text{ Cos } qt_1^*\right)U + V \text{ Cos } qt_1^*\right]/(c + 1). \tag{4.4.6b}$$

Equations (4.4.6) enable part of the stable manifold to be plotted in RIII. Given the time $t = t_1^*$ at which the response reaches B, we can determine the corresponding point on the stable manifold.

Equations which determine the stable manifold in RI are obtained in a similar manner. Points (x_0, y_0) on the stable manifold are given by

$$x_0 = -1 + C + \left[\left(\frac{c}{2} \text{ Sin } qt'^* + q \text{ Cos } qt'^*\right)U - V \text{ Sin } qt'^*\right] \tag{4.4.7a}$$

$$y_0 = \left[\frac{c}{2}(x_0 - C + 1) + (1 + D\omega + Cc) + (q \text{ Sin } qt'^*)U - \frac{c}{2} \text{ Cos } qt'^* U + V \text{ Cos } qt'^*\right]/(c + 1) \tag{4.4.7b}$$

where

$$U = [1 - C \text{ Cos } \omega t'^* - D \text{ Sin } \omega t'^*]e^{ct'^*/2} \tag{4.4.8a}$$

$$V = [c - (D\omega + Cc)\text{Cos } \omega t'^* - (-C\omega + Dc)\text{Sin } \omega t'^*]e^{ct'^*/2} \tag{4.4.8b}$$

and t'^* is the time at which the response starting on the stable manifold at $Q_s = (x_0, y_0)$ at time $t = 0$, reaches the point D on the stable manifold in RII. Computer plots of sections of the stable manifolds in RI and RIII are displayed in Fig[4.9].

4.5 EQUATIONS OF THE UNSTABLE MANIFOLDS IN RIII and RI

Let the point F at (x_0, y_0) be on the unstable manifold, SA, in RII; see Fig[4.8]. Any solution leaving

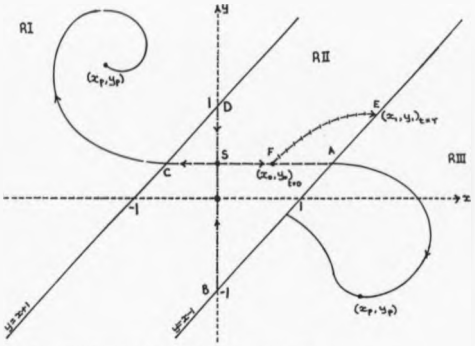

FIG[4.8] Locating points on the unstable manifold in RIII.

F at time $t = 0$ will meet the boundary line, $y = x - 1$, at time $t = \tau$(say) at $E = (x_1, y_1)$. Such a solution in RII is given by (4.1.3) where $y_0 = F^*$ and $b = 1$ from which τ and x_0 satisfy

$$F^* \cos \omega\tau + F^*\omega \sin \omega\tau = x_0 e^{\tau} - 1. \qquad (4.5.1)$$

Now reverse the procedure. Take any time τ,

$0 < \tau < 2\pi/\omega$ modulo $2\pi/\omega$, at which the solution reaches E then from (4.4.1) we can determine x_0 and the co-ordinates of E,

$$x_1 = F^* \text{ Cos } \omega\tau + F^*\omega \text{ Sin } \omega\tau + 1 \tag{4.5.2a}$$

$$y_1 = F^* \text{ Cos } \omega\tau + F^*\omega \text{ Sin } \omega\tau. \tag{4.5.2b}$$

The values x_1, y_1 and τ are the initial conditions for the response in RIII.

The complete solution in RIII is given by (4.4.1) where the constants of integration are determined using the initial conditions $x(\tau) = x_1$, $y(\tau) = y_1$. Applying these conditions to (4.4.1) gives

$$\bar{A} = \frac{1}{q}\left[\frac{c}{2} \text{ Sin } q\tau + q \text{ Cos } q\tau\right]U_1 - \frac{1}{q}V_1 \text{ Sin } q\tau \tag{4.5.3a}$$

$$\bar{B} = \frac{1}{q}\left[q \text{ Sin } q\tau - \frac{c}{2} \text{ Cos } q\tau\right]U_1 + \frac{1}{q}V_1 \text{ Cos } q\tau \tag{4.5.3b}$$

where

$$U_1 = [(F^* - C)\text{Cos } \omega\tau + (F^*\omega - D)\text{Sin } \omega\tau]e^{c\tau/2} \tag{4.5.4a}$$

$$V_1 = [1 + \{F^*(1 + c) - (D\omega + Cc)\}\text{Cos } \omega\tau + \{F^*(1 + c) - (-C\omega + Dc)\} \times \text{Sin } \omega\tau]e^{c\tau/2}. \tag{4.5.4b}$$

When ω and F are replaced by results (4.1.28) and - (4.1.29), U_1 reduces to

$$U_1 = \frac{-\omega e^{c\tau/2}}{(1 + c)} \text{ Sin } \omega\tau \tag{4.5.5}$$

and V_1 reduces to

$$V_1 = e^{c\tau/2}[1 - \text{Cos } \omega\tau + F^*\omega(1 + c) + C\omega - Dc \text{ Sin } \omega\tau]. \tag{4.5.6}$$

The Poincaré $(2\pi/\omega)$ first-return map of points along the unstable manifold SA are obtained using (4.3.1) and (4.4.3) with $t = 2\pi/\omega$. That is,

$$x_u(2\pi/\omega) = e^{-c\pi/\omega}\left[\bar{A} \text{ Cos } \frac{2\pi q}{\omega} + \bar{B} \text{ Sin } \frac{2\pi q}{\omega}\right] + C + 1 = X \tag{4.5.7a}$$

$$y_u(2\pi/\omega) = \frac{Ce^{-c\pi/\omega}}{2(1 + c)}\left[\bar{A} \text{ Cos } \frac{2\pi q}{\omega} + \bar{B} \text{ Sin } \frac{2\pi q}{\omega}\right] + \frac{e^{-c\pi/\omega}}{(c + 1)}\left[-q\bar{A} \text{ Sin } \frac{2\pi q}{\omega} + q\bar{B} \text{ Cos } \frac{2\pi q}{\omega}\right] + \frac{c}{2(1 + c)} = Y, \tag{4.5.7b}$$

By a similar procedure, point on the unstable manifold in RI are given by

$$x_u(2\pi/\omega) = e^{-c\pi/\omega}\left[\bar{A}_1 \text{ Cos } \frac{2\pi q}{\omega} + \bar{B}_1 \text{ Sin } \frac{2\pi q}{\omega}\right] + C - 1 \tag{4.5.8a}$$

$$y_u(2\pi/\omega) = \frac{Ce^{-c\pi/\omega}}{2(c + 1)}\left[\bar{A}_1 \text{ Cos } \frac{2\pi q}{\omega} + \bar{B}_1 \text{ Sin } \frac{2\pi q}{\omega}\right] + \frac{e^{-c\pi/\omega}}{(c + 1)}\left[-q\bar{A}_1 \text{ Sin } \frac{2\pi q}{\omega} + q\bar{B}_1 \text{ Cos } \frac{2\pi q}{\omega}\right] + \frac{(c + 4)}{2(c + 1)} \tag{4.5.8b}$$

where $\bar{A}_1$, $\bar{B}_1$ are given by (4.5.3) with U_1 unchanged but

$$V_1 = e^{c\tau/2}[-1 - \text{Cos } \omega\tau + F^*\omega(1 + c) + (C\omega - Dc)\text{Sin } \omega\tau]. \quad (4.5.9)$$

Computer plots of the unstable manifolds that appear in part in RI and RIII are displayed in Fig[4.9].

The piece-wise linear system (4.1.1) itself produces some interesting steady-state solutions. Fig[4.10a-f] shows a selection of those solutions in the (x, x') plane, where x' = y. The results model those of Duffing's equation when the forcing amplitude is fixed and the frequency is varied since we observe here that the solutions also pass through the same four stages as ω is decreased - see section (2.1). The period 5 and period 7 solutions fall within the chaotic band of ω-values and this has also been observed by Holmes, (1979) in Duffing's equation. When ω is given by (4.1.28), that is $\omega = 1.291$ in this case, we have a homoclinic bifurcation situation whereby solutions whose initial values (t = 0) are not on the manifolds will settle to one of two period-2 solutions as shown in Fig[4.10b]; otherwise solutions are dictated by the complex windings of the manifolds themselves and periodic solutions are no longer possible.

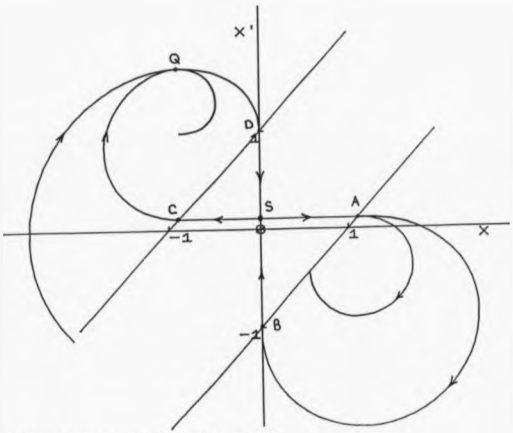

FIG[4.9] Stable and unstable manifolds. c = 0.3

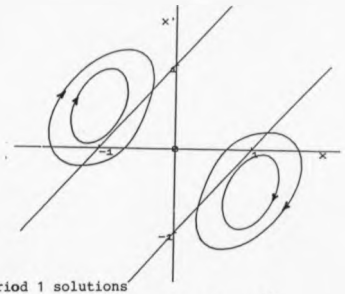

(a) Period 1 solutions

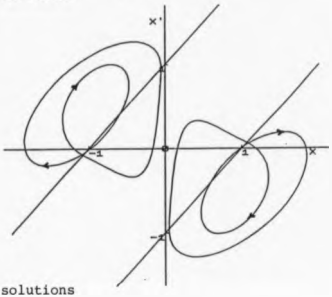

(b) Period 2 solutions

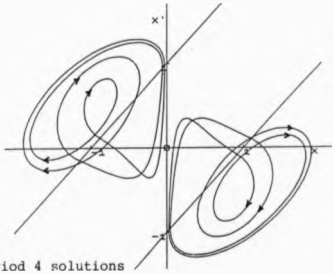

(c) Period 4 solutions

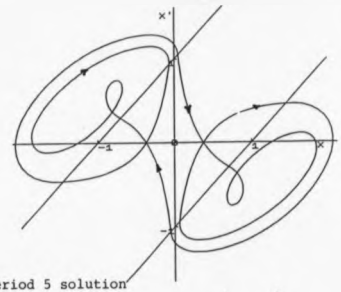

(d) Period 5 solution

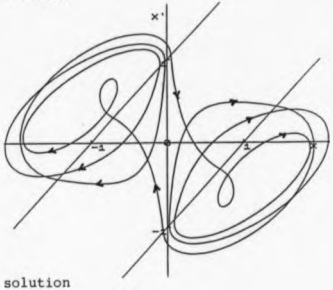

(e) Period 7 solution

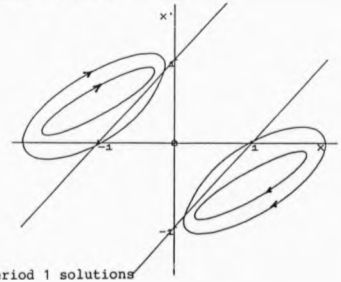

(f) Period 1 solutions

In this chapter we have been able to obtain analytically information about the stable and unstable manifolds of a piecewise linear differential equation. The co-ordinates of points of homoclinic tangency were found thus enabling the saddle connections in the (x, x') plane to be plotted and the corresponding solutions in the (x, t) plane, where it was shown that the maximum displacement was fixed regardless of the parameter value c. In addition, equations were obtained to allow, in part, computer plots of the stable and unstable manifolds. All this was possible because the differential equation was linear within each region and hence could be solved. Fortunately, we were investigating parts of the system that were readily accessible to analysis as boundary matching elsewhere, for example, would have led to the problem of solving transcendental equations. An important side to all this is that piecewise linear systems exhibit all the phenomena associated with non-linear differential equations, particularly Duffing's equation. Another piecewise linear system has been investigated by Thompson, Bokaian & Ghaffari (1983) which concerns itself with subharmonic resonances and chaotic motions of a bilinear oscillator through the behaviour of a simple forced linear oscillator with different stiffnesses for positive and negative deflections. See also Shaw & Holmes (1983).

CHAPTER 5

SADDLE CONNECTIONS

INTRODUCTION

The form of the invariant manifolds of a dynamical system plays an important role in the behaviour of the system as a whole particularly if, as a result of a change in a control parameter, a qualitative change of the invariant manifold topology occurs resulting in a corresponding qualitative change in response. Structural instability is clearly inherent in such systems and we say the behaviour is an example of global bifurcation as such dynamical changes to the system cannot be deduced from local information.

This phenomenon can be clearly seen in the very simple system

$$x' = y$$

$$y' = x - x^3$$

whose closed invariant manifolds (see Fig[1.5] - separatrices in this case) split the solution set into three regions composed of periodic solutions disposed about $x = \pm 1$ and $x = 0$. If we introduce damping then a

qualitative change to the dynamical system is seen to occur as the manifolds break at the slightest amount of friction - (see Fig[1.8]) and periodic solutions are no longer sustained.

One particular type of global bifurcation that can affect the behaviour of a dynamical system is homoclinic bifurcation resulting from the intersection of unstable and stable manifolds of the corresponding Poincaré map. Poincaré maps of Duffing's equation in Chapter 3 revealed that prior to the initial point of contact of the manifolds (homoclinic tangency) all first-returns on the stable manifolds approached one of two fixed points corresponding to stable periodic solutions. At contact the unstable manifolds break away from their respective fixed points (which, incidentally, remain for a short interval of ω-values before they too bifurcate) producing complex windings of the type plotted in Chapter 3.

Associated with each homoclinic point is a homoclinic saddle connection the appearance of which is particularly significant in the global behaviour of solutions of Duffing's equations. Whilst they are usually highly unstable solutions, nevertheless any analytic properties of their behaviour is important in understanding the full affects of homoclinic bifurcation. Few authors refer to the actual saddle solutions of Duffing's equation so it is intended in this chapter to search for these saddle connections which link correctly phased ingoing and outgoing limiting solutions of the

unstable periodic solution using a modified form of the latter equation. Fig[5.1a] depicts the simplest type of saddle connection sought.

5.1 A COORDINATE PERTURBATION APPROACH

In this and the next section a method is developed which enables us to investigate the appearance of

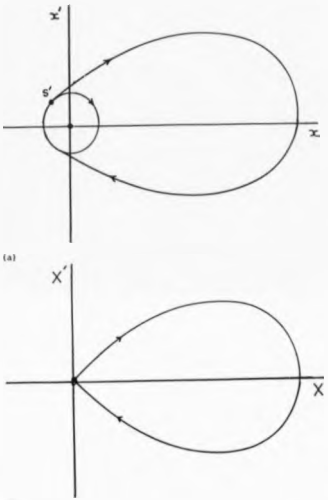

Fig[5.1] Simple saddle connections
(a) of Duffing's equation with saddle point at x',
(b) of the transformed Duffing equation with saddle point at the origin.

homoclinic saddle connections and approach homoclinic bifurcation by this method. As with Mel'nikov's method [see section (3.2)] use is made of a singular perturbation procedure based on the saddle connection or seperatrix of the unforced, undamped Duffing equation as illustrated in Fig[1.5]. An important spin-off from this approach is that we can investigate solutions which pass 'close' to the unstable periodic solution. The result is that conditions can be found for the existence of multiple loop and transverse saddle connections and certain large amplitude oscillations with odd periods and these are dealt with in subsequent sections.*

We begin by expressing Duffing's equation (1.1.1) as a perturbed Hamiltonian system by assuming that $k = \varepsilon k_0$, $F = \varepsilon f$ where ε is small and $(k_0, f) = 0(1)$ as $\varepsilon \to 0$, so that equation (1.1.1) becomes

$$x'' + \varepsilon k_0 x' - x + x^3 = \varepsilon f \cos \omega t. \qquad (5.1.1)$$

For small k and F the unstable periodic solution disposed about $x = 0$ in its averaged form is given by

$$x = \varepsilon f_0 \cos \omega t \qquad (5.1.2)$$

where

$$f_0 = -f/(1 + \omega^2)$$

based on the linear equation approximated at $(x, x') = (0, 0)$.

* See Smith and Davenport, (1988).

Representing the unstable periodic solution (5.1.2) by $x = p(t)$ then the change of variable

$$x = X(t, \varepsilon) + p(t)$$

removes the periodic component from (5.1.1) leaving

$$X'' + \varepsilon k_0 X' - X + X^3 + 3p(t)X^2 + 3p^2(t)X = 0. \qquad (5.1.3)$$

If $p(t)$ is replaced by its averaged form and coefficients to order ε only are retained, then X satisfies the approximate equation

$$X'' + \varepsilon k_0 X' - X + X^3 + 3\varepsilon f_0 X^2 \operatorname{Cos} \omega t = 0. \qquad (5.1.4)$$

The change of variable transforms the unstable periodic solution to an equilibrium saddle point at the origin in the (X, X') plane, giving simple saddle connections of the type shown in Fig[5.1b].

If $\varepsilon = 0$, Eqn(5.1.4) reduces to the Hamiltonian system with saddle connection for $X > 0$ given by

$$X = \sqrt{2}\ \operatorname{Sech}(t - t_0) \qquad (5.1.5)$$

where

$$X(t_0) = \sqrt{2}, \qquad X'(t_0) = 0$$

and

$$\lim_{t \to \pm\infty} X(t) = 0.$$

Consider now those solutions which pass close to $X = \sqrt{2}$, and in consequence pass close to the origin. In particular consider the solution $X = X(t, \varepsilon)$ both forward and backward in time, which satisfies

$$X(t_0, \varepsilon) = \sqrt{2} + \varepsilon\delta$$
$$X'(t_0, \varepsilon) = 0 \qquad (5.1.6)$$

where t_0, δ are constants.

Unfortunately, we cannot apply a simple perturbation method to Eqn(5.1.3) since the solution will not have the correct behaviour as $t \to \pm\infty$. The reason for this is that when X and ε are small (5.1.3) approximates to the linear equation

$$X'' + \varepsilon k_0 X' - X = 0 \qquad (5.1.7)$$

which has solution

$$X(t, \varepsilon) = Ae^{m_1 t} + Be^{m_2 t} \qquad (5.1.8)$$

where $m_1 = 1 - \varepsilon k_0/2$, $m_2 = -1 - \varepsilon k_0/2$ and A, B are constants of integration. The saddle behaviour at (0, 0) is such that as $t \to -\infty$

$$X \approx Ae^{m_1 t} \qquad (5.1.9a)$$

and as $t \to \infty$

$$X \approx Be^{m_2 t}. \qquad (5.1.9b)$$

The corresponding saddle behaviour based on the perturbation method is such that as $t \to -\infty$ (see (5.1.3))

$$X \sim A_s e^{t} \tag{5.1.10a}$$

and as $t \to +\infty$

$$X \sim B_s e^{-t} \tag{5.1.10b}$$

where A_s and B_s are again constants of integration. Clearly, the behaviour in this case is different from the required behaviour for large time (both positive and negative). In fact we have here a singular perturbation problem with the singular behaviour occurring at $t \to \pm\infty$.

This difficulty can be avoided by introducing a coordinate perturbation in which a simultaneous expansion in powers of ε of both the dependent and independent variable are taken generating an implicit relation between X and t through a new parameter. (For details see Jordan and Smith (1987) and Nayfeh (1973)).

Expanding $X(t, \varepsilon)$ and t in terms of the new parameter τ,

$$X(t, \varepsilon) = X_0(\tau) + X_1(\tau) + \ldots \tag{5.1.11}$$

and

$$t = \tau + \varepsilon T_1(\tau) + \ldots \tag{5.1.12}$$

where $T_1(\tau)$, ... are a set of unknown functions T_1, ... of τ. Eqns(5.1.11) and (5.1.12) are substituted into the

differential equation (5.1.4) and the boundary conditions (5.1.6).

As we do not expect that $t = t_0$ will correspond to $\tau = t_0$, suppose instead that $t = t_0$ corresponds to $\tau = \tau^*(\varepsilon)$. Then we must solve (5.1.12) for τ^*; that is

$$t_0 = \tau^* + \varepsilon T_1(\tau^*) + \ldots. \tag{5.1.13}$$

Put

$$\tau^* = t_0 + \varepsilon\tau_1 + \ldots \tag{5.1.14}$$

where $\tau_1, \ldots$ are constants.

Using Taylor's expansion we can write $T_1(\tau^*) = T_1(t_0) + \varepsilon\tau_1 T_1'(t_0) + \ldots$ and (5.1.13) becomes

$$t_0 = t_0 + \varepsilon(\tau_1 + T_1(t_0)) + \ldots, \tag{5.1.15}$$

so $\tau_1 = -T_1(t_0)$.

Thus

$$\tau^* = t_0 - \varepsilon T_1(t_0) + \ldots. \tag{5.1.16}$$

Next the derivatives of X are transformed by

$$\frac{dX}{dt} = \frac{dX}{d\tau}\cdot\frac{d\tau}{dt} = (X_0' + \varepsilon X_1' + \ldots)(1 + \varepsilon T_1'(\tau) + \ldots)^{-1}$$

$$= (X_0' + \varepsilon X_1' + \ldots)(1 - \varepsilon T_1'(\tau) + \ldots) -$$

$$= X_0' + \varepsilon(X_1' - X_0'T_1'(\tau)) + \ldots, \tag{5.1.17}$$

and

$$\frac{d^2X}{dt^2} = \frac{d\tau}{dt}\cdot\frac{d}{d\tau}[X_0' + \varepsilon(X_1' - X_0'T_1'(\tau)) + \ldots]$$

$$= (1 - \varepsilon T_1'(\tau) + \ldots)[X_0'' + \varepsilon(X_1'' - X_0''T_1'(\tau)$$

$$- X_0'T_1''(\tau)) + \ldots]$$

$$= X_0'' + \varepsilon(X_1'' - 2X_0''T_1'(\tau) - X_0'T_1''(\tau)) + \ldots. \qquad (5.1.18)$$

Thus Eqn(5.1.4) becomes, to order ε,

$$X_0'' + \varepsilon(X_1'' - 2X_0''T_1'(\tau) - X_0'T_1''(\tau)) + \varepsilon k_0X_0'$$

$$- X_0 - \varepsilon X_1 + X_0^3 + 3\varepsilon X_0^2X_1 + 3\varepsilon f_0X_0^2 \text{ Cos } \omega t = 0, \qquad (5.1.19)$$

where, for the moment, we retain the time t in Cos ωt.

Equating the coefficients of the two powers of ε in Eqn(5.1.19) gives

$$X_0'' - X_0 + X_0^3 = 0 \qquad (5.1.20)$$

and

$$X_1'' + (3X_0^2 - 1)X_1 = 2X_0''T_1' + T_1''X_0' - k_0X_0'$$

$$- 3f_0X_0^2 \text{ Cos } \omega t, \qquad (5.1.21)$$

where $T_1 = T_1(\tau)$.

The conditions on X at time $t = t_0$ become

$$X_0(\tau^*) + \varepsilon X_1(\tau^*) + \ldots = \sqrt{2} + \varepsilon\beta$$

or

$$X_0(t_0 - \varepsilon T_1(t_0) + \ldots) + \varepsilon X_1(t_0 - \varepsilon T_1(t_0) + \ldots)$$
$$+ \ldots = \sqrt{2} + \varepsilon\beta$$

or

$$X_0(t_0) + \varepsilon(X_1(t_0) - T_1(t_0)X_0'(t_0)) + \ldots = \sqrt{2} + \varepsilon\beta$$

using the Taylor expansion again.

Therefore,

$$X_0(t_0) = \sqrt{2} \tag{5.1.22}$$

and

$$X_1(t_0) - T_1(t_0)X_0'(t_0) = \beta. \tag{5.1.23}$$

The other condition on X' using (5.1.16) and (5.1.17) becomes

$$X_0'(\tau^*) + \varepsilon(X_1'(\tau^*) - X_0'(\tau^*)T_1'(\tau^*)) + \ldots = 0$$

that is

$$X_0'(t_0) + \varepsilon(-T_1(t_0)X_0''(t_0) + X_1'(t_0)$$
$$- X_0'(t_0)T_1'(t_0)) + \ldots = 0$$

so

$$X_0'(t_0) = 0 \tag{5.1.24}$$

and

$$X_1'(t_0) = T_1(t_0)X_0''(t_0). \tag{5.1.25}$$

The solution of Eqn(5.1.20) subject to conditions (5.1.22) and (5.1.24) is the unperturbed solution

$$X_0 = \sqrt{2}\ \mathrm{Sech}(\tau - t_0). \tag{5.1.26}$$

Substituting this result into Eqn(5.1.21) gives

$$X_1'' + (6\ \mathrm{Sech}^2(\tau - t_0) - 1)X_1 = f(\tau) \tag{5.1.27}$$

where

$$\begin{aligned} f(\tau) = {} & 2T_1'\sqrt{2}\ \mathrm{Sech}(\tau - t_0)(1 - 2\ \mathrm{Sech}^2(\tau - t_0)) \\ & - (T_1'' - k_0)\sqrt{2}\ \mathrm{Sinh}(\tau - t_0)\ \mathrm{Sech}^2(\tau - t_0) \\ & - 6f_0\ \mathrm{Sech}^2(\tau - t_0)\ \mathrm{Cos}\ \omega t. \end{aligned} \tag{5.1.28}$$

Now as $\tau \to \infty$, the dominant terms of (5.1.28) are such that

$$\begin{aligned} f(\tau) \approx {} & 2\sqrt{2}(k_0 + 2T_1' - T_1'')(e^{-(\tau-t_0)} + 0(e^{-3(\tau-t_0)})) \\ & - 32T_1'\sqrt{2}(e^{-3(\tau-t_0)} + 0(e^{-5(\tau-t_0)})) \\ & + 0(e^{-2(\tau-t_0)}) \end{aligned} \tag{5.1.29}$$

and the corresponding linear differential equation modelling the behaviour as $\tau \to \infty$ is

$$X_1'' + (24e^{-2(\tau-t_0)} - 1)X_1 = De^{-(\tau-t_0)} \tag{5.1.30}$$

where $D = 2\sqrt{2}(k_0 + 2T_1' - T_1'')$.

Eqn(5.1.30) has solution

$$X_1(\tau) = a_0 e^{(\tau - t_0)}, \quad a_0 \text{ constant} \tag{5.1.31}$$

which produces exponential growth as $\tau \to \infty$. In a similar way when $\tau \to -\infty$ we find the corresponding linear equation yielding a solution

$$X_1(\tau) = b_0 e^{-(\tau - t_0)}, \quad b_0 \text{ constant} \tag{5.1.32}$$

which also produces unwanted exponential growth. Such solutions can be avoided by choosing T_1 correctly. We do this by eliminating those terms in (5.1.28) that give rise to these unbounded exponential solutions by putting

$$2T_1'\sqrt{2}\ \mathrm{Sech}(\tau - t_0) - (T_1'' - k_0)\sqrt{2}\ \mathrm{Sinh}(\tau - t_0)$$

$$\mathrm{Sech}^2(\tau - t_0) = 0. \tag{5.1.33}$$

Thus

$$T'' - 2\ \mathrm{Coth}(\tau - t_0)T' = k_0$$

and we note that there is a singularity at $\tau = t_0$.

Hence,

$$\frac{d}{d\tau}\left(\frac{T'}{\mathrm{Sinh}^2(\tau - t_0)}\right) = \frac{k_0}{\mathrm{Sinh}^2(\tau - t_0)}$$

$$\Rightarrow \frac{T_1'}{\mathrm{Sinh}^2(\tau - t_0)} = A_1 - k_0\ \mathrm{Coth}(\tau - t_0).$$

Thus

$$T_1' = A_1 \operatorname{Sinh}^2(\tau - t_0) - \frac{k_0}{2} \operatorname{Sinh}(\tau - t_0)$$

$$\Rightarrow T_1 = \frac{A_1}{4} \operatorname{Sinh} 2(\tau - t_0) - \frac{A_1}{2}(\tau - t_0)$$

$$- \frac{k_0}{4} \operatorname{Cosh} 2(\tau - t_0) + B_1. \qquad (5.1.34)$$

We require a continuous smooth co-ordinate perturbation which is such that the local saddle behaviour matches the behaviour given by (5.1.9). As $\tau \to -\infty$ the local approximation given by (5.1.26) is $X(\tau) = 2\sqrt{2}e^{\tau - t_0}$. This must agree locally with (5.1.9a), that is $X(\tau) = Ae^{h(\tau)}$, where $h(\tau) = \tau + \varepsilon(T_1(\tau) - \frac{k_0}{2}\tau) + \ldots$. Hence, $T_1(\tau) \simeq \frac{k_0}{2}\tau$ as $\tau \to -\infty$ as there are no ε-terms present in solution (5.1.9a). A similar argument reveals that $T_1(\tau) \simeq -\frac{k_0}{2}\tau$ as $\tau \to \infty$.

Applying these conditions to Eqn(5.1.34) and adding the further condition that $T_1(t_0)$ is the same for both solutions it transpires that for $\tau > t_0$ we put $A_1 = k_0$ and for $\tau < t_0$ we put $A_1 = -k_0$ with $B_1 = 0$ in both cases. Hence, when $\tau > t_0$,

$$T_1 = -\frac{k_0}{4}e^{-2(\tau - t_0)} - \frac{k_0}{2}(\tau - t_0)$$

and when $\tau < t_0$

$$T_1 = -\frac{k_0}{4}e^{2(\tau-t_0)} + \frac{k_0}{2}(\tau - t_0)$$

which can be combined in the one smooth solution

$$T_1 = -\frac{k_0}{4}e^{-2|\tau - t_0|} - \frac{k_0}{2}|\tau - t_0|. \qquad (5.1.35)$$

Note that $T_1(t_0) = -k_0/4$ and $T_1'(t_0) = 0$.

It follows that X_1 now satisfies the equation

$$X_1'' + (6\,\mathrm{Sech}^2(\tau - t_0) - 1)X_1 = g(\tau) \qquad (5.1.36)$$

where

$$g(\tau) = -2\sqrt{2}k_0\,\mathrm{Sech}^3(\tau - t_0)[e^{-2|\tau-t_0|} - 1]\,\mathrm{sgn}(\tau - t_0)$$
$$- 6f_0\,\mathrm{Sech}^2(\tau - t_0)\,\mathrm{Cos}\,\omega t. \qquad (5.1.37)$$

Finally in this section we consider the effect the time-transformation has on the trigonometrical term $\mathrm{Cos}\,\omega t$. Substituting in the time-transformation (5.1.12) gives

$$-6f_0\,\mathrm{Sech}^2(\tau - t_0)\,\mathrm{Cos}\,\omega(\tau - \varepsilon T_1(\tau) + \ldots).$$

For τ large and positive $T_1(\tau) \approx -\frac{k_0}{2}\tau$. We can write

$$\mathrm{Cos}\,\omega t = \mathrm{Cos}\,\omega\tau + o(1)$$

provided that $-\frac{\varepsilon}{2}k_0\tau$ is 'small', and this will be valid

at large 'time', $\tau = p(\varepsilon)$ provided that $\varepsilon p(\varepsilon) \to 0$ as $\varepsilon \to 0$. However, as $\tau \to \infty$, the amplitude term, $\mathrm{Sech}^2(\tau - t_0)$ can be approximated by $ke^{-2\tau} \sim ke^{-2p(\varepsilon)}$ which is exponentially small as $p(\varepsilon) \to \infty$, $\varepsilon \to 0$. Even though the cosine function may get out of phase for $|\tau|$ large the amplitude term disposes of it anyway. The same argument applies when τ is large and negative.

Substituting in (5.1.27) the function $T_1(\tau)$ given by (5.1.34) and replacing Cos ωt by Cos $\omega\tau$ gives the new equation for X_1,

$$X_1'' + (6\ \mathrm{Sech}^2(\tau - t_0) - 1)X_1 = g(\tau, t_0) \qquad (5.1.38)$$

where

$$g(\tau, t_0) = -2\sqrt{2}k_0\ \mathrm{Sech}^3(\tau - t_0)[e^{-2|\tau - t_0|} - 1]$$
$$\mathrm{sgn}(\tau - t_0) - 6f_0\ \mathrm{Sech}^2(\tau - t_0)\ \mathrm{Cos}\ \omega\tau \qquad (5.1.39)$$

subject to initial conditions (5.1.23) and (5.1.25).

5.2 SIMPLE SADDLE CONNECTIONS

Although it is possible to obtain explicitly the perturbation $X_1(\tau)$ given by (5.1.38) it is unnecessary at this juncture since the conditions for saddle connections to occur can be obtained using the solutions of the homogeneous linear differential equation

$$X'' + [6\ \mathrm{Sech}^2(\tau - t_0) - 1]X = 0 \qquad (5.2.1)$$

which is equation (5.1.38) with the forcing term $g(\tau)$ set to zero.

This type of equation has been much investigated by such authors as Cesari (1970), Bellman (1950) and Hille (1969) and an interesting feature of this linear equation is that an exact solution can be constructed. It is easy to show that (5.2.1) has a solution $u_1(\tau)$ given by

$$u_1(\tau, t_0) = \mathrm{Sinh}(\tau - t_0)\ \mathrm{Sech}^2(\tau - t_0). \qquad (5.2.2)$$

Using Abel's formula (see Kreider (1966)) it is possible to find the general solution of (5.2.1) now that we have one nontrivial solution of the equation. A second solution of (5.2.1) is found using

$$u_2(\tau, t_0) = u_1(\tau, t_0)\int \frac{d\tau}{[u_1(\tau, t_0)]^2}$$

$$= \mathrm{Sinh}(\tau - t_0)\ \mathrm{Sech}^2(\tau - t_0)\int \frac{\mathrm{Cosh}^4(\tau - t_0)\,d\tau}{\mathrm{Sinh}^2(\tau - t_0)} \qquad (5.2.3)$$

giving

$$u_2(\tau, t_0) = \tfrac{3}{2}(\tau - t_0)\ \mathrm{Sinh}(\tau - t_0)\ \mathrm{Sech}^2(\tau - t_0) -$$

$$- \tfrac{3}{2}\ \mathrm{Sech}(\tau - t_0) + \tfrac{1}{2}\ \mathrm{Cosh}(\tau - t_0). \qquad (5.2.4)$$

Note that

$$u_1(t_0, t_0) = 0 \qquad u_1'(t_0, t_0) = 1$$

$$u_2(t_0, t_0) = -1 \qquad u_2'(t_0, t_0) = 0.$$

Employing the method of variation of parameters whereby a particular solution for the nonhomogeneous linear differential equation (5.1.38) can be constructed out of the general solution of its associated homogeneous equation (see Kreider, 1966), the general solution of (5.1.38) can be written

$$X_1(\tau) = A_0u_1(\tau, t_0) + B_0u_2(\tau, t_0) + \int_{t_0}^{\tau} G(\tau, s)ds \tag{5.2.5}$$

where

$$G(\tau, s) = \frac{u_2(\tau, t_0)u_1(s, t_0) - u_1(\tau, t_0)u_2(s, t_0)}{W[u_1(s, t_0), u_2(s, t_0)]}.$$

The Wronskian, $W[\ ]$, of the linearly independent solutions $u_1(s, t_0)$, $u_2(s, t_0)$ turns out to be 1. The general solution, therefore, can be written

$$X_1(\tau) = A_0u_1(\tau, t_0) + B_0u_2(\tau, t_0) + \int_{t_0}^{\tau} \{u_2(\tau, t_0) \cdot u_1(s, t_0) - u_1(\tau, t_0)u_2(s, t_0)\}g(s, t_0)ds \tag{5.2.6}$$

where from (5.1.23) and (5.1.25)

$$X_1(t_0) = \beta$$

$$X_1'(t_0) = \frac{k_0\sqrt{2}}{4}. \tag{5.2.7}$$

These boundary conditions are satisfied when

$$B_0 = -\beta$$

and

$$A_0 = \frac{k_0\sqrt{2}}{4} \tag{5.2.8}$$

hence, tne particular solution of (5.1.38) is

$$X_1(\tau) = \frac{k_0}{4}\sqrt{2}u_1(\tau, t_0) - \beta u_2(\tau, t_0) + \int_{t_0}^{\tau} \{u_2(\tau, t_0)$$

$$u_1(s, t_0) - u_1(\tau, t_0)u_2(s, t_0)\}g(s, t_0)ds. \tag{5.2.9}$$

Now the main solution

$$X(t) = X_0(\tau) + \varepsilon X_1(\tau) + \ldots$$

starts from the origin if $X \to 0$ as $\tau \to -\infty$. This is immediately satisfied by $X_0(\tau)$. Thus we require that

$$\lim_{\tau \to -\infty} X_1(\tau) = 0.$$

As $\tau \to -\infty$ so $u_1(\tau, t_0) \to 0$ and $u_2(\tau, t_0) \to \infty$, hence we can write (5.2.9) as

$$X_1(-\infty) = 0 = -\beta u_2(-\infty, t_0) + u_2(-\infty, t_0)\int_{t_0}^{\tau} u_1(s, t_0)$$

$$g(s, t_0)ds$$

from which

$$\beta = \int_{t_0}^{-\infty} u_1(s, t_0)g(s, t_0)ds. \tag{5.2.10}$$

The solution also approaches the origin as $\tau \to \infty$ with $u_1(\tau) \to 0$ and $u_2(\tau) \to \infty$ as $\tau \to \infty$. This time it turns out that

$$\beta = \int_{t_0}^{\infty} u_1(s, t_0)g(s, t_0)ds. \tag{5.2.11}$$

Finally a saddle connection occurs when the result of the two integrals (5.2.10) and (5.2.11) are equal, that is,

$$\int_{t_0}^{-\infty} u_1(s, t_0)g(s, t_0)ds = \int_{t_0}^{\infty} u_1(s, t_0)g(s, t_0)ds. \tag{5.2.12}$$

Hence a saddle connection occurs if t_0 satisfies

$$\int_{-\infty}^{\infty} u_1(s, t_0)g(s, t_0)ds = 0. \tag{5.2.13}$$

Denote the integral on the left of (5.2.13) by $I(t_0)$. Then, evaluation of the integral (see Appendix B) leads to

$$I(t_0) = \tfrac{2}{3}k_0\sqrt{2} - f\pi\omega \operatorname{Sech}(\tfrac{1}{2}\pi\omega) \operatorname{Sin} \omega t_0 = 0 \qquad (5.2.14)$$

since $f_0 = -\dfrac{F}{(1+\omega^2)}$.

Real solutions of (5.2.14) exist provided that

$$|\operatorname{Sin} \omega t_0| = \left|\frac{2k_0\sqrt{2}\ \operatorname{Cosh}(\tfrac{1}{2}\pi\omega)}{3f\pi\omega}\right| \leq 1 \qquad (5.2.15)$$

but as the expression is always greater than zero then $t_0 \in [0, \pi/\omega[\bmod \pi/\omega$. Single saddle connections must occur at the critical time $t_0 = \pi/2\omega$, hence the corresponding critical forcing amplitude and frequency, F_c and ω_c, are related by

$$F_c = \frac{2\sqrt{2}k\ \operatorname{Cosh}(\tfrac{1}{2}\pi\omega_c)}{3\pi\omega_c} \qquad (5.2.16)$$

which agrees with the previous result of Chapter 3 obtained using Mel'nikov's method. See also Holmes (1979) and Barenblatt (1983). This technique gives the saddle connections which lie in the $X > 0$ half plane for which $t_0 = \pi/2\omega \pmod{2\pi/\omega}$. The saddle connections for $X < 0$ are considered in section (5.4) although computer plots are shown prior to this.

Fig(5.2a,c] display saddle connections for parameters $F = 0.26843$, $\omega = 1.2$ and $F = 0.2$, $\omega = 1.0837$ with $k = 0.316$ throughout. These values should be compared to the critical values $F = 0.266$, $\omega = 1.2$ and $F = 0.25$, $\omega = 1.0967$ predicted by (5.2.16). The saddle

connections in the $X > 0$ half-plane were obtained by solving numerically the differential equation (5.1.4), using a standard Runge-Kutta method, with the correct initial conditions (X, X') located in the first quadrant close to the saddle point S at time $t = 0$. As $X'(0) = m_1 X(0)$ on the saddle solution close to S, where $m_1 = 1 - k/2$, one need only search for the correct $X(0)$ such that the solution runs back into S again. The same procedure is employed to find saddle connections in the $X < 0$ half-plane but with initial condition this time located in the third quadrant. In either case, if the initial conditions are not chosen carefully, the solution will not return to the saddle point. An alternative approach is to fix X and X' close to S and search for the correct starting times.

Fig[5.2b,d] show the Duffing saddle connections corresponding to the right-hand sides of Fig[5.2a,c] respectively. The displacement $x(t)$ is obtained by adding the unstable $2\pi/\omega$-periodic displacement, given by (5.1.2), to the displacement $X(t)$. The periodic solution, $p(t)$, is affected at all times by the value of $X(t)$ thus destroying its periodicity although for t large (positive and negative) the periodicity of the solution is practically restored since the contribution from $X(t)$ for these times is neglegible. The peaks, in both cases occur at $t_0 = 5\pi/2\omega$ (a solution of $\sin \omega t_0 = 1$) with maximum displacements $\sqrt{2} + \varepsilon\beta \approx 1.445$ throughout.

When the control parameter F is increased or ω

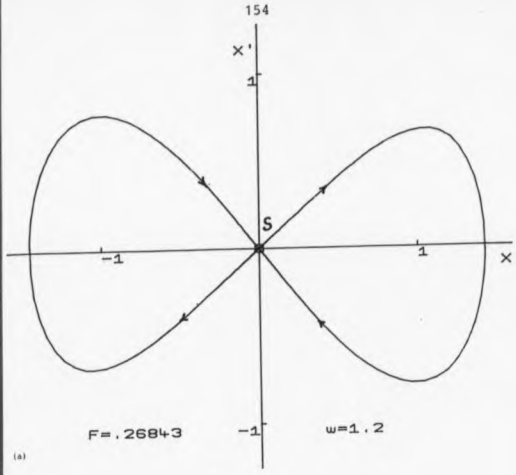

(a)

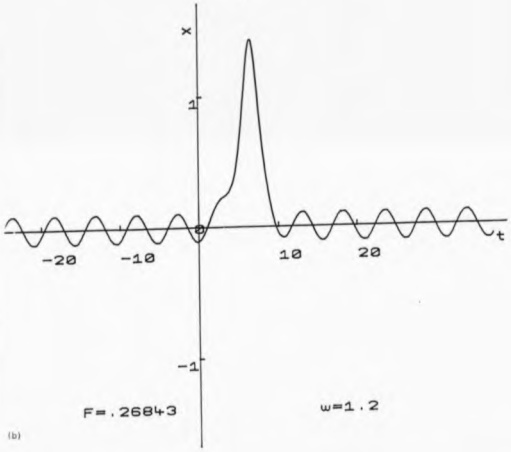

(b)

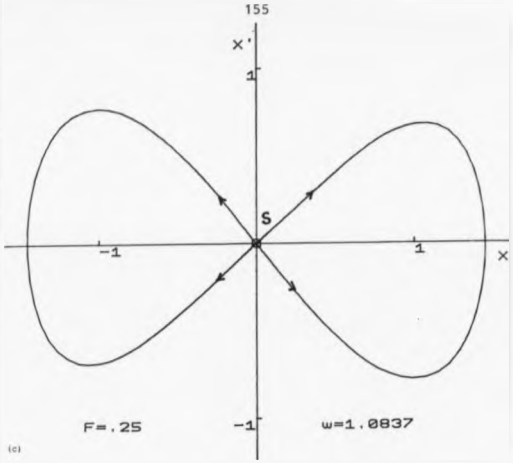

(c)

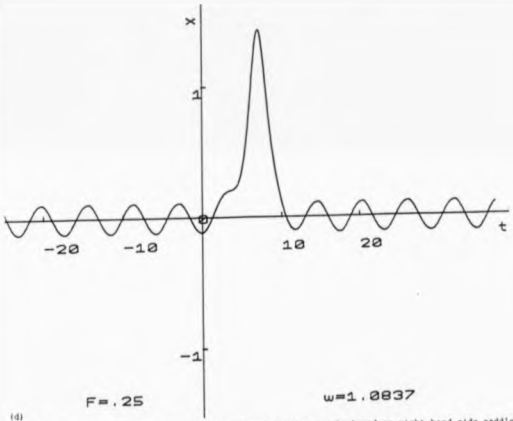

(d)

FIG[5.2] Single saddle connections and displacement/time graphs based on right-hand side saddle solutions.

decreased beyond the critical values associated with homoclinic tangency each tangency point bifurcates to become a pair of transverse homoclinic intersections. Likewise, the single saddle connections in each of the two half-planes also bifurcate into pairs of simple saddle connections for which intersection times with the $X > 0$ axis are given by solutions of (5.2.15) in the principle range $0 \leq t < \pi/\omega$. Let these times be t_{01} and t_{02} where $t_{01} < t_{02}$. To determine where each of these solutions cuts the X-axis we need to find the value of β using either (5.2.10) or (5.2.11) where t_0 is replaced by t_{01} (t_{02}). Choosing (5.2.11)

$$\beta = \int_{t_{01}}^{\infty} u_1(s)g(s)ds \tag{5.2.17}$$

gives [see Appendix D]

$$\beta = \frac{\sqrt{2}}{3}k_0 - 6f_0[I \text{ Cos } \omega t_{01} - J \text{ Sin } \omega t_{01}] \tag{5.2.18}$$

where

$$I = \frac{1}{6}(\omega^2 + 2) + \frac{\pi\omega}{12}(\omega^2 + 1) \text{ Tanh}(\tfrac{1}{2}\pi\omega) - \frac{2}{3}\omega^2(\omega^2 + 1) \sum_{n=0}^{\infty} \frac{1}{\omega^2 + (4n + 1)^2} \tag{5.2.19}$$

$$J = \frac{\pi\omega}{12}(\omega^2 + 1) \text{ Sech}(\tfrac{1}{2}\pi\omega). \tag{5.2.20}$$

Hence, the saddle connections cut the X-axis where

$$X(t_{01},\ \varepsilon) = \sqrt{2} - 6f_0\varepsilon I \cos \omega t_{01} + O(\varepsilon^2) \qquad (5.2.21)$$

$$X(t_{02},\ \varepsilon) = \sqrt{2} - 6f_0\varepsilon I \cos \omega t_{01} + O(\varepsilon^2) \qquad (5.2.22)$$

since $J \sin \omega t_{01} = J \sin \omega t_{02} = -\frac{\sqrt{2}k_0}{3}$.

The double saddle connections shown in Fig[5.3a,c] were computed in the same way as the single connections in Fig[5.2]. For a known forcing amplitude F or forcing frequency ω the corresponding parameter (ω or F) can be found from result (5.2.16) enabling a search to be undertaken in the vicinity of the predicted value. Initial conditions chosen very close to S at times $t = 0$ give intersection times t_{01}, t_{02} such that $t_{01} + t_{02} = (4n + 1)\pi/\omega$, $n = (0, 1, 2, \ldots)$ for solutions in the $X > 0$ half plane and $t_{01} + t_{02} = (4n + 3)\pi/\omega$ for solutions in the $X < 0$ half plane. This difference in time totals is explained in section (5.4). Also, the two formulae assume that t_{01} and t_{02} are solutions of (5.2.15) within the same half cycle. If this is not the case, it depending upon the initial conditions, we can state simply that the time total $t_{01} + t_{02}$ will be an odd integer multiple of π/ω in either half plane.

Listed in Table [5.1] are all the initial conditions (at $t = 0$), the X-intersections and intersection times for all the saddle connections in Fig[5.3a] and Fig[5.3c].

Finally, Fig[5.3b] and Fig[5.3d] show pairs of

saddle connections of Duffing's equation obtained from Fig[5.3a] and Fig[5.3b] respectively for X > 0.

TABLE [5.1]

	X	X'	t_{01}	t_{02}	$X(t_{01})$	$X(t_{02})$
Fig[5.3a] F = .28 ω = 1.2	0.01415	0.0119	6.225		1.477	
	0.00793	0.0067		6.7		1.407
	-0.13048	-0.1094	3.6		-1.477	
	-0.07365	-0.062		4.0875		-1.407
Fig[5.3c] F = .25 ω = 1.0	0.00464	0.0039	7.45		1.49	
	0.00247	0.0021		8.025		1.403
	-0.0673	-0.0567	4.33		-1.494	
	-0.03606	-0.0304		4.875		-1.403

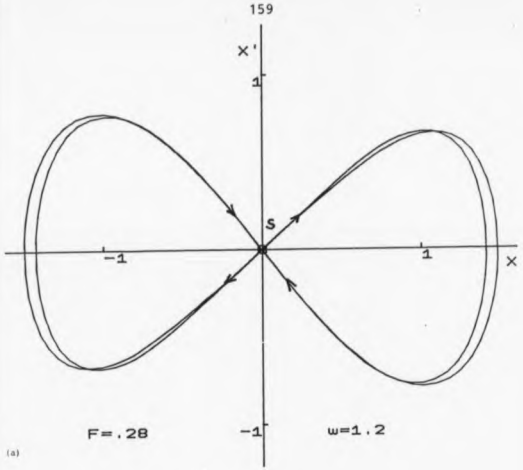

(a)

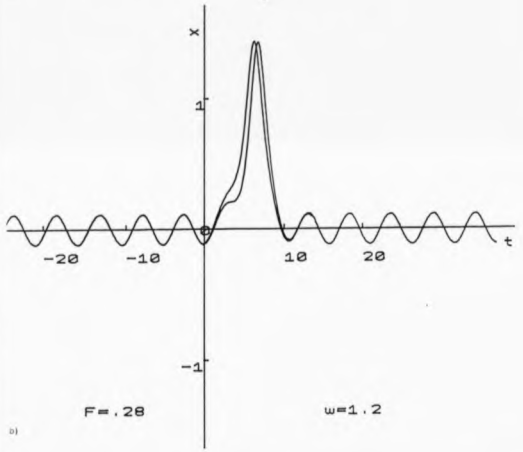

(b)

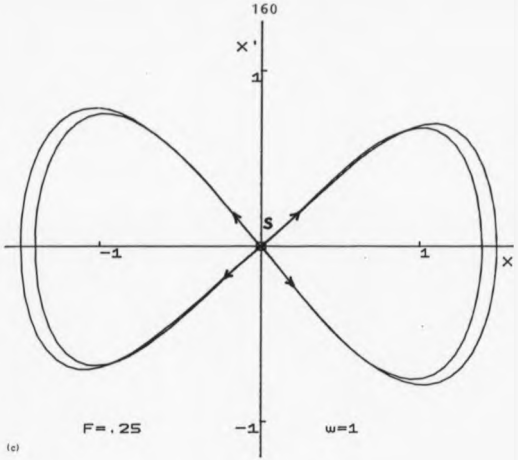

(c)

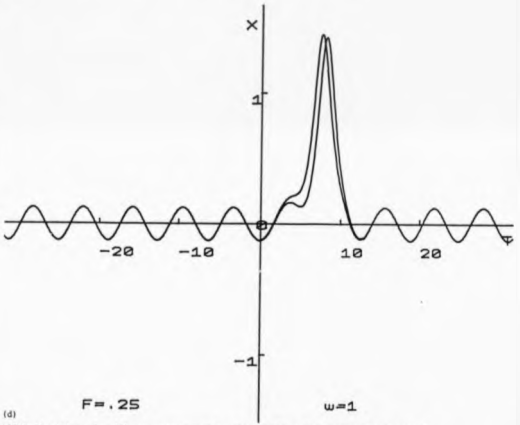

(d)

FIG[5.3] Pairs of saddle connections and corresponding displacement/time graphs.

5.3 DOUBLE LOOP CONNECTIONS

The question arises: are 'single loop' saddle connections the only type possible? Or can we have saddle connections which loop X = 1 more than once before entering X = 0 (and similarly X = -1)? In Fig[5.4] the loop which has tangential contact at B with the unstable

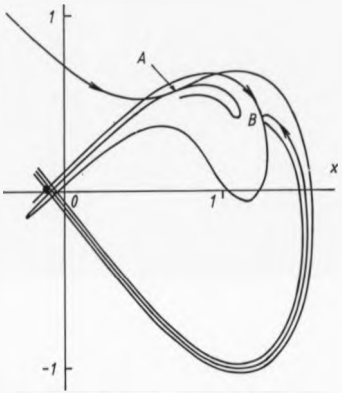

FIG(5.4) manifold behaviour corresponding to multiple loop saddle connections.

manifold of Duffing's equation (5.1.1) is a segment of the stable manifold at prior times. The first return of B occurs at A where the stable manifold has contact with an interior loop of the unstable manifold. The saddle connection which passes through both B and P reveals at least two loops which surround X = 1. For $F > F_c$ or $\omega < \omega_c$ there must exist many saddle connections which loop X = 1 (likewise X = -1) many times before returning to the saddle point or the unstable periodic solution of Duffing's equation.

Consider an unstable solution from S in the (X, X') plane which first cuts the positive X-axis at P at time $t = t_0$ in Fig[5.5a]. Call this solution $X_u(t, \varepsilon)$. At point P, $X_u(t_0, \varepsilon) = \sqrt{2} + \varepsilon\beta$ and $X_u'(t_0, \varepsilon) = 0$. As the solution continues it cuts the positive X axis again at Q at time t_1 at which point $X_u'(t_1, \varepsilon) = 0$, or, from (5.1.17)

$$X_{u0}'(\tau_1) + \varepsilon(X_{u1}'(\tau_1) - X_{u0}''(\tau_1)T_1'(\tau_1)) + \ldots O(\varepsilon^2) = 0 \qquad (5.3.1)$$

where $t_1 = \tau_1 + \varepsilon T_1(\tau_1) + \ldots O(\varepsilon^2)$.

The solution $X_u(t, \varepsilon)$ takes the form

$$X_u(t, \varepsilon) = X_{u0}(\tau) + \varepsilon X_{u1}(\tau) + \ldots O(\varepsilon^2)$$

where

$$X_{u0}(\tau) = \sqrt{2}\ \mathrm{Sech}(\tau - t_0) \qquad (5.3.2a)$$

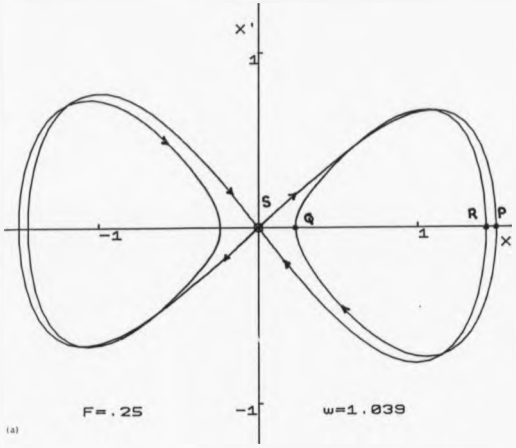

(a)

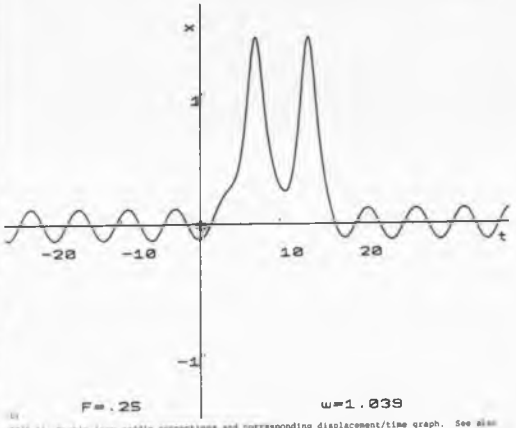

(b)

(10)(5.5) Double loop saddle connections and corresponding displacement/time graph. See also Fig(5.9).

and

$$X_{u1}(\tau) = \frac{k_0}{4}u_1(\tau, t_0) + u_2(\tau, t_0)\int_{-\infty}^{\tau} u_1(s, t_0)g(s, t_0)ds$$

$$- u_1(\tau, t_0)\int_{t_0}^{\tau} u_2(s, t_0)g(s, t_0)ds \qquad (5.3.2b)$$

where β has been replaced in (5.2.9) by its integral form (5.2.10). An important requirement here is that the time difference between points P and Q should be large, in fact we would expect that $t_1 - t_0 \to \infty$ as $\varepsilon \to 0$ since, in this limit, the solution must approach the separatrix of the unperturbed system. This requirement is clearly met by those solutions that pass slowly close to the saddle point S and we can find t_1 by considering the dominant terms only of the boundary condition (5.3.1). Noting that the dominant terms of $u_1(\tau_1, t_0)$ and $u_2(\tau_1, t_0)$ are $\mathrm{Sinh}(\tau_1 - t_0)\ \mathrm{Sech}^2(\tau - t_0)$ and $\frac{1}{2}\mathrm{Sech}(\tau_1 - t_0)\ \mathrm{Sinh}^2(\tau_1 - t_0)$ respectively, (5.3.1) reduces to

$$-2\sqrt{2}e^{-(\tau_1 - t_0)} + \frac{\varepsilon}{4}e^{(\tau_1 - t_0)}\int_{-\infty}^{\tau_1} u_1(s, t_0)g(s, t_0)ds = 0 \qquad (5.3.3)$$

for $\tau_1 - t_0$ large. In addition this large time difference allows us to replace the upper limit of the integral in (5.3.3) by ∞ since the integral remainder is asymptotically negligible. Therefore, using the result of (5.2.13), (5.3.3) becomes

$$-2\sqrt{2}e^{-(\tau_1-t_0)} + \frac{\varepsilon}{4}e^{(\tau_1-t_0)}I(t_0) = 0. \tag{5.3.4}$$

Hence t_1 or τ_1 satisfies

$$t_1 - t_0 = \tau_1 - t_0 = -\frac{1}{2}\ln\varepsilon - \frac{1}{2}\ln\{\sqrt{2}I(t_0)/16\} + o(1). \tag{5.3.5}$$

At this time,

$$\begin{aligned} X_u(t_1) &= X_{u0}(\tau_1) + \varepsilon X_{u1}(\tau_1) + \ldots \\ &= \sqrt{2}\,\mathrm{Sech}(\tau_1 - t_0) + \frac{\varepsilon}{4}k_0\sqrt{2}u_1(\tau_1, t_0) \\ &\quad + \varepsilon u_2(\tau_1, t_0)\int_{-\infty}^{\tau_1} u_1(s, t_0)g(s, t_0)ds \\ &\quad - \varepsilon u_1(\tau_1, t_0)\int_{t_0}^{\tau_1} u_2(s, t_0)g(s, t_0)ds \end{aligned} \tag{5.3.6}$$

from (5.3.2). Now for τ_1 large (positive) the following asymptotic approximations hold,

$$X_{u0}(\tau_1) \approx 2\sqrt{2}e^{-(\tau_1-t_0)} \tag{5.3.7a}$$

$$u_1(\tau_1, t_0) \approx 2e^{-(\tau_1-t_0)} \tag{5.3.7b}$$

$$u_2(\tau_1, t_0) \approx \frac{1}{4}e^{(\tau_1-t_0)} \tag{5.3.7c}$$

$$\int_{-\infty}^{\tau_1} u_1(s, t_0)g(s, t_0)ds \approx I(t_0) \tag{5.3.7d}$$

yielding the leading order approximation

$$X(t_1) \approx 2\sqrt{2}e^{-(\tau_1 - t_0)} + \frac{1}{4}\varepsilon e^{(\tau_1 - t_0)} I(t_0) + o(\varepsilon). \qquad (5.3.8)$$

Substituting in the time $\tau_1 - t_0$ given in (5.3.5) the intersection with the X axis is given by

$$X_u(t_1) \approx 2^{\frac{1}{2}}[\varepsilon I(t_0)]^{\frac{1}{2}} + \ldots + o(\sqrt{\varepsilon}). \qquad (5.3.9)$$

The same approach can be applied to the solution SRQ. Call this solution $X_s(t, \varepsilon)$ and assume that it passes through R at time $t = t_2$. This solution can be expressed in the form

$$X_s(t, \varepsilon) = X_{s0}(\tau) + \varepsilon X_{s1}(\tau) \qquad (5.3.10)$$

where

$$X_{s0}(\tau) = \sqrt{2}\ \mathrm{Sech}(\tau - t_2) \qquad (5.3.11a)$$

and

$$X_{s1}(\tau) = \frac{k_0}{4}\sqrt{2}u_1(\tau, t_2) - u_2(\tau, t_2)\int_{\tau}^{\infty} u_1(s, t_2)g(s, t_2)ds$$

$$- u_1(\tau, t_2)\int_{t_2}^{\tau} u_2(s, t_2)g(s, t_2)ds \qquad (5.3.11b)$$

where, as in the previous case, β has been replaced in (5.2.9) but this time by its integral form (5.2.11). At Q, $X_s'(t_1, \varepsilon) = 0$ or

$$X_{s0}'(\tau_1) + \varepsilon(X_{s1}'(\tau_1) - X_{s0}'(\tau_1)T_1'(\tau_1)) + \ldots O(\varepsilon^2) = 0$$

(5.3.12)

where $t_1 = \tau_1 + \varepsilon T_1(\tau_1) + \ldots O(\varepsilon^2)$ as before.

Again we look to asymptotic conditions to help us find the time t_2. Here the behaviour of $X_s(t_1, \varepsilon)$ has to be considered for large negative time since the time difference at Q and R is such that $t_1 - t_2 \to -\infty$ as $\varepsilon \to 0$ for the solution to approach the separatrix of the unperturbed system. Considering only the dominant terms of (5.3.12) the boundary condition reduces to

$$2\sqrt{2}e^{(\tau_1 - t_2)} + \frac{\varepsilon}{4}e^{-(\tau_1 - t_2)}\int_{-\infty}^{\tau_1} u_1(s, t_2)g(s, t_2)ds = 0$$

(5.3.13)

for $\tau_1 - t_2$ large (negative). Hence, t_1 (and τ_1) satisfy

$$t_1 - t_2 = \tau_1 - t_2 = \frac{1}{2}\ln\varepsilon + \frac{1}{2}\ln[-\sqrt{2}I(t_2)/16] + o(1).$$

(5.3.14)

At this time

$$X_s(t_1) = X_{s0}(\tau) + \varepsilon X_{s1}(\tau_1) + \ldots O(\varepsilon^2)$$

$$= \sqrt{2}\,\mathrm{sech}(\tau_1 - t_2) + \frac{\varepsilon}{4}k_0\sqrt{2}u_1(\tau_1, t_2)$$

$$+ \varepsilon u_2(\tau_1, t_2)\int_{\tau_1}^{\infty} u_1(s, t_2)g(s, t_2)ds$$

$$-\varepsilon u_1(\tau_1, t_2)\int_{t_2}^{\tau_1} u_2(s, t_2)g(s, t_2)\,ds. \qquad (5.3.15)$$

For τ_1 large negative the following asymptotic approximations hold,

$$X_{s0}(\tau_1) \approx 2\sqrt{2}e^{(\tau_1 - t_2)} \tag{5.3.16a}$$

$$u_1(\tau_1, t_2) \approx -2e^{(\tau_1 - t_2)} \tag{5.3.16b}$$

$$u_2(\tau_1, t_2) \approx \frac{1}{4}e^{-(\tau_1 - t_2)} \tag{5.3.16c}$$

$$\int_{\tau_1}^{\infty} u_2(s, t_2)g(s, t_2)ds \approx I(t_2) \tag{5.3.16d}$$

yielding the leading order approximation

$$X_s(t_1) \approx 2\sqrt{2}e^{(\tau_1 - t_2)} - \frac{3}{4}e^{-(\tau_1 - t_2)}I(t_2) + o(\varepsilon). \tag{5.3.17}$$

As before substitute in the time $\tau_1 - t_2$ given in (5.3.14) and the intersection with the X-axis is given by

$$X_s(t_1) \approx 2^{\frac{3}{2}}[-\varepsilon I(t_2)]^{\frac{1}{2}} + \ldots o(\sqrt{\varepsilon}). \tag{5.3.18}$$

For continuity of solution at Q we require

$$X_u(t_1) = X_s(t_1) \tag{5.3.19}$$

for the same time t_1 given by both (5.3.5) and (5.3.14). Hence,

$$I(t_0) = -I(t_2) \tag{5.3.20}$$

and from (5.3.5) and (5.3.14)

$$t_0 - t_2 = \ln\varepsilon + \ln[\sqrt{2}I(t_0)/16]$$

or

$$8\sqrt{2}e^{-(t_2-t_0)} = \varepsilon I(t_0). \qquad (5.3.21)$$

From (5.3.20) and (5.3.21) it follows that

$$\text{Sin } \omega t_0 = F_c(k - 12e^{-(t_2-t_0)})/(Fk) = M \qquad (5.3.22)$$

$$\text{Sin } \omega t_2 = F_c(k + 12e^{-(t_2-t_0)})/(Fk) = N > 0 \qquad (5.3.23)$$

in terms of the original parameters. Real solutions for t_0 and t_2 exist if $|M| \leq 1$ and $|N| \leq 1$. Suppose that $M = x - y$ and $N = x + y$ where

$$x = F_c/(Fk) \geq 0$$

and

$$y = \frac{12F_c}{(Fk)}e^{-(t_2-t_0)} \geq 0$$

then Fig[5.6] shows the regions of solutions satisfying the two conditions where $|M| \leq 1$ has 'positive' shading (///) and $|N| \leq 1$ has 'negative' shading (\\\). Clearly, $|N| \leq 1$ guarantees solutions for both inequalities. Further we expect the following conditions to hold,

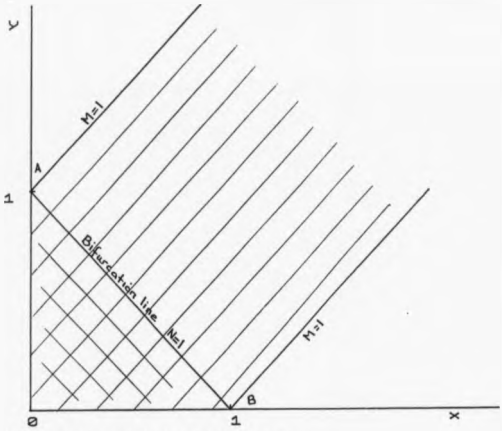

FIG[5.6] Solutions exist for t_0 and t_2 in the region OAB.

$$0 \leq F_c/(Fk) \leq 1 \qquad (5.3.24a)$$

and

$$0 \leq \frac{12F_c}{(Fk)^2}e^{-(t_2-t_0)} \leq 1. \qquad (5.3.24b)$$

Therefore real solutions for t_0 and t_2 can exist only if

$$F \geq F_c\{k + 12e^{-(t_2-t_0)}\}/k \qquad (5.3.25)$$

and bifurcation take place at equality in (5.3.25) where $\sin \omega t_2 = 1$. Consequently, we can write

$$\begin{aligned}\cos \omega(t_2 - t_0) &= \cos \omega t_2 \cos \omega t_0 + \sin \omega t_2 \sin \omega t_0 \\ &= \sin \omega t_0 \\ &= \frac{F_c}{F}\left\{1 - \frac{12}{k}e^{-(t_2-t_0)}\right\} \\ &= \frac{F_c}{F}\left\{1 - \left(\frac{F}{F_c} - 1\right)\right\}, \quad \text{from N = 1} \\ &= \frac{2F_c}{F} - 1.\end{aligned}$$

Hence,

$$F = F_c \sec^2\{\tfrac{1}{2}\omega(t_2 - t_0)\}. \qquad (5.3.26)$$

Therefore, the critical values of F are given by simultaneous solutions of

$$F = F_c \sec^2\{\tfrac{1}{2}\omega(t_2 - t_0)\} = F_c\{k + 12e^{-(t_2-t_0)}\}/k \qquad (5.3.27)$$

given by the intersections of the two curves in Fig[5.7].

Solutions of (5.3.27) appear in pairs about the time values $\omega(t_2 - t_0) = 2n\pi$ (n = 1, 2, 3, ...). Each pair of F values, (F_1, F_2), (F_3, F_4) ... corresponds to homoclinic tangency on 'outgoing' and 'ingoing' windings

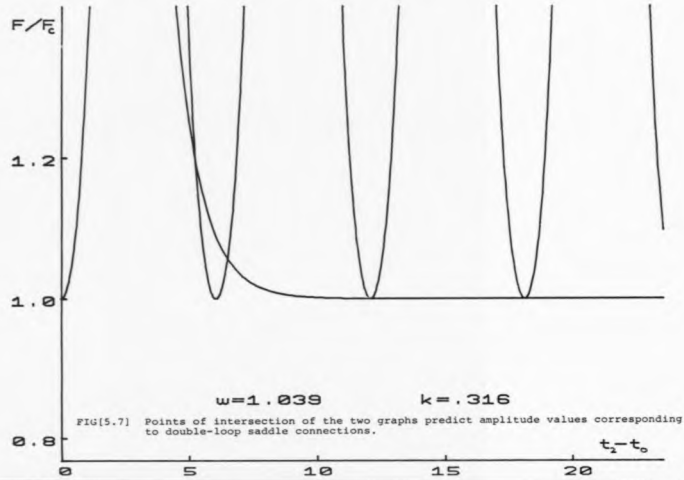

FIG[5.7] Points of intersection of the two graphs predict amplitude values corresponding to double-loop saddle connections.

of the unstable manifold of the Poincaré map as depicted in Fig[5.8]. This is strongly suggested by Fig[3.4e] and Fig[5.4]. Clearly, there is a discrete unbounded set of such homoclinic tangency points of the type shown that approach the initial $F = F_c$ tangency point. As $t_2 - t_0 \to \infty$ double loop connections pass slowly very close to the saddle point at $X = 0$. In this limit these

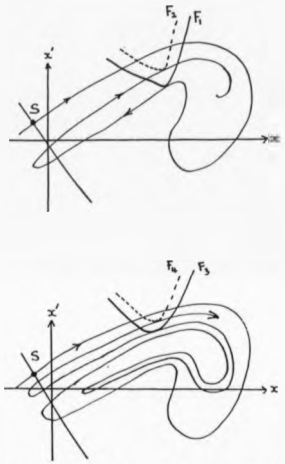

FIG[5.8] Manifold behaviour showing homoclinic tangencies corresponding to double loop saddle connection. NB. For each new F-value here there is a corresponding change in the manifold diagram.

solutions tend to the single loop connection associated with $F = F_c$. In fact, (5.3.27) confirms that as $t_2 - t_0 \to \infty$ so $F \to F_c$.

As $t_2 - t_0 \to \infty$ we can easily estimate the solutions of (5.3.27) using Taylor's series. Let these solutions occur when $t_2 - t_0 = 2n\pi/\omega + \varepsilon$, $\varepsilon << 1$. Substituting these times into (5.3.27) and expanding in terms of ε up to ε^2, ε satisfies,

$$(\omega^2 k - 24E_n)\varepsilon^2 + 48E_n\varepsilon - 48E_n = 0 \qquad (5.3.28)$$

where $E_n = \exp(-2n\pi/\omega)$. Hence,

$$\varepsilon_{1,2} = \frac{-24E_n \pm 4\sqrt{3E_n(\omega^2 k - 12E_n)}}{(\omega^2 k - 24E_n)}, \quad \omega^2 k \neq 24E \qquad (5.3.29)$$

and double loop saddle connections occur, approximately, when

$$F = F_c \operatorname{Sec}\left\{\frac{\omega}{2}\varepsilon_1\right\}$$

and (5.3.30)

$$F = F_c \operatorname{Sec}\left\{\frac{\omega}{2}\varepsilon_2\right\}$$

or

$$F = F_c\left\{k + 12E_n e^{-\varepsilon_1}\right\}$$

and (5.3.31)

$$F = F_c\left\{k + 12E_n e^{-\varepsilon_2}\right\}.$$

The first pair of solutions (F_1, F_2) satisfying (5.3.27), marked in Fig[5.7], yield critical amplitudes of $F_1 = 0.291$ and 0.255 when $\omega = 1.039$. Numerical investigations found double loop connections at $F = 0.29$ and $F = 0.25$ showing good agreement with the predicted values. The antisymmetric solution pairs are displayed in Fig[5.5a] and Fig[5.9a] respectively.

Fig[5.5b] and Fig[5.9b] show the corresponding saddle connections of Duffing's equation drawn in the (x, t) plane for these parameter values as described in section (5.2). Here the double loop connections translate into the two maximum displacements that run both from and into the almost periodic cosinusoidal response of the unstable periodic solution of Duffing's equation. The second peak must occur at time t_2 satisfying $x(t_2) = X(t_2)$. This is certainly the case for $F = 0.25$, $\omega = 1.039$ but for the slightly larger amplitude of $F = 0.29$ agreement is not so good.

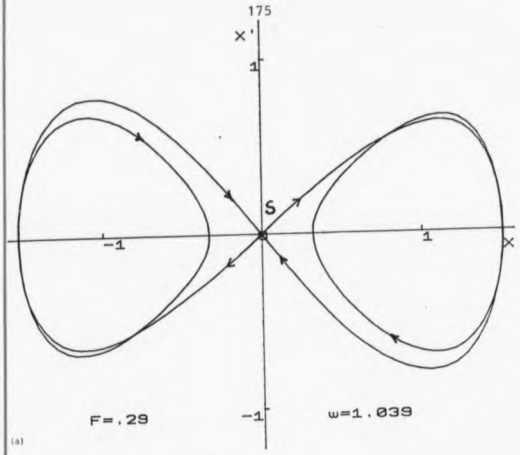

(a)

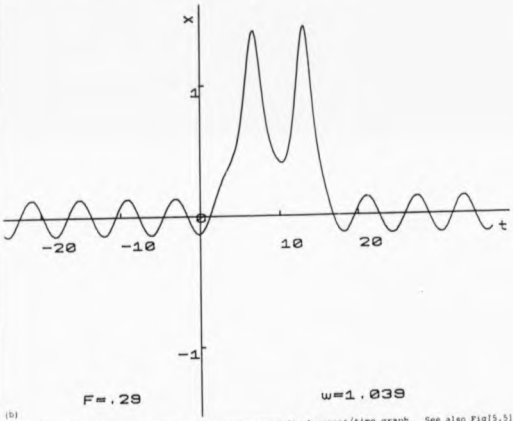

(b)

FIG[5.9] Double saddle connection and corresponding displacement/time graph. See also Fig[5.5].

5.4 CONNECTIONS FOR X < 0

So far the analysis has been confined to saddle connections contained completely in the X > 0 half-plane. Figs[5.2], [5.3], [5.5] and [5.9] reveal that saddle connections also exist in the negative X < 0 half-plane. In order to analyse these connections we introduce two simple transformations of the displacement X and the time t of equation (5.1.4) by writing $X = -\bar{X}$ and $t = \bar{t} + \pi/\omega$. $\bar{X}$ now satisfies the equation

$$\bar{X}'' + \varepsilon k_0 \bar{X}' - \bar{X} + \bar{X}^3 + 3\varepsilon f_0 \bar{X}^2 \operatorname{Cos} \omega\bar{t} = 0 \qquad (5.4.1)$$

where $\bar{X}'$ means differentiation with respect to $\bar{t}$. It has turned out to be the same equation as (5.1.4) which means we are able to analyse (5.4.1) as before but for $\bar{X} > 0$. Thus the conditions for a saddle connection [see (5.2.14)] become

$$I(\bar{t}_0) = \tfrac{2}{3}k_0\sqrt{2} - f\pi\omega \operatorname{Sech}(\tfrac{1}{2}\pi\omega) \operatorname{Sin} \omega\bar{t}_0 = 0 \qquad (5.4.2)$$

or

$$\tfrac{2}{3}k_0\sqrt{2} + f\pi\omega \operatorname{Sech}(\tfrac{1}{2}\pi\omega) \operatorname{Sin} \omega t_0 = 0. \qquad (5.4.3)$$

Hence, the intersection times with the negative X-axis occur (in the critical case) when $\operatorname{Sin} \omega t_0 = -1$ yielding the same result relating F_c and ω_c given by (5.2.16).

The conditions for double loop connections obtained from (5.3.22) and (5.3.23) are

$$\text{Sin } \omega\bar{t}_0 = \frac{F_c}{F}\left[1 - \frac{12}{k}e^{-(\bar{t}_2-\bar{t}_0)}\right] \tag{5.4.4}$$

$$\text{Sin } \omega\bar{t}_2 = \frac{F_c}{F}\left[1 + \frac{12}{k}e^{-(\bar{t}_2-\bar{t}_0)}\right]. \tag{5.4.5}$$

That is,

$$\text{Sin } \omega t_0 = -\frac{F_c}{F}\left[1 - \frac{12}{k}e^{-(t_2-t_0)}\right] \tag{5.4.6}$$

$$\text{Sin } \omega t_2 = -\frac{F_c}{F}\left[1 + \frac{12}{k}e^{-(t_2-t_0)}\right]. \tag{5.4.7}$$

In the critical case when $\text{Sin } \omega t_2 = -1$

$$\text{Cos } \omega(t_2 - t_0) = -\text{Sin } \omega t_0$$
$$= \frac{F_c}{F}\left[1 - \frac{12}{k}e^{-(t_2-t_0)}\right]$$

and Eqns(5.3.26) and (5.3.27) remain unchanged.

These results show conclusively that for each saddle connection in the $X > 0$ half plane there corresponds a saddle connection in the $X < 0$ half plane such that the two connections are antisymmetric, and critical times differ by π/ω.

5.5 TRANSVERSE CONNECTIONS

It was shown in section (5.2) that as the parameter values of the Duffing system are varied and the manifolds proceed through a homoclinic point of tangency then the

corresponding single saddle connection bifurcates into two totally separate simple saddle connections. Between these two solutions a third type of solution exists that leaves the saddle point and crosses into the opposite half-plane before returning to the saddle point again. Such a solution will be called a transverse connection of which two types exist. Firstly, there are those that leave the saddle point in the first quadrant of the (X, X') plane and return to the saddle point again through the second quadrant; and secondly, there are those that leave the saddle point in the third quadrant and return through the fourth quadrant. The parameter values are the same for both types, the initial conditions dictating which one of the two solutions will occur. Examples of the two types of non-symmetric transverse connections appear in Fig[5.10a,b] for $F = 0.28$, $\omega = 1.2$. We concentrate our investigations on the first type.

First consider a solution SPQ in Fig[5.10a] that passes through P at time t_0 arriving at Q at time t_1, where t_1 satisfies $X_u(t_1, \varepsilon) = 0$. Assume that the solution after leaving the saddle point S comes close to the saddle point again for large τ. In this case we can find the time t_1 at Q as before by only considering dominant terms of (5.3.2). Putting (5.3.8) equal to zero,

$$2\sqrt{2}e^{-(\tau_1-t_0)} + \frac{1}{4}ce^{(\tau_1-t_0)}I(t_0) = 0 \qquad (5.5.1)$$

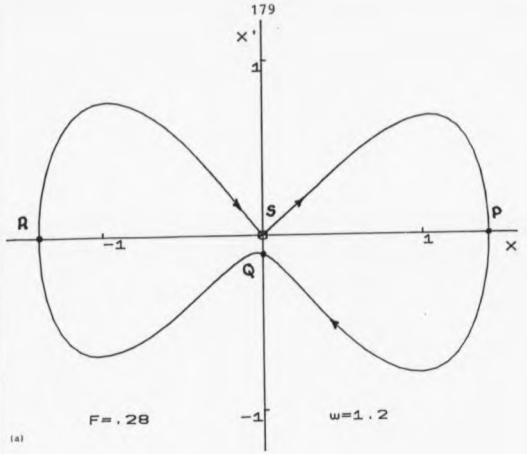

(a)

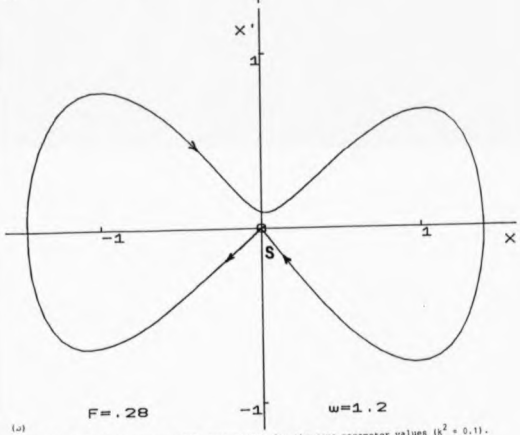

(a)

FIG[5.10] Pair of transverse saddle connections for the same parameter values ($k^2 = 0.1$).

gives

$$t_1 - t_0 = \tau_1 - t_0 = -\frac{1}{2}\ln\left[-\frac{\sqrt{2}}{16}\varepsilon I(t_0)\right]. \qquad (5.5.2)$$

Real solutions for t_1 only occur when $I(t_0) < 0$ and this only happens when $t_a < t_0 < t_b$, where t_a, t_b are solutions of $\sin \omega t = F_c/F$, $F > F_c$. When $I(t_0) > 0$, (5.5.2) has no real solutions implying that solutions in the (X, X') plane do not cross into the next half plane so transverse connections are not possible.

At Q, $X_u'(t_1, \varepsilon)$ is given by (5.3.4) with time t_1 given by (5.5.2). That is,

$$\begin{aligned} X_u'(t_1, \varepsilon) &= -2\sqrt{2}e^{-(\tau_1 - t_0)} + \frac{\varepsilon}{4}e^{(\tau_1 - t_0)}I(t_0) \\ &= \left[2\sqrt{2}e^{-(\tau_1 - t_0)} + \frac{\varepsilon}{4}e^{(\tau_1 - t_0)}I(t_0)\right] \\ &\quad - 4\sqrt{2}e^{-(\tau_1 - t_0)} \\ &= -4\sqrt{2}e^{-(\tau_1 - t_0)} \qquad \text{(using (5.5.1))} \\ &= -2^{\frac{1}{2}}[-\varepsilon I(t_0)]^{\frac{1}{2}}. \qquad (5.5.3) \end{aligned}$$

Likewise, no first derivative exists for X' unless $I(t_0) < 0$.

Next consider the solution QRS that passes through R at time t_2 in the other half-plane, $X < 0$. Solutions in this half-plane are given by $\bar{X}_s(\bar{t}, \varepsilon)$ where $\bar{X}_s(\bar{t}, \varepsilon) = -X_s(t, \varepsilon)$ and $t = \bar{t} + \pi/\omega$ - see section (5.4).

As before we solve the boundary condition $\bar{X}_s(t_1, \varepsilon) = 0$ at Q for $\tau_1 - t_2$ large negative but this time consider dominant terms only of solution (5.3.15). Putting (5.3.17) equal to zero it turns out that

$$t_1 - t_2 = \tau_1 - t_2 = \tfrac{1}{2}\ln\left[\frac{\sqrt{2}\varepsilon}{16} I(\bar{t}_2)\right] \tag{5.5.4}$$

and also at Q for this time from (5.3.13)

$$X_s'(t_1, \varepsilon) = -2^{\frac{1}{2}}[\varepsilon I(\bar{t}_2)]^{\frac{1}{2}}. \tag{5.5.5}$$

The solutions match if the time t_1 given by (5.5.2) and (5.5.4) are the same and $X_u'(t_1, \varepsilon) = X_s'(t_1, \varepsilon)$. From (5.5.3) and (5.5.5)

$$I(\bar{t}_2) = -I(t_0) \tag{5.5.6}$$

and from (5.5.2) and (5.5.4)

$$t_2 - t_0 = -\tfrac{1}{2}\ln\left[-\frac{\sqrt{2}\varepsilon}{16} I(t_0)\right] - \tfrac{1}{2}\ln\left[\frac{\sqrt{2}\varepsilon}{16} I(\bar{t}_2)\right]$$

$$= -\ln\left[-\frac{\sqrt{2}\varepsilon}{16} I(t_0)\right].$$

Hence,

$$8\sqrt{2}e^{-(t_2-t_0)} = -\varepsilon I(t_0) = \varepsilon I(t_2 - \pi/\omega). \tag{5.5.7}$$

For transverse saddle connections

$$\text{Sin } \omega t_0 = F_c\{k + 12e^{-(t_2-t_0)}\}/(Fk) \tag{5.5.8}$$

$$\text{Sin } \omega t_2 = F_c(-k + 12e^{-(t_2-t_0)})/(Fk). \qquad (5.5.9)$$

As in section (5.2), bifurcation occurs when Sin $\omega t_0 = 1$, or when

$$F = F_c(k + 12e^{-(t_2-t_0)})/k \qquad (5.5.10)$$

and we can write as before,

$$\text{Cos } \omega(t_2 - t_0) = \text{Sin } \omega t_2 = 1 - 2F_c/F \qquad (5.5.11)$$

and we can determine the time t_2. Hence, the critical values of F satisfy,

$$F = \frac{2F_c}{1 - \text{Cos } \omega(t_2 - t_0)} = F_c(k + 12e^{-(t_2-t_0)})/k \qquad (5.5.12)$$

given by the intersections of the two curves in Fig[5.11].

Solution this time appear in pairs about the time values $\omega(t_2 - t_0) = (2n - 1)\pi$, (n = 1, 2, 3, ...) there being a phase difference of π/ω between results for the transverse case and the double loop case. These times correspond to homoclinic tangency situations which allow for transverse connections to run from one half-plane to the other.

Such solutions prompt one into thinking about the behaviour of the manifolds of the Poincaré map which enable such connections to occur. Previous results of Poincaré maps, both here and in relevant literature, do not show such

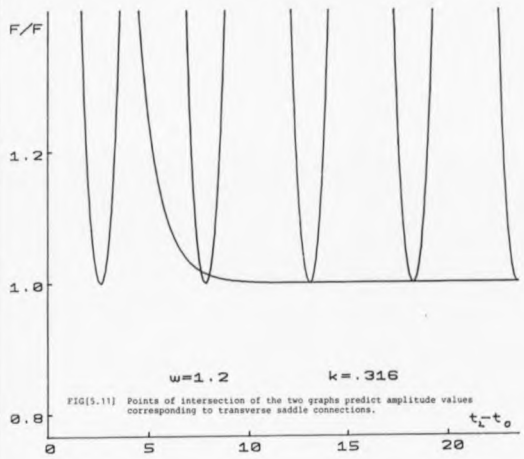

FIG[5.11] Points of intersection of the two graphs predict amplitude values corresponding to transverse saddle connections.

manifold behaviour. Despite the endless possibilities of complex windings accompanied by countless homoclinic points the feeling is towards intersections of the unstable manifolds by both stable manifolds has partly portrayed in Fig[5.12], where x and y are homoclinic points of two different transverse connections of the first type. The first return of the homoclinic point x will occur close to the saddle point S with subsequent

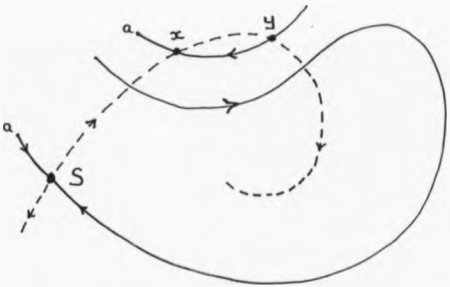

FIG[5.12] Intersections of the unstable manifold by both stable manifolds.

first returns on the stable manifold running into S from the left. (The small a's denote subsequent connection.)

A further sketch of the manifolds based on computer plots is shown in Fig[5.13] where the complex windings of the left-hand stable manifold are revealed. Starting at the point A we can follow the behaviour of this manifold as it runs backwards and forward between the half-planes cutting the unstable manifold as previously depicted in

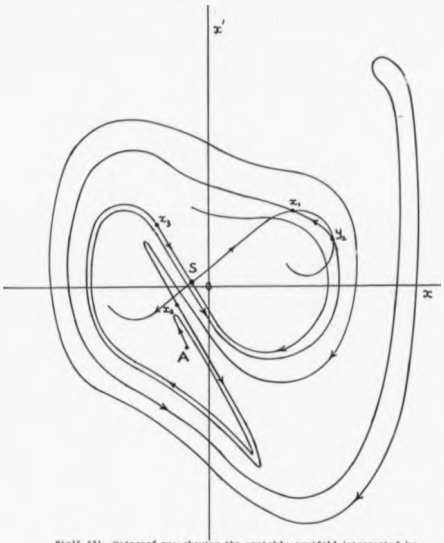

Fig[5.13] Poincaré map showing the unstable manifold intersected by both stable manifolds.

Fig[5.12] at x_1 and y_2. We expect the right-hand stable manifold to behave in a similar way producing homoclinic points corresponding to the second type of transverse connection. Three first-returns of a typical transverse connection are marked x_1, x_2 and x_3.

Finally, Fig[5.14] show two examples of transverse saddle connections of Duffing's equation. These were obtained by solving numerically Eqn(5.1.4), with initial

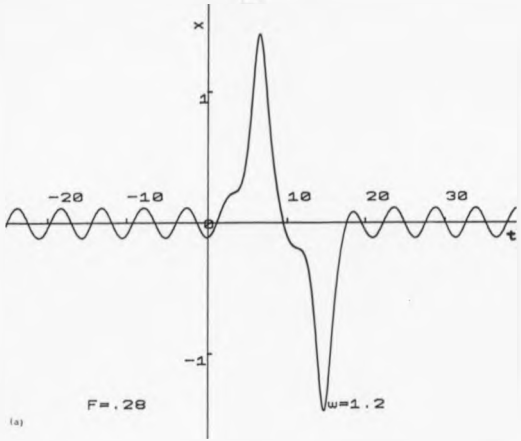

(a)

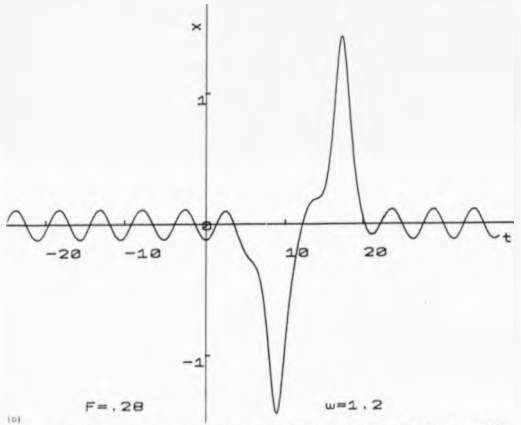

(b)

FIG[5.14] Displacement/time graphs based on the right-hand sides of the double loop connection of Fig[5.10].

conditions used to obtain Fig[5.10a,b], and then adding the periodic term given by (5.1.2). Here the intersection time t_0 satisfies the two equations, $x(t_0) = X(t_0)$ and $x(t_0 - \pi/\omega) = X(t_0 - \pi/\omega)$ corresponding to the two types of saddle connections.

5.6 MULTIPLE LOOP CONNECTIONS

The method outlined in section (5.3) to investigate double-loop connections can be extended to investigate the existence of multiple loop connections. Consider a multiple loop type solution as drawn in Fig[5.15] where the solution curve loops round many times before returning to the saddle point S and denote the time of

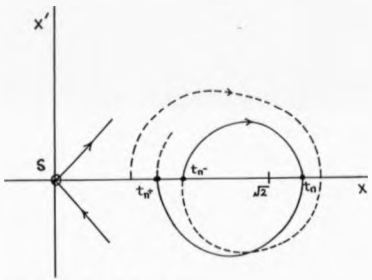

Fig[5.15] Multiple loop type solution.

the n^{th} intersection at $X = \sqrt{2} + \varepsilon\beta_n$. Prior and post intersections are labelled t_{n+} and t_{n-} respectively, where to this approximation t_{n-} and τ_{n-} are interchangeable. To assist the analysis assume as we have done throughout that the time differences $t_n - t_{n-}$, $t_{n+} - t_n$, ... are large.

The solution that passes through P_n where $X = \sqrt{2} + \varepsilon\beta_n$ at time t_n has solution

$$X(t) = X_0(\tau, t_n) + \varepsilon X_1(\tau, t_1), \ \ldots O(\varepsilon^2) \tag{5.6.1}$$

where

$$X_0(\tau, t_n) = \sqrt{2}\ \mathrm{Sech}(\tau - t_n) \tag{5.6.2}$$

and

$$X_1(\tau, t_n) = \frac{k_0}{4}\sqrt{2}u_1(\tau, t_n) - \beta_n u_2(\tau, t_n) + \int_{t_n}^{\tau} \{u_2(\tau, t_n)u_1(s, t_n) - u_1(\tau, t_n) u_2(s, t_n)\}g(s, t_n)ds. \tag{5.6.3}$$

Acting on the assumption that $\tau_{n+} - t_n$ is large positive then we would expect both $X_0(\tau_{n+}, t_n)$ and $X_1(\tau_{n+}, t_n)$ to tend to zero as $\tau_{n+} \to \infty$. This is clearly true for $X_0(\tau_{n+}, t_n)$ so for $X_1(\tau_{n+}, t_n)$ we require

$$0 = -\beta_n u_2(\tau_{n+}, t_n) + u_2(\tau_{n+}, t_n)\int_{t_n}^{\tau_{n+}+\infty} u_1(s, t_n)$$

$$g(s, t_n)ds \qquad (5.6.4)$$

hence,

$$\beta_n = \int_{t_n}^{\infty} u_1(s, t_n)g(s, t_n)ds, \quad n = 2, 3, 4, \ldots N \qquad (5.6.5)$$

with

$$\beta_1 = -\int_{-\infty}^{t_1} u_1(s, t_1)g(s, t_1)ds.$$

As before intersection times at Q_n and Q_{n+1} satisfy the equations $X'(\tau_{n-}) = 0$, $X'(\tau_{n+}) = 0$. Considering significant terms only of the boundary conditions these times satisfy

$$-2\sqrt{2}e^{-(\tau_{n+}-t_n)} + \frac{\varepsilon}{4}e^{(\tau_{n+}-t_n)}\left[-\beta_n + \int_{t_n}^{\infty} u_n(s, t_n)\right.$$

$$\left. g(s, t_n)ds\right] = 0 \quad \text{and} \qquad (5.6.6)$$

$$2\sqrt{2}e^{(\tau_{n-}-t_n)} - \frac{\varepsilon}{4}e^{-(\tau_{n-}-t_n)}\left[-\beta_n + \int_{t_n}^{-\infty} u_n(s, t_n)\right.$$

$$\left. g(s, t_n)ds\right] = 0. \qquad (5.6.7)$$

At Q_{n+1} and Q_n,

$$X(\tau_{n+},\ \varepsilon) = 2^{\frac{1}{2}}\left[\varepsilon\left\{-\beta_n + \int_{t_n}^{\infty} u_1(s,\ t_n)g(s,\ t_n)ds\right\}\right] \tag{5.6.8}$$

$$X(\tau_{n-},\ \varepsilon) = 2^{\frac{1}{2}}\left[\varepsilon\left\{-\beta_n + \int_{t_n}^{-\infty} u_1(s,\ t_n)g(s,\ t_n)ds\right\}\right]. \tag{5.6.9}$$

For continuity of solutions at Q_n we require

$$\left.\begin{aligned} t_{n-} &= t_{(n-1)+} \\ X(t_{n-}) &= X(t_{(n-1)+}) \end{aligned}\right\}\ n = 2,\ 3,\ 4,\ \ldots N. \tag{5.6.10}$$

We can now solve for $\beta_1,\ \beta_2,\ \ldots\beta_n$ using (5.6.8) and (5.6.9).

Let $P_n(s) = u_1(t_n,\ s)g(t_n,\ s)$ then

$$-\beta_2 + \int_{t_2}^{-\infty} P_2(s)ds = -\beta_1 + \int_{t_1}^{\infty} P_1(s)ds$$

so

$$\beta_2 = -I(t_1) - \int_{-\infty}^{t_2} P_2(s)ds. \tag{5.6.11}$$

Likewise,

$$-\beta_3 + \int_{t_3}^{-\infty} P_3(s)ds = -\beta_2 + \int_{t_2}^{\infty} P_2(s)ds$$

and

$$\beta_3 = -I(t_2) - I(t_1) - \int_{-\infty}^{t_3} P_3(s)ds. \tag{5.6.12}$$

Therefore,

$$\beta_n = -\left\{\sum_{r=1}^{n-1} I(t_r)\right\} - \int_{-\infty}^{t_3} P_n(s)ds \tag{5.6.13}$$

when n = N

$$\beta_N = -\left\{\sum_{r=1}^{N-1} I(t_r)\right\} - \int_{-\infty}^{t_N} P_N(s)ds \tag{5.6.14}$$

but since

$$\beta_N = \int_{t_N}^{\infty} P_N(s)ds \tag{5.6.15}$$

$$\sum_{r=1}^{N} I(t_r) = 0 \tag{5.6.16}$$

see result (5.3.20) where t_0 should be read as t_n.

Arrival times at Q_{n+1} and Q_n are given by

$$t_{n+} = t_n - \frac{1}{2}\ln\varepsilon - \frac{1}{2}\ln\left[\frac{\sqrt{2}}{16}\left\{-\beta_n + \int_{t_n}^{\infty} P_n(s)ds\right\}\right] \tag{5.6.17}$$

$$t_{n-} = t_n + \frac{1}{2}\ln\varepsilon + \frac{1}{2}\ln\left[\frac{\sqrt{2}}{16}\left\{-\beta_n + \int_{t_n}^{-\infty} P_n(s)ds\right\}\right] \tag{5.6.18}$$

by solving Eqn(5.6.6) and (5.6.7).

Continuiity of time implies that

$$t_n + \frac{1}{2}\ln\varepsilon + \frac{1}{2}\ln\left[\frac{\sqrt{2}}{16}\left(-\beta_n + \int_{t_n}^{-\infty} P_n(s)\,ds\right)\right]$$

$$= t_{n-1} - \frac{1}{2}\ln\varepsilon - \frac{1}{2}\ln\left[\frac{\sqrt{2}}{16}\left(-\beta_{n-1} + \int_{t_{n-1}}^{\infty} P_{n-1}(s)\,ds\right)\right] \tag{5.6.19}$$

or

$$t_2 - t_1 = -\ln\varepsilon - \ln\left[\frac{\sqrt{2}}{16} I(t_1)\right] \tag{5.6.20}$$

using (5.6.11).

Likewise

$$t_3 - t_2 = -\ln\varepsilon - \ln\left[\frac{\sqrt{2}}{16}(I(t_1) + I(t_2))\right] \tag{5.6.21}$$

using (5.6.12). Therefore,

$$t_n - t_{n-1} = -\ln\varepsilon - \ln\left[\frac{\sqrt{2}}{16}\sum_{r=1}^{n-1} I(t_r)\right]. \tag{5.6.22}$$

Hence,

$$e^{-(t_2-t_1)} = \frac{\varepsilon\sqrt{2}}{16} I(t_1) \tag{5.6.23}$$

$$e^{-(t_3-t_2)} - e^{-(t_2-t_1)} = \frac{\varepsilon\sqrt{2}}{16} I(t_2) \tag{5.6.24}$$

$$\vdots \qquad \vdots \qquad \vdots$$

$$e^{-(t_N-t_{N-1})} - e^{-(t_{N-1}-t_{N-2})} = \frac{\varepsilon\sqrt{2}}{16} I(t_{N-1}) \tag{5.6.25}$$

and

$$-e^{-(t_N-t_{N-1})} = \frac{\varepsilon\sqrt{2}}{16} I(t_N) \tag{5.6.26}$$

using (5.6.16).

Since

$$I(t_n) = \frac{2}{3}k_0\sqrt{2} - \frac{2\sqrt{2}k_0 F}{F_c}\text{Sin } \omega t_n$$

we can write these equations as

$$F \text{ Sin } \omega t_1 = F_c\left[1 - \frac{12}{k}e^{-(t_2-t_1)}\right] \tag{5.6.27}$$

$$F \text{ Sin } \omega t_2 = F_c\left[1 - \frac{12}{k}\left[e^{-(t_3-t_2)} - e^{-(t_2-t_3)}\right]\right] \tag{5.6.28}$$

$$\vdots \qquad\qquad \vdots$$

$$F \text{ Sin } \omega t_N = F_c\left[1 + \frac{12}{k}e^{-(t_N-t_{N-1})}\right]. \tag{5.6.29}$$

Based on results of previous sections it seems likely that the critical time will occur when Sin $\omega t_N = 1$ in which case

$$F = F_c\left[1 + \frac{12}{k}e^{-(t_N-t_{N-1})}\right]. \tag{5.6.30}$$

We know that this is the case when N = 2 from section (5.3) but for N > 2 it has not been established that it

is true. Finally, the set of equations (5.6.27) - (5.6.29) have to be solved numerically, due to the presence of transcendental functions, in the order t_N, t_{N-1}, ..., t_1.

5.7 PERIODIC SOLUTIONS

Having investigated transverse connections of the type shown in Fig[5.10a,b] it seems natural to ask whether large amplitude periodic solutions can be investigated in a similar way. Such solutions would be disposed about the origin in the (X, X') plane and run in 'close' to the origin thus satisfying a necessary pre-requisite of the method used. Greenspan and Holmes (1983) have shown that there exist subharmonic solutions that appear to fit this description.

Consider a closed solution SPQRS as shown in Fig[5.16] in which we make the usual assumptions that QP and QR are approximately $\sqrt{2}$ and Q and S are 'close' to the origin. Let the solution start at S at time t_0 and pass through P, Q, R at times t_1, t_2, t_3 respectively, returning to S at time t_4. Let

$$X(t_1, \varepsilon) = \sqrt{2} + \varepsilon\bar{s}_1, \qquad X(t_3, \varepsilon) = -\sqrt{2} - \varepsilon\bar{s}_3.$$

Consider separately solutions SPQ and QRS that meet at the point Q at the same time. Solution SPQ, passing through P at time t_1, is given by (5.6.2) and (5.6.3) with n = 1. As Q is considered 'close' to the origin

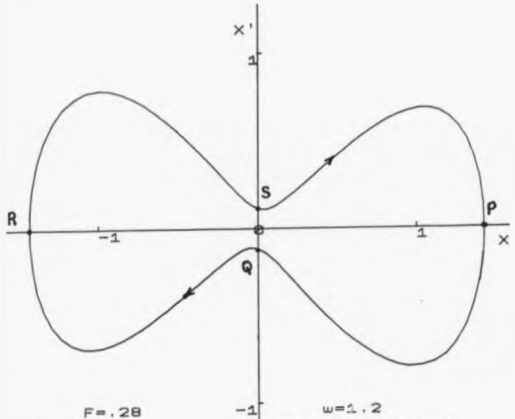

FIG[5.16] Period 3 solution. Notice how the solution runs in 'close' to the origin.

then we expect the time difference $t_2 - t_1$ to be large positive. Considering significant terms only of (5.6.2) and (5.6.3) for $t_2 - t_1$ large and letting the upper limit of the integral of (5.6.3) tend to ∞, the solution passes through Q at time t_2 that satisfies

$$2\sqrt{2}\, e^{-(t_2-t_1)} + \frac{\sqrt{3}}{4} e^{(t_2-t_1)} I(t_1) = 0. \qquad (5.7.1)$$

Solving for t_2 and substituting it into the significant terms of $X'(t, \varepsilon)$ gives

$$X'(t_2, \varepsilon) = -2^{\frac{1}{2}}[-\varepsilon I(t_1)]^{\frac{1}{2}} \tag{5.7.2}$$

at Q where $I(t_1) > 0$.

The other solution QRS, in the $X < 0$ half-plane, passes through R at time t_3 and is given by

$$\begin{aligned}\bar{X}(t, \varepsilon) &= \bar{X}_0(\bar{\tau}, \varepsilon) + \varepsilon\bar{X}_1(\bar{\tau}, \varepsilon) + \ldots \\ &= -X_0(\tau - \pi/\omega, \varepsilon) - \varepsilon X_1(\tau - \pi/\omega, \varepsilon) + \ldots\end{aligned} \tag{5.7.3}$$

where X_0 and X_1 are again given by (5.6.2) and (5.6.3) but with $n = 3$. Solving for $X = 0$ at S for $t_2 - t_3$ large negative,

$$2\sqrt{2}e^{(\bar{t}_2-\bar{t}_3)} - \frac{\varepsilon}{4}e^{-(\bar{t}_2-\bar{t}_3)}I(\bar{t}_3) = 0 \tag{5.7.4}$$

or

$$2\sqrt{2}e^{(t_2-t_3)} - \frac{\varepsilon}{4}e^{-(t_2-t_3)}I(t_3 - \pi/\omega) = 0. \tag{5.7.5}$$

Put the time t_2 obtained from (5.7.5) into the significant terms of $X'(t, \varepsilon)$ and

$$X'(t_2, \varepsilon) = -2^{\frac{1}{2}}[\varepsilon I(t_3 - \pi/\omega)]^{\frac{1}{2}}. \tag{5.7.6}$$

For solutions to match at Q we require

$$-2^{\frac{3}{4}}[-\varepsilon I(t_1)]^{\frac{1}{4}} = -2^{\frac{3}{4}}[\varepsilon I(t_3 - \pi/\omega)] \tag{5.7.7}$$

that is

$$-I(t_1) = I(t_3 - \pi/\omega) \tag{5.7.8}$$

and from (5.7.1) and (5.7.5)

$$e^{-2(t_2-t_1)} = -\frac{\sqrt{2}\varepsilon}{16} I(t_1)$$

$$e^{2(t_2-t_3)} = \frac{\sqrt{2}\varepsilon}{16} I(t_3 - \pi/\omega)$$

hence

$$t_2 = \tfrac{1}{2}(t_1 + t_3). \tag{5.7.9}$$

Next we consider solutions QPS and QRS that match at S with time difference $2m\pi/\omega$ where m is a positive integer. As before we take the solutions through P and R at times t_1 and t_2 respectively and match at S using the results for time differences tending to $\mp\infty$. On QPS we solve for $X = 0$ at S with $t_0 - t_1$ large negative, hence t_0 satisfies

$$2\sqrt{2}e^{(t_0-t_1)} + \frac{\varepsilon}{4}e^{-(t_0-t_1)}[-I(t_1)] = 0. \tag{5.7.10}$$

Solving for t_0 and substituting into the significant terms of $X'(t, \varepsilon)$,

$$X'(t_0, \varepsilon) = 2^{\frac{3}{4}}[\varepsilon I(t_1)]^{\frac{1}{4}} \tag{5.7.11}$$

at S.

On QRS we also solve for X = 0 at S but with $t_4 - t_3$ large positive, hence t_4 satisfies

$$2\sqrt{2}e^{-(\bar{t}_4-\bar{t}_3)} + \frac{\varepsilon}{4}e^{(\bar{t}_4-\bar{t}_3)}I(\bar{t}_3) = 0, \tag{5.7.12}$$

or

$$2\sqrt{2}e^{-(t_4-t_3)} + \frac{\varepsilon}{4}e^{(t_4-t_3)}I(t_3 - \pi/\omega) = 0 \tag{5.7.13}$$

whilst at S for time t_4

$$X'(t_4, \varepsilon) = 2^{\frac{1}{2}}[-\varepsilon I(t_3 - \pi/\omega)]^{\frac{1}{2}}, \tag{5.7.14}$$

$I(t_3 - \pi/\omega) > 0$.

For solutions to match at S we again require

$$I(t_1) = -I(t_3 - \pi/\omega)$$

as before and for continuity of time from (5.7.10) and (5.7.13)

$$e^{2(t_0-t_1)} = \frac{\sqrt{2}\varepsilon}{16}I(t_1) \tag{5.7.15}$$

$$e^{-2(t_4-t_3)} = -\frac{\sqrt{2}\varepsilon}{16}I(t_3 - \pi/\omega) \tag{5.7.16}$$

hence

$$t_0 - t_1 = -t_4 + t_3.$$

Periodicity occurs if $t_4 = t_0 + 2m\pi/\omega$, hence

$$t_0 = \tfrac{1}{2}(t_1 + t_3) - m\pi/\omega. \qquad (5.7.17)$$

Also, for results (5.7.11) and (5.7.2) to hold

$$I(t_1) = 0 \qquad (5.7.18)$$

similarly,

$$I(t_3 - \pi/\omega) = 0. \qquad (5.7.19)$$

From (5.7.18) and (5.7.19)

$$\text{Sin } \omega t_1 = -\text{Sin } \omega t_3 = F_c/F \qquad \text{see (5.2.14)} \qquad (5.7.20)$$

Assuming that the time taken to travel from P to R is approximately the same as the time taken to travel from R to P then the solutions t_1 and t_2 must differ by a multiple of π. In fact,

$$\omega t_2 = \omega t_1 + (2n - 1)\pi \qquad (n = 1, 2, 3, \ldots)$$

and the time difference is an odd multiple of π. Hence, a complete closed-loop stable solution will have period $(2n - 1)$.

Stable solutions of period 3 and 5 have both been found by employing the method of this chapter. We know that solutions which cross into the opposite half-plane cut the positive X-axis at time $t_0 = (4n - 3)\pi/2\omega$, $(n = 1, 2, 3, \ldots)$, where $X(t_0) = \sqrt{2} + \varepsilon\beta_1$. The period 3 solution was found by considering the behaviour of the

two transverse solutions, see Fig[5.10a,b], obtainable from the same parameter values, $F = 0.28$, $\omega = 1.2$, $k = 0.312$. Together their forms suggest that a periodic solution might exist for the same parameters. Choosing $X(t_0)$ close to $\sqrt{2}$ together with $X'(t_0) = 0$ one searches numerically for a possible periodic (closed-loop) solution. The resulting period 3 solution is shown in Fig[5.16].

Using the transformation given in section (5.1) along with the actual (x, X') values used to obtain Fig[5.16] we can plot the approximate solution of Duffing's equation, in the (x, x') plane by putting

$x(t) = X(t) - \frac{F}{(1 + \omega^2)} \cos \omega t,$

$x'(t) = X'(t) + \frac{F\omega}{(1 + \omega^2)} \sin \omega t$ the result of which is shown in Fig[5.17a]. This should be compared with the actual solution in Fig[5.17b] obtained from Duffing's equation (5.1.1). Similarly, Fig[5.18] displays both the approximate period 5 solution and the actual period 5 solution for the values $F = .3$, $\omega = 2.8$, $k = 0.06$. Agreement here is extremely good.

Finally, as the period of these solutions increases so the domain of attraction grows smaller thus making it harder to find higher odd period solutions. However, it is known that such solutions in the (X, X') plane will run closer and closer into the origin as the period increases.

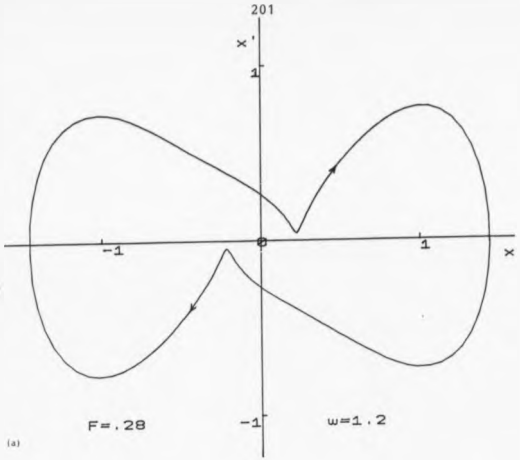

(a)

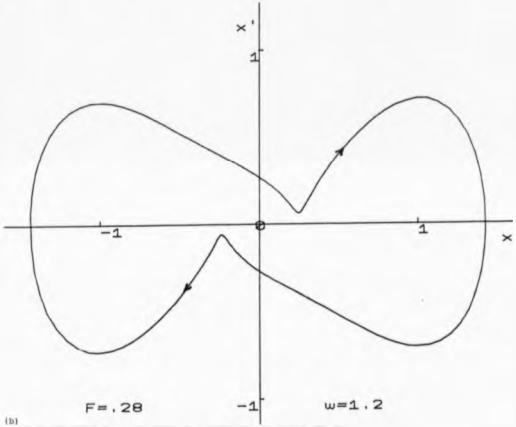

(b)

FIG(5.77) Period 1 solutions: (a) Approximate solution, (b) Exact solution.

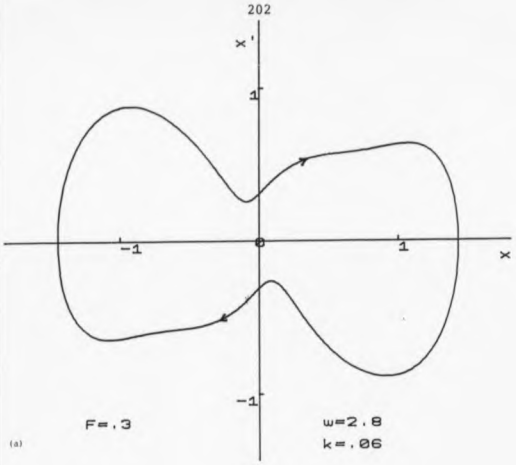

(a)

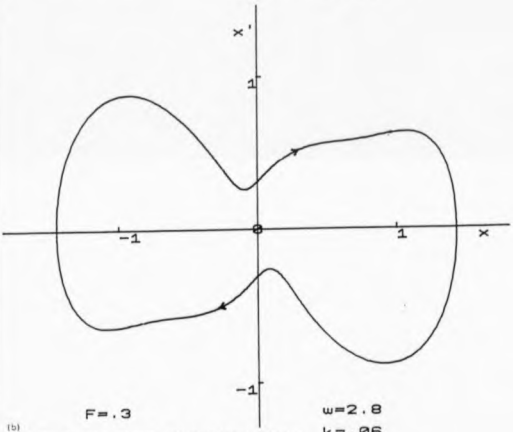

(b)

FIG[5,18] Period 5 solution. (a) Approximate solution, (b) Exact solution.

This chapter has illustrated the application of a combined averaging and singular perturbation method to some typical saddle connections associated with the saddle point of the Poincaré section of the Duffing oscillator. These include the single, double, transverse and multiple loop connections and period (2n - 1) solutions. All these solutions have the common feature that they may be viewed as perturbations of the separatrix of the undamped and unforced Duffing equation. All perturbations have the property that they cut the X-axis at $\pm\sqrt{2} + O(\varepsilon)$, pass close to the origin and that the time difference between these two points is large. Further, we have obtained specific values of F corresponding to bifurcation associated with the types of saddle connections referred to previously in particular Holmes' result obtained using Mel'nikov's method.

CHAPTER 6

THE EXACT SOLUTION OF THE TRANSFORMED DUFFING EQUATION

6.1 THE EQUATION OF THE SADDLE CONNECTION

It was shown in Chapter 5, section 1, that the equation

$$X'' + \varepsilon k_0 X' - X + X^3 + 3\varepsilon f_0 X^2 \cos \omega t = 0 \qquad (6.1.1)$$

could be solved using a standard perturbation technique along with a given time-transformation. This resulted in two linear second-order differential equations:

$$X_0'' - X_0 + X_0^3 = 0 \qquad (6.1.2)$$

with boundary conditions given by (5.1.22), (5.1.24) and

$$X_1'' + (3X_0^2 - 1)X_1 = 2X_0''T_1' + T_1''X_0' - k_0X_0' - 3f_0X_0^2 \cos \omega\tau \qquad (6.1.3)$$

with boundary conditions given by (5.1.23) and (5.1.25) and differentiation throughout with respect to τ. $T_1 = T_1(\tau)$ is part of the given time-transformation (see 5.1.12) and is given by (5.1.34). The solution of (6.1.2) subject to the given boundary conditions turned

out to be $X_0(\tau) = \sqrt{2}\ \mathrm{Sech}(\tau - t_0)$ which corresponds to the separatrix of the undamped, unforced equation, $\varepsilon = 0$. Substituting the result for X_0 into (6.1.3) and replacing T_1 and its derivatives produced the new equation for X_1, namely,

$$X_1'' + (6\ \mathrm{Sech}^2(\tau - t_0) - 1)X_1 = g(\tau) \qquad (6.1.4)$$

where

$$g(\tau) = -2\sqrt{2}k_0\ \mathrm{Sech}^3(\tau - t_0)\{e^{-2|\tau - t_0|} - 1\}\ \mathrm{sgn}(\tau - t_0)$$

$$- 6f_0\ \mathrm{Sech}^2(\tau - t_0)\ \mathrm{Cos}\ \omega\tau.$$

Fortunately, we found in Chapter 5 that the conditions for various saddle connections could be obtained without the need to solve Eqn(6.1.4) completely thus removing consideration of certain integrals. However, all such integrals must be evaluated here in order to obtain those solutions that leave the origin at time $t = -\infty$. Of course, we are only interested in those solutions that cross the X-axis, in the (X, X') plane, at time $t = (4n + 1)\pi/2\omega$ ($n = 0, 1, 2, \ldots$), at a point close to $\sqrt{2}$. The remainder of this chapter is taken up with solving (6.1.4) to produce an overall solution of (6.1.1) and finally we make use of particular solutions to determine the positions of homoclinic points of Duffing's equation.

We will solve (6.1.4) in two parts. To begin with

consider the equation

$$X_1'' + (6\,\mathrm{Sech}^2(\tau - t_0) - 1)X_1 = -M\,\mathrm{Sech}^3(\tau - t_0)$$
$$[e^{-2|\tau - t_0|} - 1]\,\mathrm{sgn}(\tau - t_0) \qquad (6.1.5)$$

($M = 2\sqrt{2}k_0$), the right-hand side of which is continuous at $\tau = t_0$. Two solutions occur, one for $\tau < t_0$ and one for $\tau > t_0$ which must match smoothly at $\tau = t_0$. Let the two particular solutions be, for $\tau < t_0$,

$$X_{11}(\tau) = a_1\,\mathrm{Cosh}(\tau - t_0) + b_1\,\mathrm{Sinh}(\tau - t_0) + c_1\,\mathrm{Sech}(\tau - t_0), \qquad (6.1.6)$$

and for $\tau > t_0$

$$X_{12}(\tau) = A_3u_1(\tau) + B_3u_2(\tau) + a_2\,\mathrm{Cosh}(\tau - t_0) + b_2\,\mathrm{Sinh}(\tau - t_0) + c_2\,\mathrm{Sech}(\tau - t_0) \qquad (6.1.7)$$

where the complementary solutions of (6.1.5) were shown in Chapter 5 to be

$$u_1(\tau) = \mathrm{Sinh}(\tau - t_0)\,\mathrm{Sech}^2(\tau - t_0)$$

$$u_2(\tau) = \tfrac{3}{2}(\tau - t_0)\,\mathrm{Sinh}(\tau - t_0)\,\mathrm{Sech}^2(\tau - t_0) - \tfrac{3}{2}\,\mathrm{Sech}(\tau - t_0) + \tfrac{1}{2}\,\mathrm{Cosh}(\tau - t_0).$$

Here A_3 and B_3 are chosen in order to obtain a continuous and smooth solution and a_1, a_2, b_1, b_2, c_1, c_2 are

constants to be determined. Substituting X_{11} into (6.1.5) it turns out, on equating like terms, that

$$a_1 = M/3, \quad b_1 = M/3, \quad c_1 = -M/2, \quad \tau < t_0 \tag{6.1.9}$$

and on substituting X_{12},

$$a_2 = -M/3, \quad b_2 = M/3, \quad c_2 = M/2, \quad \tau > t_0. \tag{6.1.10}$$

For matching to occur at $\tau = t_0$ we require

$$X_{11}(t_0) = X_{12}(t_0)$$

and

$$X_{11}'(t_0) = X_{12}'(t_0)$$

which results in

$$\begin{aligned} A_3 &= 0 \\ B_3 &= M/3. \end{aligned} \tag{6.1.11}$$

Hence, a particular solution of (6.1.5), continuous and smooth at $\tau = t_0$, is given by

$$X_{11p}(\tau) = \frac{2}{3}\sqrt{2}k_0 e^{(\tau - t_0)} - \sqrt{2}k_0 \operatorname{Sech}(\tau - t_0), \quad \tau \leq t_0 \tag{6.1.12}$$

$$X_{12p}(\tau) = \sqrt{2}k_0(\tau - t_0)\operatorname{Sinh}(\tau - t_0)\operatorname{Sech}^2(\tau - t_0) - \frac{\sqrt{2}}{3}k_0 \operatorname{Cosh}(\tau - t_0) + 2\frac{\sqrt{2}}{3}k_0 \operatorname{Sinh}(\tau - t_0), \quad \tau \geq t_0. \tag{6.1.13}$$

We note that $X_{12p}(\tau)$ contains exponential growth terms and that $X_{11p}(t_0) = X_{12p}(t_0) = -\sqrt{2}k_0/3$.

The remaining part of Eqn(6.1.4) is

$$X_1'' + (6\,\mathrm{Sech}^2(\tau - t_0) - 1)X_1 = N\,\mathrm{Sech}^2(\tau - t_0)\,\mathrm{Cos}\,\omega\tau \tag{6.1.14}$$

where $N = -6f_0$. The Sech^2 term can be removed from the right-hand side of (6.1.14) by writing

$$X_1 = \frac{N}{6}\,\mathrm{Cos}\,\omega\tau + v \tag{6.1.15}$$

which transforms (6.1.14) to

$$v'' + (6\,\mathrm{Sech}^2(\tau - t_0) - 1)v = \frac{N}{6}(1 + \omega^2)\,\mathrm{Cos}\,\omega\tau \tag{6.1.16}$$

where the independent solutions of the homogeneous equation given by (6.1.8) still apply here. The remaining solution of (6.1.16) is found using the integral formula

$$v = \frac{N}{6}(1 + \omega^2)u_2(\tau)\int u_1(\tau)\,\mathrm{Cos}\,\omega\tau\,d\tau - \frac{N}{6}(1 + \omega^2)u_1(\tau)\int u_2(\tau)\,\mathrm{Cos}\,\omega\tau\,d\tau. \tag{6.1.17}$$

To this end consider the integral

$$\int \mathrm{Sech}(\tau - t_0)e^{i\omega\tau}d\tau.$$

Using the series

$$\text{Sech}(\tau - t_0) = 2 \sum_{n=0}^{\infty} (-1)^n e^{-(2n+1)(\tau - t_0)}, \quad \tau > t_0, \tag{6.1.18}$$

we have, after interchanging the operations of summation and integration

$$\int \text{Sech}(\tau - t_0) e^{i\omega\tau} d\tau = -2 \sum_{n=0}^{\infty} \frac{(-1)^n e^{-(2n+1)(\tau - t_0)} e^{i\omega\tau} (2n + 1 + i\omega)}{D} + C \tag{6.1.19}$$

where $D = (2n + 1)^2 + \omega^2$.

Therefore,

$$\int \text{Sech}(\tau - t_0) \text{ Cos } \omega\tau \, d\tau = 2 \sum_{n=0}^{\infty} \frac{(-1)^n e^{-(2n+1)(\tau - t_0)}}{D} [-(2n + 1) \text{ Cos } \omega\tau + \omega \text{ Sin } \omega\tau] + c_1 \tag{6.1.20}$$

and

$$\int \text{Sech}(\tau - t_0) \text{ Sin } \omega\tau \, d\tau = 2 \sum_{n=0}^{\infty} \frac{(-1)^n e^{-(2n+1)(\tau - t_0)}}{D} [-(2n + 1) \text{ Sin } \omega\tau - \omega \text{ Cos } \omega\tau] + d_1. \tag{6.1.21}$$

For $\tau < t_0$ use

$$\text{Sech}(\tau - t_0) = 2 \sum_{n=0}^{\infty} (-1)^n e^{(2n+1)(\tau - t_0)}, \tag{6.1.22}$$

then

$$\int \text{Sech}(\tau - t_0)\ \text{Cos}\ \omega\tau\ d\tau =$$

$$2 \sum_{n=0}^{\infty} \frac{(-1)^n e^{(2n+1)(\tau - t_0)}}{D} [(2n + 1)\ \text{Cos}\ \omega\tau + \omega\ \text{Sin}\ \omega\tau] + c_2 \qquad (6.1.23)$$

and

$$\int \text{Sech}(\tau - t_0)\ \text{Sin}\ \omega\tau\ d\tau =$$

$$2 \sum_{n=0}^{\infty} \frac{(-1)^n e^{(2n+1)(\tau - t_0)}}{D} [(2n + 1)\ \text{Sin}\ \omega\tau - \omega\ \text{Cos}\ \omega\tau] + d_2. \qquad (6.1.24)$$

Matching of solutions must take place at $\tau = t_0$. Let $\tau \to t_0$ in (6.1.20) and (6.1.23), then for $\tau > t_0$

$$\int \text{Sech}(\tau - t_0)\ \text{Cos}\ \omega\tau\ d\tau \to$$

$$2 \sum_{n=0}^{\infty} \frac{(-1)^n}{D} [-(2n + 1)\ \text{Cos}\ \omega t_0 + \omega\ \text{Sin}\ \omega t_0] + c_1 \qquad (6.1.25)$$

and for $\tau < t_0$

$$\int \text{Sech}(\tau - t_0)\ \text{Cos}\ \omega\tau\ d\tau \to$$

$$2 \sum_{n=0}^{\infty} \frac{(-1)^n}{D} [(2n + 1)\ \text{Cos}\ \omega t_0 + \omega\ \text{Sin}\ \omega t_0] + c_2. \qquad (6.1.26)$$

Clearly at $\tau = t_0$ there is a discontinuity unless c_1 and c_2 are chosen to correct this.

From Jolley p. 165

$$\text{Sech } \theta = 4\pi \sum_{n=0}^{\infty} \frac{(2n + 1)(-1)^n}{[(2n + 1)^2\pi^2 + 4\theta^2]}. \qquad (6.1.27)$$

Put $\theta = \frac{1}{2}\pi\omega$. Then

$$\text{Sech}(\tfrac{1}{2}\pi\omega) = \frac{4}{\pi} \sum_{n=0}^{\infty} \frac{(2n + 1)(-1)^n}{D}. \qquad (6.1.28)$$

For matching to occur at $\tau = t_0$, results (6.1.25) and (6.1.26) are set equal to each other giving

$$c_1 - c_2 = 4 \sum_{n=0}^{\infty} \frac{(2n + 1)(-1)^n}{D} \text{Cos } \omega t_0$$

$$= \pi \text{ Sech}(\tfrac{1}{2}\pi\omega) \text{ Cos } \omega t_0.$$

Choose

$$c_1 = \frac{\pi}{2} \text{Sech}(\tfrac{1}{2}\pi\omega) \text{ Cos } \omega t_0 = -c_2. \qquad (6.1.29)$$

Similarly

$$d_1 = \frac{\pi}{2} \text{Sech}(\tfrac{1}{2}\pi\omega) \text{ Sin } \omega t_0 = -d_1. \qquad (6.1.30)$$

Hence,

$$I_c = \int \text{Sech}(\tau - t_0) \text{ Cos } \omega\tau \, d\tau \qquad (6.1.31)$$

$$= \frac{\pi}{2} \text{Sech}(\tfrac{1}{2}\pi\omega) \text{ Cos}(\omega t_0) \text{ sgn}(\tau - t_0)$$

$$2 \sum_{n=0}^{\infty} \frac{(-1)^n e^{-(2n+1)|\tau - t_0|}}{D} [-(2n + 1) \text{ Cos}(\omega\tau)$$

$$\text{sgn}(\tau - t_0) + \omega \text{ Sin}(\omega\tau)]$$

for all τ, and

$$I_s = \int \text{Sech}(\tau - t_0)\ \text{Sin}\ \omega\tau\ d\tau \qquad (6.1.32)$$

$$= \frac{\pi}{2}\ \text{Sech}(\tfrac{1}{2}\pi\omega)\ \text{Sin}(\omega t_0)\ \text{sgn}(\tau - t_0)$$

$$+ 2 \sum_{n=0}^{\infty} \frac{(-1)^n e^{-(2n+1)|\tau - t_0|}}{D}[-(2n+1)\ \text{Sin}(\omega\tau)$$

$$\text{sgn}(\tau - t_0) - \omega\ \text{Cos}\ \omega\tau]$$

for all τ.

We now have smooth continuous solutions on $\mathbb{R}$.

These results enable the integration required for (6.1.17) to be expressed in terms of I_c and I_s. The three remaining integrals are:

1. $$\int \text{Sinh}(\tau - t_0)\ \text{Sech}^2(\tau - t_0)\ \text{Cos}\ \omega\tau\ d\tau =$$

$$-\text{Cos}\ \omega\tau\ \text{Sech}(\tau - t_0) - \omega I_s. \qquad (6.1.33)$$

2. $$\frac{3}{2}\int (\tau - t_0)\ \text{Sinh}(\tau - t_0)\ \text{Sech}^2(\tau - t_0)\ \text{Cos}\ \omega\tau\ d\tau =$$

$$-\frac{3}{2}(\tau - t_0)\ \text{Sech}(\tau - t_0)\ \text{Cos}\ \omega\tau + \frac{3}{2} I_c + \frac{3}{2}\frac{\omega d}{d\omega} I_c$$

$$+ \frac{3}{2}\omega t_0 I_s. \qquad (6.1.34)$$

3. $$\frac{1}{2}\int \text{Cosh}(\tau - t_0)\ \text{Cos}\ \omega\tau\ d\tau =$$

$$-\frac{1}{2(1+\omega^2)}(\text{Sinh}(\tau - t_0)\ \text{Cos}\ \omega\tau + \omega\ \text{Sinh}(\tau - t_0)$$

$$\text{Sin}\ \omega\tau). \qquad (6.1.35)$$

The complete general formulae is

$$X_1(\tau) = A_0u_1(\tau) + B_0u_2(\tau) + \bar{X}_1(\tau) + \frac{N}{6}\,\mathrm{Cos}\,\omega\tau$$

$$+ \frac{N(1+\omega^2)}{6}[u_2(\tau)\{-\mathrm{Cos}\,\omega\tau\,\mathrm{Sech}(\tau - t_0) - \omega I_s\}]$$

$$- u_1(\tau)\left\{-\frac{3}{2}(\tau - t_0)\,\mathrm{Sech}(\tau - t_0)\,\mathrm{Cos}\,\omega\tau\right.$$

$$+ \frac{3}{2}\frac{d}{d}I_c + \frac{3}{2}t_0I_s + \frac{\mathrm{Sinh}(\tau - t_0)\,\mathrm{Cos}\,\omega\tau}{2(1+\omega^2)}$$

$$\left. + \frac{\omega\,\mathrm{Cosh}(\tau - t_0)\,\mathrm{Sin}\,\omega\tau}{2(1+\omega^2)}\right\} \qquad (6.1.36)$$

where

$$\bar{X}_1(\tau) = X_{11p}(\tau), \quad \tau \leqslant t_0$$

$$\bar{X}_1(\tau) = X_{12p}(\tau), \quad \tau \geqslant t_0.$$

It finally remains to determine the arbitrary constants A_0 and B_0 using the boundary conditions given by (5.1.46) namely,

$$X_1(t_0) = \beta \qquad (6.1.37a)$$

$$X_1'(t_0) = \tfrac{1}{2}\sqrt{2}k_0 \qquad (6.1.37b)$$

where β is the point at which the solution curve meets the X-axis and is given by (5.2.10) as

$$\beta = -\int_{-\infty}^{t_0} u_1(s)g(s)\,ds.$$

This integral can be evaluated explicitly [see Appendix D] to give

$$\beta = N(I \text{ Cos } \omega t_0 + J \text{ Sin } \omega t_0) - \frac{\sqrt{2}}{3}k_0 \qquad (6.1.38)$$

where

$$I = \frac{1}{6}(\omega^2 + 2) + \frac{1}{12}\pi\omega(\omega^2 + 1)\,\text{Tanh}(\tfrac{1}{2}\pi\omega) - \frac{2}{3}\omega^2(\omega^2 + 1)\sum_{n=1}^{\infty}\frac{1}{[(4n + 1)^2 + \omega^2]}, \qquad (6.1.39)$$

$$J = \frac{1}{12}\pi\omega(\omega^2 + 1)\,\text{Sech}(\tfrac{1}{2}\pi\omega). \qquad (6.1.40)$$

Together (6.1.37a), (6.1.36) and (6.1.38) give

$$B_0 = -\frac{N}{12}\pi\omega(\omega^2 + 1)\,\text{Sech}(\tfrac{1}{2}\pi\omega)\,\text{Sin } \omega t_0,$$

or

$$B_0 = f_0\frac{\pi}{2}\omega(\omega^2 + 1)\,\text{Sech}(\tfrac{1}{2}\pi\omega)\,\text{Sin } \omega t_0. \qquad (6.1.41)$$

Next A_0 is found by satisfying condition (6.1.37b). Differentiating (6.1.36) at time $\tau = t_0$,

$$X_1'(t_0) = A_0 + \frac{2}{3}\sqrt{2}k_0 - \frac{\omega}{4}N \text{ Sin } \omega t_0 + \frac{N}{3}(1 + \omega^2)\left[-\frac{3}{2}\omega\frac{d}{d\omega}I_c - \frac{3}{2}\omega t_0 I_s\right]. \qquad (6.1.42)$$

At $\tau = t_0$,

$$I_s = -2\sum_{n=0}^{\infty}\frac{(-1)^n\omega}{D}\,\text{Cos } \omega t_0$$

and

$$\frac{d}{d}I_c = 2\sum_{n=0}^{\infty}\frac{(-1)^n}{D}\,\text{Sin}\;\omega t_0 + 2\sum_{n=0}^{\infty}\frac{(-1)^n\omega t_0}{D}\,\text{Cos}\;\omega t_0$$

$$- 4\sum_{n=0}^{\infty}\frac{(-1)^n\omega^2}{D}\text{Sin}\;\omega t_0$$

and so

$$-\frac{3}{2}\frac{d}{d\omega}I_c - \frac{3}{2}\omega t_0 I_c = -3\omega\sum_{n=0}^{\infty}\frac{(-1)^n[2n+1)^2 - \omega^2]}{D}\,\text{Sin}\;\omega t_0. \tag{6.1.43}$$

Hence,

$$A_0 = \frac{\omega}{4}N\,\text{Sin}\;\omega t_0 + N\frac{\omega}{2}(1+\omega^2)\sum_{n=0}^{\infty}\frac{(-1)^n[(2n+1)^2 - \omega^2]}{D^2}$$

$$\times\,\text{Sin}\;\omega t_0 - \frac{5}{12}\sqrt{2}k_0$$

or

$$A_0 = -\frac{3}{2}f_0\,\text{Sin}\;\omega t_0 - 3f_0\omega(1+\omega^2)\sum_{n=0}^{\infty}\frac{(-1)^n[(2n+1)^2 - \omega^2]}{D^2}$$

$$\text{Sin}\;\omega t_0 - \frac{5}{12}\sqrt{2}k_0, \tag{6.1.44}$$

and solution (6.1.36) is complete.

The solution of Equation (6.1.1) takes the form

$$X(\tau) = X_0(\tau) + \varepsilon X_1(\tau) + \ldots O(\varepsilon^2) \tag{6.1.45}$$

where $X_0(\tau) = \sqrt{2}\;\text{Sech}(\tau - t_0)$

and $X_1(\tau)$ is given by (6.1.36)

but is still a general solution since t_0 is arbitrary and it has not been shown fully that $X(\tau)$ satisfies all the conditions of a simple saddle connection. It remains to determine those values of t_0 such that $X(\tau) \to 0$, $X'(\tau) \to 0$ as $\tau \to \pm\infty$. Clearly these conditions are met by $X_0(\tau)$ but $X_1(\tau)$ contains exponential growth terms which must be eliminated. To this end and to establish simultaneously the particular values of t_0 consider the growth terms of $X_1(\tau)$ as $\tau \to \infty$, which are given by

$$\frac{1}{4}e^{\tau}\left[B_0 + \frac{2}{3}\sqrt{2}k_0 - \frac{N\omega}{12}(1+\omega^2)\pi \operatorname{Sech}(\tfrac{1}{2}\pi\omega) \operatorname{Sin} \omega t_0\right]. \tag{6.1.46}$$

Equating to zero the expression in the brackets removes the growth term and gives the time t_0 when simple saddle connections occur, that is, when

$$F \operatorname{Sin} \omega t_0 = \frac{2\sqrt{2}k_0 \operatorname{Cosh}(\frac{1}{2}\pi\omega)}{3\pi\omega}$$

which agrees with result (5.1.53) as expected.

To determine the co-ordinates of the homoclinic points of tangency we must return to Eqn(6.1.1) where the parametric form of the solution is given by

$$X(t) = X_0(\tau) + \varepsilon X_1(\tau) + \ldots + O(\varepsilon^2) \tag{6.1.47a}$$

$$t = \tau + \varepsilon T_1(\tau) + \ldots + O(\varepsilon^2). \tag{6.1.47b}$$

Homoclinic points occur when $t_0 = \pi/2\omega$ and $t = 0$.

When $t = 0$, let $\tau = \tau_+^* = \tau_0 + \varepsilon\tau_1 + \ldots$ where $\tau_0, \tau_1, \ldots$ are constants. Hence, from (6.1.47b)

$$0 = \tau_+^* + \varepsilon T_1(\tau_+^*) + \ldots + O(\varepsilon^2)$$

or

$$0 = \tau_0 + \varepsilon(\tau_1 + T_1(0)) + \ldots + O(\varepsilon^2).$$

Equating powers of ε,

$$\tau_0 = 0 \tag{6.1.48}$$

and

$$\tau_1 = -T_1(0)$$

$$= \frac{k_0}{2}\left(\frac{1}{2}e^{-2t_0} + t_0\right), \qquad \text{using result (5.1.35).} \tag{6.1.49}$$

Hence, when $t = 0$,

$$\tau_+^* = \varepsilon\frac{k_0}{2}\left(\frac{1}{2}e^{-2t_0} + t_0\right) + O(\varepsilon^2). \tag{6.1.50}$$

We are now in a position to write down the co-ordinates of homoclinic points of tangency of Duffing's equation obtainable from the equation for simple saddle connections. Such points have co-ordinates given by

$$(x_H, x_H')_{t_0=\pi/2\omega} \tag{6.1.51}$$

where

$$x_H = X(\tau_+^*) - \frac{F_c}{(1+\omega^2)} \cos(\omega\tau_+^*) \tag{6.1.52}$$

$$x_H' = X'(\tau_+^*) + \frac{\omega F_c}{(1+\omega^2)} \sin(\omega\tau_+^*) \tag{6.1.53}$$

and $X > 0$.

Similarly, when $X < 0$, the co-ordinates are given by

$$x_H = X(\tau_-^*) - \frac{F_c}{(1+\omega^2)} \cos(\omega\tau_-^*) \tag{6.1.54}$$

$$x_H' = X'(\tau_-^*) + \frac{F_c\omega}{(1+\omega^2)} \sin(\omega\tau_-^*) \tag{6.1.55}$$

where

$$\begin{aligned} \tau_+^* &= \tau^* \quad (t_0 = \pi/2\omega), \\ \tau_-^* &= \tau^* \quad (t_0 = -\pi/2\omega), \end{aligned} \tag{6.1.56}$$

and F_c is given by (5.2.16).

Taking $k = 0.4, 0.3, 0.2, 0.1$ and ω ranging from 0.6 to 2 in steps of 0.1, Table [6.1] displays the coordinates of the homoclinic points corresponding to these parameter values. From Fig[3.4d] the coordinates of the particular homoclinic point of tangency ($x > 0$) are given as (0.66, 0.63) which should be compared to the co-ordinates (0.65, 0.663) obtained using (6.1.52) and (6.1.53). Here $y = x'$.

Table [6.1]

The following tables display the coordinates (x, y) of one of the homoclinic points corresponding to each of the parameter sets F, ω and k listed.

F =	k =	ω =	x =	y =
0.296	0.400	0.600	0.069	0.286
0.286	0.400	0.700	0.200	0.385
0.285	0.400	0.800	0.325	0.479
0.290	0.400	0.900	0.444	0.562
0.301	0.400	1.000	0.556	0.631
0.317	0.400	1.100	0.660	0.685
0.337	0.400	1.200	0.756	0.723
0.362	0.400	1.300	0.843	0.745
0.391	0.400	1.400	0.924	0.752
0.426	0.400	1.500	0.997	0.747
0.466	0.400	1.600	1.064	0.730
0.512	0.400	1.700	1.125	0.703
0.566	0.400	1.800	0.181	0.668
0.626	0.400	1.900	0.234	0.624

(a)

F =	k =	ω =	x =	y =
0.222	0.300	0.600	0.097	0.260
0.215	0.300	0.700	0.218	0.358
0.214	0.300	0.800	0.336	0.451
0.218	0.300	0.900	0.448	0.535
0.226	0.300	1.000	0.554	0.605
0.238	0.300	1.100	0.652	0.660
0.253	0.300	1.200	0.743	0.700
0.271	0.300	1.300	0.825	0.726
0.294	0.300	1.400	0.900	0.738
0.319	0.300	1.500	0.968	0.739
0.350	0.300	1.600	1.030	0.729
0.384	0.300	1.700	1.087	0.710
0.424	0.300	1.800	1.138	0.683
0.470	0.300	1.900	1.186	0.650

(b)

F =	k =	ω =	x =	y =
0.148	0.200	0.600	0.129	0.238
0.143	0.200	0.700	0.240	0.332
0.142	0.200	0.800	0.350	0.424
0.145	0.200	0.900	0.456	0.506
0.151	0.200	1.000	0.555	0.576
0.158	0.200	1.100	0.647	0.632
0.169	0.200	1.200	0.731	0.674
0.181	0.200	1.300	0.808	0.703
0.196	0.200	1.400	0.877	0.720
0.213	0.200	1.500	0.940	0.726
0.233	0.200	1.600	0.997	0.723
0.256	0.200	1.700	1.048	0.713
0.283	0.200	1.800	1.095	0.695
0.313	0.200	1.900	1.137	0.672

(c)

Finally, plotting the coordinates of the homoclinic points given in Table [6.1] where x' = y, produces the three curves displayed in Fig[6.1] below. Notice that each curve has a turning point at x = 1.

In addition to locating (approximately) the co-ordinates of the homoclinic points we are also able to draw the saddle connections through them using the exact formula given by (6.1.36) and its derivative.

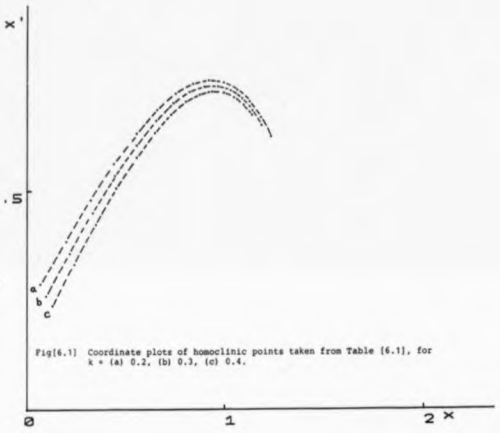

Fig[6.1] Coordinate plots of homoclinic points taken from Table [6.1], for k = (a) 0.2, (b) 0.3, (c) 0.4.

6.2 CONCLUDING REMARKS

Despite being one of the simplest non-linear ordinary differential equations under current study, Duffing's equation is imbued with rich 'dynamical' phenomena. Through its ability to model the behaviour of certain physical systems it became necessary to analyse and explain why certain types of behaviour occurred. Throughout this thesis, not only has the reader's attention been drawn to the various phenomena on offer, but, I would like to think, I have shed some light on why some of these strange events occur. Some of the phenomena at present are unfortunately inaccessible to analysis; however, nowadays researchers can turn to that invaluable mathematical aid - the computer, to help solve, make general observations and to draw conclusions when analysing O.D.E.'s of this type. This has certainly been the case here. However, many important questions still remain unanswered.

We still do not know, for example, what causes period doubling in systems such as these. No-one as yet has been able to produce any sort of parameter link that acts as a trigger for this change in behaviour. The nearest we came to understanding period doubling was through the use of a simple unimodal (non-linear) iteration scheme, guided by Feigenbaum (1983). It turned out that the scheme exhibited behaviour similar to that observed in Duffing's equation.

Although only briefly mentioned early on in the

thesis we again do not know what causes the hysterisis affect commonly referred to as the 'jump'-phenomena. What interaction of the various forces acting within the system causes it to 'jump' to a higher or lower amplitude response? Surely this and the previous question are necessary areas of further study.

Chapter 4 showed us that it was possible to find smooth piece-wise linear systems that also behaved in the same way as Duffing's equation exhibiting all the different phenomena thought solely to belong to the domain of non-linear systems. Undoubtedly, such systems are earier to analyse and through further research into such equations it may be possible to answer some of the many outstanding questions of non-linear systems.

The program of work presented in chapters 5 and 6 is certainly capable of further development. The perturbed solution given by Equation (5.1.3) deserves further investigation particularly in the area of stability of high amplitude odd-periodic solutions. The period 3 and 5 solutions obtained in chapter 5 appeared strongly stable but were not investigated. Perturbing the initial conditions slightly on such solutions one could follow the subsequent behaviour of the system and possibly establish stability criteria using similar methods employed in chapter 5. From numerical evidence it appears that an increase in the period of such solutions is accompanied by a significant decrease in the parameter regions of stability.

The method employed in chapter 5 revealed disjoint sets of amplitude values for which critical homoclinic tangencies were observed corresponding to particular types of multiple loop saddle connections. It is conjectured that there is an interlacing of critical tangencies within the Poincaré map and hence between amplitude values since all sets have sequences of amplitude values that tend to F_c.

The averaging and perturbation method employed in this thesis is not intended exclusively for Duffing's equation but could easily be applied to other systems with singular perturbation structures. The transformed equation helped to computer plot saddle connections which otherwise would have been difficult to draw. The exact solution of the simple saddle connections in the new system was obtained thus enabling the coordinates of the homoclinic tangency points to be found. It is possible that this approach could reveal and make accessible similar facts hidden in other dynamical systems.

The number of unanswered questions surrounding Duffing's equation alone will keep researchers occupied for many years to come. In the short period in which I have studied it, it has proved fascinating and extremely worthwhile. It has certainly opened my eyes to the unpredictable behaviour inherent in nonlinear systems which until recently thought was not possible. I wonder, finally, if Duffing, himself, was fully aware of the amount of interest that would one day be aroused by his

equation which forms a basis of research into nonlinear phenomena today.

APPENDIX A

THE FUNCTION $\Delta'(t_0)$

The form of the integrand in (3.3.6) suggests that integration here to obtain an expression for $\Delta'(t_0)$ might well prove difficult. However, due to the disappearance of many awkward terms, since $p_1 = 0$ and p_0, q_0, q_1 are each of single variable type, the integral actually reduces to

$$\Delta'(t_0) = -\int_{-\infty}^{\infty} p_0(x_0(t - t_0), y_0(t - t_0)) - q_1(x_0(t - t_0), y_0(t - t_0))dt \qquad A1$$

where $p_0 = y(t - t_0)$,

$q_1 = f \cos \omega t - k_0 y(t - t_0)$

and $y_0(t - t_0) = -\sqrt{2}\ \mathrm{Sech}^2(t - t_0)\ \mathrm{Sinh}(t - t_0)$.

[$y_0 = x_0'$ where $x_0' = \sqrt{2}\ \mathrm{Sech}(t - t_0)$ is the solution of the unperturbed, $\varepsilon = 0$, equation on which Mel'nikov's method is based.]

Upon substitution A1 becomes

$$\Delta'(t_0) = \int_{-\infty}^{\infty} (k_0 y_0^2 - f y_0 \cos \omega t)dt \qquad A2$$

$$= k_0 \int_{-\infty}^{\infty} y_0^2 dt - f \int_{-\infty}^{\infty} y_0 \cos \omega t\, dt \qquad A3$$

$$= I_1 + I_2.$$

First consider the integral I_1,

$$= 2k_0\int_{-\infty}^{\infty} \text{Sech}^4(t - t_0)\ \text{Sinh}^2(t - t_0)dt$$

$$= \frac{2}{3}k_0\int_{-\infty}^{\infty} \frac{d}{dt}[\text{Tanh}^3(t - t_0)]dt$$

$$= \frac{2}{3}k_0\Big|_{-\infty}^{\infty} \text{Tanh}^3(t - t_0)$$

$$= \frac{4}{3}k_0. \qquad \text{A4}$$

Next consider the integral I_2 given by

$$I_2 = \sqrt{2}f\int_{-\infty}^{\infty} \text{Sech}^2(t - t_0)\ \text{Sinh}(t - t_0)\ \text{Cos}\ \omega t\ dt \qquad \text{A5}$$

which contains both hyperbolic and trigonometrical terms. Write $x = t - t_0$ then A5 upon this change of variable becomes

$$I_2 = \sqrt{2}f\int_{-\infty}^{\infty} \text{Sech}^2 x\ \text{Sinh}\ x\ \text{Cos}\ \omega(x + t_0)dt \qquad \text{A6}$$

which, after expanding the Cosine term can be written as

$$I_{2a} + I_{2b}$$

where

$$I_{2a} = \sqrt{2}f\ \text{Cos}\ \omega t_0\int_{-\infty}^{\infty} \text{Sech}^2 x\ \text{Sinh}x\ \text{Cos}\ \omega x\ dx \qquad \text{A7}$$

and

$$I_{2b} = -\sqrt{2}f \text{ Sin } \omega t_0 \int_{-\infty}^{\infty} \text{Sech}^2 x \text{ Sin } x \text{ Sin } \omega x \, dx. \qquad \text{A8}$$

Integral I_{2a} is zero, since it is over the product of an odd and an even function.

Integral I_{2b} is evaluated by the method of residues (see Spiegel, 1974) as follows.

Start by applying the method of integration by parts so that

$$I_{2b} = M\int_{-\infty}^{\infty} [-\text{Sin } \omega x \text{ Sech } x] + \omega M \int_{-\infty}^{\infty} \text{Cos } \omega x \text{ Sech } x \, dx,$$

$$M = -\sqrt{2}f \text{ Sin } \omega t_0$$

$$= \omega M \int_{-\infty}^{\infty} \text{Cos } \omega x \text{ Sech } x \, dx, \quad \text{since Sech}(\pm\infty) = 0. \qquad \text{A9}$$

Next consider the integral

$$\oint_c \frac{e^{i\omega z}}{\text{Cosh } z} dz \quad \text{where } z = x + yi \qquad \text{A10}$$

of which integral A9 is part, and c is a rectangle having vertices at $-R$, R, $R + \pi i$, $-R + \pi i$ (see Fig[A.1]). The poles of $e^{i\omega z}/\text{Cosh } z$ are simple and occur where $\text{Cosh } z = 0$, i.e. $z = (n + \frac{1}{2})\pi i$, $n = 0, \pm 1, \pm 1, \ldots$. The only pole enclosed by c is $\pi i/2$.

The residue of $\frac{e^{i\omega z}}{\text{Cosh } z}$ at $z = \pi i/2$ is

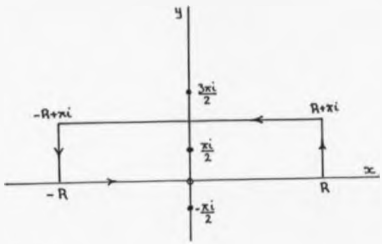

FIG[A.1]

$$\lim_{z \to \pi i/2} (z - \pi i/2)\frac{e^{i\omega z}}{\text{Cosh } z} = \frac{e^{-\omega\pi/2}}{\text{Sinh}(\pi i/2)} \quad \text{using L'Hopital's rule}$$

$$= \frac{e^{-\omega\pi/2}}{i \text{ Sin}(\pi/2)}$$

$$= -ie^{-\omega\pi/2}.$$

Then by the residue theorem

$$\oint_C \frac{e^{i\omega z}}{\text{Cosh } z} = 2\pi i(-ie^{-\omega\pi/2}) = 2\pi e^{-\omega\pi/2}. \qquad \text{A11}$$

This can be written

$$\int_{-R}^{R} \frac{e^{i\omega x}}{\text{Cosh } x}dx + \int_{0}^{\pi} \frac{e^{i\omega(-R+iy)}}{\text{Cosh}(R + iy)}dy$$

$$+ \int_{R}^{-R} \frac{e^{i\omega(x+\pi i)}}{\text{Cosh}(x + \pi i)}dx + \int_{\pi}^{0} \frac{e^{i\omega(-R+iy)}}{\text{Cosh}(-R + iy)}dy = 2\pi e^{-\omega\pi/2}.$$

As $R \to \infty$ the second and fourth integrals on the left approach zero. To show this let us consider the second integral. Since

$$|\text{Cosh}(R + iy)| = \left|\frac{e^{R+iy} + e^{-R-iy}}{2}\right|$$

$$\geq \frac{1}{2}\left\{|e^{R+iy}| - |e^{-R-iy}|\right\}$$

$$= \frac{1}{2}(e^{R} - e^{-R})$$

$$\geq \frac{1}{4}e^{R}$$

we have

$$\left|\int_0^{\pi} \frac{e^{i\omega(R+iy)}}{\text{Cosh}(R + iy)}dy\right| \leq \int_0^{\pi} \frac{e^{i\omega R}}{\frac{1}{4}e^{R}}dy = 4\pi e^{(i\omega-1)R}$$

and the result follows on noting that the right-side approaches zero as $R \to \infty$. In a similar manner it can be shown that the fourth integral on the left of A11 approaches zero as $R \to \infty$. Hence A11 becomes

$$\lim_{R\to\infty}\left\{\int_{-R}^{R} \frac{e^{i\omega x}dx}{\text{Cosh } x} + \int_{R}^{-R} \frac{e^{i\omega(x+\pi i)}}{\text{Cosh}(x + \pi i)}dx\right\} = 2\pi e^{-\omega\pi/2}$$

or

$$\lim_{R\to\infty}\left\{\int_{-R}^{R} \frac{e^{i\omega x}}{\text{Cosh } x}dx + e^{-\omega\pi}\int_{-R}^{R} \frac{e^{i\omega x}}{\text{Cosh } x}dx\right\} = 2\pi e^{-\omega\pi/2}$$

or

$$\lim_{R\to\infty}\left\{(1 + e^{-\omega\pi})\int_{-R}^{R} \frac{e^{i\omega x}}{\text{Cosh } x}dx\right\} = 2\pi e^{-\omega\pi/2}$$

hence,

$$\int_{-\infty}^{\infty} \frac{e^{i\omega x}}{\text{Cosh } x}dx = \frac{2\pi e^{-\omega\pi/2}}{1 + e^{-\omega\pi}} \qquad \text{A13}$$

$$= \frac{2\pi}{e^{\omega\pi/2} + e^{-\omega\pi/2}}$$

$$= \pi \text{ Sech}(\pi\omega/2). \qquad \text{A14}$$

Expanding the left side of AB and taking the real part only,

$$\int_{-\infty}^{\infty} \frac{\text{Cos } \omega x}{\text{Cosh } x}dx = \int_{-\infty}^{\infty} \text{Cos } \omega x \text{ Sech } x \, dx = \pi \text{ Sech}(\omega\pi/2). \qquad \text{A15}$$

Therefore,

$$I_{2b} = -\sqrt{2}f\pi\omega \text{ Sech}(\omega\pi/2)\text{Sin}\omega t_o \qquad \text{A16}$$

and

$$\Delta'(t_0) = \tfrac{4}{3}k_0 - \sqrt{2}f\pi\omega \text{ Sech}(\omega\pi/2)\text{Sin}\omega t_o. \qquad \text{A17}$$

APPENDIX B

FINDING $I(t_0)$

From equation (5.2.13) we know that $I(t_0)$ is given by

$$I(t_0) = \int_{-\infty}^{\infty} u_1(s, t_0) g(s, t_0) ds \qquad B1$$

where

$$u_1(s, t_0) = \text{Sinh}(s - t_0)\text{Sech}^2(s - t_0)$$

and

$$g(s, t_0) = g_1(s, t_0) + g_2(s, t_0)$$

where

$$g_1(s, t_0) = -2\sqrt{2}k_0 \text{ Sech}^3(s - t_0)[e^{-2|s-t_0|} - 1] \times \text{sgn}(s - t_0)$$

and

$$g_2(s, t_0) = -6f_0 \text{ Sech}^2(s - t_0) \text{ Cos } \omega s.$$

First consider the integral

$$I_1 = \int_{-\infty}^{\infty} u_1(s, t_0) g_1(s, t_0) ds \qquad B2$$

$$= -2\sqrt{2}k_0\int_{-\infty}^{\infty} \text{Sinh}(s - t_0)\ \text{Sech}^5(s - t_0)[e^{-2|s-t_0|} - 1]$$

$$\text{sgn}(s - t_0)ds. \qquad \text{B3}$$

As the integrand $u_1(s, t_0)g(s, t_0)$ in B3 is an even function we can write B3 as

$$-4\sqrt{2}k_0\int_0^{\infty} \text{Sinh } u\ \text{Sech}^5 u[e^{-2u} - 1]\ du \qquad \text{B4}$$

where $u = s - t_0$. Expressing e^{-2u} as $(\text{Cosh } u - \text{Sinh } u)^2$ and expanding, B4 becomes

$$-4\sqrt{2}k_0\int_0^{\infty} \text{Sinh } u\ \text{Sech}^5 u[\text{Cosh}^2 u - 2\ \text{Sinh } u\ \text{Cosh } u$$

$$+ \text{Sinh}^2 u - 1]du$$

$$= -8\sqrt{2}k_0\int_0^{\infty} (\text{Sinh } u\ \text{Sech}^5 u - \text{Sech}^2 u\ \text{Tan}^2 u$$

$$- \text{Sinh } u\ \text{Sech}^5 u)du$$

$$= -8\sqrt{2}k_0\left[-\frac{1}{2}\text{Sech}^2 u - \frac{1}{3}\text{Tanh}^3 u + \frac{1}{4}\text{Sech}^4 u\right]$$

$$= -8\sqrt{2}k_0\left[-\frac{1}{3} + \frac{1}{2} - \frac{1}{4}\right]$$

$$= \frac{2}{3}\sqrt{2}k_0 \qquad \text{B5}$$

which is not dependent upon the time t_0.

Next consider the integral

$$I_2 = \int_{-\infty}^{\infty} u_1(s, t_0) g_2(s, t_0) ds \qquad B6$$

$$= -6f_0 \int_{-\infty}^{\infty} \text{Sinh}(s - t_0) \text{Sech}^4(s - t_0) \text{ Cos } \omega s \, ds \qquad B7$$

$$= -6f_0 \int_{-\infty}^{\infty} \text{Sinh } v \text{ Sech}^4 v \text{ Cos } \omega(v + t_0) dv \qquad B8$$

where $v = s - t_0$.

Expanding the cosine term in B8 gives the two integrals

$$-6f_0 \text{ Cos } \omega t_0 \int_{-\infty}^{\infty} \text{Sinh } v \text{ Sech}^4 v \text{ Cos } \omega v \, dv$$

$$+ 6f_0 \text{ Sin } \omega t_0 \int_{-\infty}^{\infty} \text{Sinh } v \text{ Sech}^4 v \text{ Sin } \omega v \, dv. \qquad B9$$

The first integral is zero since the integrand is an odd function. This leaves

$$I_2 = 6f_0 \text{ Sin } \omega t_0 \int_{-\infty}^{\infty} \text{Sinh } v \text{ Sech}^4 v \text{ Sin } \omega v \, dv \qquad B10$$

$$= 2\omega f_0 \text{ Sin } \omega t_0 \int_{-\infty}^{\infty} \text{Sech}^3 v \text{ Cos } \omega v \, dv \qquad B11$$

applying integration by parts. To complete the integration it is necessary to consider the complex integral

$$I_3 = \int_{-\infty}^{\infty} e^{i\omega v} \text{ Sech } v \, dv \qquad B12$$

to which we apply integration by parts twice. Hence, it can be shown that

$$\int_{-\infty}^{\infty} e^{i\omega v} \operatorname{Sech}^3 v \, dv = \frac{(1 + \omega^2)}{2} \int_{-\infty}^{\infty} e^{i\omega v} \operatorname{Sech} v \, dv. \qquad B13$$

Taking the real parts only then

$$\int_{-\infty}^{\infty} \operatorname{Cos} \omega v \operatorname{Sech}^3 v \, dv = \frac{(1 + \omega^2)}{2} \int_{-\infty}^{\infty} \operatorname{Cos} \omega v \operatorname{Sech} v \, dv \qquad B14$$

$$= \frac{(1 + \omega^2)}{2} \pi \operatorname{Sech}(\tfrac{1}{2}\pi\omega) \qquad B15$$

see Appendix A.

Therefore,

$$I_2 = f_0(1 + \omega^2)\pi\omega \operatorname{Sech}(\tfrac{1}{2}\pi\omega) \operatorname{Sin} \omega t_0. \qquad B16$$

Since $I(t_0) = I_1 + I_2$ then

$$I(t_0) = \frac{2}{3}\sqrt{2}k_0 + f_0(1 + \omega^2)\pi\omega \operatorname{Sech}(\tfrac{1}{2}\pi\omega) \operatorname{Sin} \omega t_0 \qquad B17$$

$$= \frac{2}{3}\sqrt{2}k_0 - f\pi\omega \operatorname{Sech}(\tfrac{1}{2}\pi\omega) \operatorname{Sin} \omega t_0 \qquad B18$$

since $f_0 = -\frac{f}{1 + \omega^2}$.

APPENDIX C

THE DERIVATIVE OF THE STABLE MANIFOLD AT THE HOMOCLINIC POINT A

Points (x_0, y_0) on the stable manifold in RIII are given in section (4.4) parametrically by

$$x_0(t_1^*) = 1 + C + \left[\left(\frac{c}{2}\,\text{Sin}\ qt_1^* + q\,\text{Cos}\ qt_1^*\right)u - v\,\text{Sin}\ qt_1^*\right]/q \qquad C1$$

$$y_0(t_1^*) = \left[\frac{c}{2}(x_0 - C - 1) + (-1 + Dw + Cc) + \left(q\,\text{Sin}\ qt_1^* - \frac{c}{2}\,\text{Cos}\ qt_1^*\right)u + v\,\text{Cos}\ qt_1^*\right]/(c + 1) \qquad C2$$

where t_1^* is the time a solution through (x_0, y_0), started at time $t = 0$, reaches the point B - a point on the stable manifold on the boundary of RII and RIII (see Fig[4.7]). U and V are given by (4.4.3a) and (4.4.3b) respectively. The slope at any point on the stable manifold in RIII is given by C1, C2 above is obtained by taking the separate derivatives of x_0 and y_0 where differentiation is with respect to t_1^*. Therefore,

$$\frac{dx_0}{dt_1^*} = \left[U'\left(\frac{c}{2}\,\text{Sin}\ qt_1^* + q\,\text{Cos}\ qt_1^*\right) + U\left(\frac{cq}{2}\,\text{Cos}\ qt_1^* - q^2\,\text{Sin}\ qt_1^*\right) - V'\,\text{Sin}\ qt_1^* - V_q\,\text{Cos}\ qt_1^*\right]/q \qquad C3$$

and

$$\frac{dy_0}{dt_1^*} = \left[\frac{c}{2}\frac{dx_0}{dt_1^*} + U'\left(q \sin qt_1^* - \frac{c}{2}\cos qt_1^*\right) + U\left(q^2 \cos qt_1^* + \frac{cq}{2}\sin qt_1^*\right) + V' \cos qt_1^* - Vq \sin qt_1^*\right]/(1 + c). \qquad C4$$

Each of the two previous results C3 and C4 can be greatly simplified if we consider that the time t_1^* corresponding to the initial homoclinic point A satisfies (4.1.17) and (4.1.18). That is,

$$\cos \omega t_1^* = -C, \qquad \sin \omega t_1^* = -D. \qquad C5$$

and $\quad \tan \omega t_1^* = \omega(2 + c)/c.$

Hence,

$$U(t_1^*) = 0 \qquad U'(t_1^*) = 0 \qquad C6$$

$$V(t_1^*) = 0 \qquad V'(t_1^*) = -\omega^2 e^{ct_1^*/2}.$$

Consequently, the derivatives C3 and C4 reduce to

$$\frac{dx_0}{dt_1^*} = \frac{\omega^2}{q} e^{ct_1^*/2} \sin qt_1^* \qquad C7$$

and

$$\frac{dy_0}{dt_1^*} = \frac{c\omega^2}{2q} e^{ct_1^*/2} \sin qt_1^* - \frac{\omega^2}{(1 + c)} e^{-ct_1^*/2} \cos qt_1^* \qquad C8$$

respectively.

Therefore, the slope at the homoclinic point A on the stable manifold is given by

$$\frac{dy_0}{dx_0} = \frac{c}{2} - \frac{q}{(1+c)} \cot(qt_1^*) \qquad C9$$

which is zero if

$$\frac{2q}{c(1+c)} = \tan(qt_1^*). \qquad C10$$

It is difficult to tell from the Poincaré map in Fig[4.5] that the slope of the stable manifold at A is not zero. But in this case, where c = 0.3, a solution from A at time t = 0 arrives at B at time $t_1^* = 4.0937$. With q = 1.1303 and ω = 1.229 it turns out that

$$\frac{dy_0}{dx_0} = 0.0755$$

at A. Hence A is a transverse homoclinic point and we expect there to be a second such point (in this case) very close to A.

APPENDIX D

INTEGRAL EVALUATION OF THE CONSTANT β

In Chapter 5 we investigated saddle solutions of the transformed Duffing equation, (5.1.4). To this end we considered these solutions which passed close to $X = \sqrt{2}$ by writing $X(t_0) = \sqrt{2} + \varepsilon\beta$, where t_0 and β were constants. However, it was not necessary there to evaluate explicitly either integral (5.2.10) or (5.2.11) to determine β. In Chapter 6, however, β is required explicitly in order to obtain the arbitrary constants of integration A_0, B_0 of the exact solution of equation (5.1.4).

Consider the integral (5.2.10) which can be written

$$\beta = -\int_{-\infty}^{t_0} u_1(s)g(s)ds. \qquad D1$$

A similar integral was evaluated in Appendix B but there the upper limit of integration was set to $s = \infty$. Despite this difference we can make use of some of the results obtained there. Firstly, we know from Appendix B that the integral D1 can be split into two separate integrals which we will call $I_a(t_0)$ and $I_b(t_0)$ respectively. Writing

$$I_a(t_0) = -2\sqrt{2}k_0 \int_{-\infty}^{t_0} \text{Sinh}(s - t_0)\ \text{Sech}^3(s - t_0) \left[e^{2(s-t_0)} - 1 \right] ds \qquad \text{D2}$$

and using the results of Appendix B,

$$I_a(t_0) = -2\sqrt{2}k_0 \int_{-\infty}^{t_0} \left[-\frac{1}{2}\,\text{Sech}^2(s - t_0) + \frac{1}{4}\,\text{Sech}^4(s - t_0) + \frac{1}{3}\,\text{Tanh}^3(s - t_0) \right]$$

$$= -\frac{\sqrt{2}}{3}k_0. \qquad \text{D3}$$

The second integral is written

$$I_b(t_0) = 6f_0 \int_{-\infty}^{t_0} \text{Sinh}(s - t_0)\ \text{Sech}^4(s - t_0)\ \text{Cos}\ \omega s\ ds \qquad \text{D4}$$

which, upon the change of variable $s - t_0 = -u$, becomes

$$I_b(t_0) = -6f_0 \int_0^{\infty} \text{Sinh}\ u\ \text{Sech}^4 u\ \text{Cos}\ \omega(u - t_0)\, du. \qquad \text{D5}$$

Expanding the cosine term and splitting into two further integrals,

$$I_b(t_0) = I_{b1}(t_0) + I_{b2}(t_0),$$

where

$$I_{b1}(t_0) = -6f_0\ \text{Cos}\ \omega t_0 \int_0^{\infty} \text{Sinh}\ u\ \text{Sech}^4 u\ \text{Cos}\ \omega u\ du \qquad \text{D6}$$

$$I_{b2}(t_0) = -6f_0 \text{ Sin } \omega t_0 \int_0^\infty \text{Sinh } u \text{ Sech}^4 u \text{ Sin } \omega u \, du. \qquad D7$$

These integrals can be evaluated using the integral result

$$\int_0^\infty e^{i\omega u} \text{ Sech } u \, du = M + iN \qquad D8$$

where from Gradshteyn (1965)

$$M = \frac{\pi}{2} \text{ Sech}\left(\frac{\omega\pi}{2}\right) \qquad D9$$

and

$$N = -\frac{\pi}{2} \text{ Tanh}\left(\frac{\omega\pi}{2}\right) - \frac{i}{2}\left[\psi\left(\frac{1 + \omega i}{4}\right) - \psi\left(\frac{1 - \omega i}{4}\right)\right]$$

$$= -\frac{\pi}{2} \text{ Tanh}\left(\frac{\omega\pi}{2}\right) + 4\omega \sum_{n=0}^{\infty} \frac{1}{[(4n + 1)^2 + \omega^2]}, \qquad D10$$

where $\psi(z)$ is the psi function.

Applying the method of integration by parts three times to D8 we have

$$\int_0^\infty e^{i\omega u} \text{ Sinh } u \text{ Sech}^4 u \, du = i\omega(1 + \omega^2)(M + iN) + \frac{(2 + \omega^2)}{6}. \qquad D11$$

Taking the real and imaginary parts of result D11 separately

$$\int_0^\infty \text{Sinh } u \text{ Sech}^4 u \text{ Cos } \omega u \, du = \frac{(2 + \omega^2)}{6} - \frac{\omega}{6}(1 + \omega^2)N \qquad D12$$

and

$$\int_0^\infty \text{Sinh } u \text{ Sech}^4 u \text{ Sin } \omega u \, du = \frac{\omega}{6}(1 + \omega^2)M. \qquad \text{D13}$$

Hence,

$$I_{b1}(t_0) = \left\{-f_0(\omega^2 + 2) - f_0\frac{\pi\omega}{2}(\omega^2 + 1)\,\text{Tanh}\left(\frac{\pi\omega}{2}\right) + 4f_0\omega^2(1 + \omega^2)\sum_{n=0}^{\infty}\frac{1}{[(4n + 1)^2 + \omega^2]}\right\}.\text{Cos } \omega t_0 \qquad \text{D14}$$

and

$$I_{b2}(t_0) = -f_0\frac{\pi\omega}{2}(\omega^2 + 1)\,\text{Sech}\left(\frac{\pi\omega}{2}\right)\,\text{Sin } \omega t_0 \qquad \text{D15}$$

written as NI and NJ respectively in (6.1.38).

REFERENCES

1. R.H. ABRAHAM AND C.D. SHAW, "Dynamics, the geometry of behaviour. Part one: Periodic Behaviour", Aerial Press, California, 1982.

2. R.H. ABRAHAM AND C.D. SHAW, "Dynamics, the geometry of behaviour. Part two: Chaotic Behaviour", Aerial Press, California, 1983.

3. R.H. ABRAHAM AND C.D. SHAW, "Dynamics, the geometry of behaviour. Part three: Global Behaviour", Aerial Press, California, 1984.

4. H. BAI-LIN, "Chaos", World Scientific, 1984.

5. G.I. BARENBLATT, G. IOOSS AND D.D. JOSEPH, "Nonlinear Dynamics and Turbulence", Pitman, London, 1983.

6. S. BECKET, U. SCHOCK, C.D. SHULTZ, T. WEIDLICH AND F. KAISER, Experiments on the bifurcation behaviour of a forced nonlinear pendulum, Physics Letters, Vol. 107A, No. 8 (1985), 347-350.

7. J.G. BYATT-SMITH, 2π Periodic solutions of Duffing's equations with negative stiffness, SIAM J. Appl. Math., Vol. 47, No. 1 (1987), 60-91.

8. L. CESARI, "Asymptotic behaviour and stability problems in ordinary differential equations", Springer-Verlag, New York, 1971.

9. J. COSTE AND N. PEYRAUD, A new type of period-doubling bifurcations in one-dimensional transformations with two extrema, Physica 5D (1982), 415-420.

10. M.J. FEIGENBAUM, Quantitative universality for a class of nonlinear transformations, Journal of Statistical Physics, Vol. 19, No. 1, 1978.

11. M.J. FEIGENBAUM, Universal behaviour in nonlinear systems, Physica 7D (1983), 16-39.

12. I.S. GRADSHTEYN AND I.M. RYZHIK, "Table of Integrals, Series and Products", Academic Press, New York, 1965.

13. J. GUCKENHEIMER AND P. HOLMES, "Nonlinear Oscillations, Dynamical Systems, and Bifurcations of Vector Fields", Springer-Verlag, New York, 1983.

14. J. GUCKENHEIMER, Multiple bifurcation problems of codimension two, SIAM J. Math. Anal. Vol. 15, No. 1, 1984, 1-49.

15. E. HILLE, "Lectures on Ordinary Differential Equations", Addison-Wesley, California, 1969.

16. C. HAYASHI, "Nonlinear Oscillations in Physical Systems", McGraw-Hill, New York, 1969.

17. C. HAYASHI, Y. UEDA AND H. KAWAKAMI, Transformation theory as applied to the solutions of non-linear

differential equations of the second order, Int. J. Non-linear Mechanics, Vol. 4, pp 235-255 (1969).

18. M. HÉNON, A two-dimensional mapping with a strange attractor, Commun. Math. Phys. 50, 69-77 (1976).

19. M. HÉNON, On the numerical computation of Poincaré maps, Physica 5D (1982), 412-414.

20. A.V. HOLDEN, "Chaos", Manchester University Press, Manchester, 1986.

21. P. HOLMES, A nonlinear oscillator with a strange attractor, Phil. Trans. Roy. Soc. A292 (1979), 419-448.

22. P. HOLMES AND D. WHITLEY, On the attracting set for Duffing's equation, Physica 7D (1983), 111-123.

23. D.W. JORDAN AND P. SMITH, "Nonlinear Ordinary Differential Equations", Clarendon Press, Oxford (1987).

24. D.L. KREIDER, R.G. KULLER, D.R. OSTBERG AND F.W. PERKINS, "An Introduction to Linear Analysis", Addison-Wesley, Massachusetts (1966).

25. T.Y. LI AND J. YORKE, Period three implies chaos, Amer. Math. Monthly, 82 (1975), pp 985-992.

26. V.K. MEL'NIKOV, On the stability of the centre for time-periodic perturbations, 1963, Trans. Moscow Math. Soc. 12(1), 1-57.

27. S. MAEZAWA, On the stability of forced vibration in piecewise-linear system, Proc. 4th Conference on Nonlinear Oscillations, Prague (1968), 361-371.

28. F.C. MOON AND P.J. HOLMES, A magentoelastic strange attractor, Journal of Sound and Vibration (1979), 65(2), 275-296.

29. F.C. MOON, Experimental models for strange attractor vibrations in elastic systems, New App. to Nonlinear Problems in Dynamics, edited by P.J. Holmes, SIAM, Philadelphia (1980).

30. A.D. MOROZOV, A complete qualitative investigation of Duffing's equation, J. Diff. Eqns. Vol. 12, No. 2 (1976), 164-174.

31. A. NAYFEH, "Perturbation Methods", Wiley-Interscience, New York (1973).

32. M. ODYNIEC AND L.O. CHUA, Josephson-Function Circuit Analysis Via Integral Manifolds, IEEE Transactions on Circuits and Systems, Vol. CAS-30, No. 5, 1983.

33. J. PALIS, JR. AND W. de MALO, "Geometric Theory of Dynamical Systems", Springer-Verlag (1982).

34. U. PARLITZ AND W. LAUTERBORN, Superstructure in the bifurcation set of the Duffing equation, Physics Letters, Vol. 107A, No. 8 (1985), 351-355.

35. L. PŮST, Vibration of nonlinear mechanical systems with nonanalytic characteristics, Proc. 4th Conference on Nonlinear Oscillations, Prague (1968), 441-458.

36. R. RÄTY, J. VON BOEHM AND H.M. ISOMÄKI, Absence of inversion-symmetric limit cycles of even periods and the chaotic motion of Duffing's oscillator, Physics Letters, Vol. 103A, No. 6, 7 (1984).

37. D. RUELLE, Strange attractors, The Mathematical Intelligencer 2 (1980), 126-137.

38. R. SEYDEL, Attractors of a Duffing equation - dependence on the exciting frequency, Physica 17D (1985), 308-312.

39. R. SHAW, Strange Attractors, Chaotic Behaviour, and Information Flow, Z. Naturforsch. 36a, 80-112 (1981).

40. S.W. SHAW AND P.J. HOLMES, A periodically forced piecewise linear oscillator, Journal of Sound and Vibration (1983), 90(1), 129-155.

41. M. SHUB, "Global Stability of Dynamical Systems", Springer-Verlag, New York, 1978.

42. P. SMITH AND N.M. DAVENPORT, A perturbation method for saddle connection and homoclinic bifurcation in Duffing's equation, Dynamics and Stability of Systems, Vol. 2. (To be published 1988.)

43. M.R. SPIEGEL, "Complex Variables", Schaum's Outline Series, McGraw-Hill, 1964.

44. J.M.T. THOMPSON, A.R. BOKAIAN AND R. GHAFFARI, Subharmonic resonances and chaotic motions of a bilinear oscillator, IMA j. App. Math. (1983), 31, 207-234.

45. J.M.T. THOMPSON AND H.B. STEWART, "Nonlinear Dynamics and Chaos", John Wiley & Sons, 1986.

46. W.Y. TSENG AND J. DUGUNDJI, Nonlinear vibrations of a buckled beam under harmonic excitation, J. Appl. Math. (1971).

47. Y. UEDA, Randomly transitional phenomena in the system governed by Duffing's equation, J. Stat. Phys. Vol. 20, No. 2, 1979.

48. Y. UEDA, Steady motions exhibited by Duffing's equation: A picture book of regular and chaotic motions, New Approaches to Nonlinear Problems in Dynamics, edited by P.J. Holmes, SIAM, Philadelphia (1980).

49. P.W. WILLIAMS, "Numerical Computation", Nelson, Great Britain, 1972.